Università degli Studi di Padova

Dipartimento di Fisica e Astronomia "Galileo Galilei"

Master Degree in Physics

Inflationary Imprints on the Large Scale Structure of the Universe

Thesis supervisors:

Prof. Marco Peloso

Prof. Massimo Pietroni

Candidate:

Nicola Tranquilli

Academic Year 2019-2020

Non conformatevi a questo mondo,
ma lasciatevi trasformare rinnovando il vostro modo di pensare.
— Rm, 12,2

Contents

Introduction

The last two decades have been extremely successful for cosmology, especially from the observational point of view. Different full-sky surveys have probed the physics at the largest cosmological scales and data have measured or constrained many different cosmological parameters with increasing accuracy. Among many, we can cite weak-lensing observations [1], WMAP [2] and Planck [3] for CMB measurements and large-scale structure maps as SDSS [4].

It is well-known that Inflation [5], a phase of the early universe in which the universe exponentially expanded, is the predominant model describing the early universe and has been receiving robust evidences from all kind of observations. Besides, Inflation provides an exceptional possibility to test physics at energies which cannot be reached in any terrestrial experiment whatsoever. Thanks to Inflation, we can explain the homogeneity and isotropy of the universe but also understand the structure formation of the universe, which was seeded during this stage, before standard model particles thermalized: in fact, Inflation is responsible in transforming the quantum fluctuations of the inflaton field into macroscopic and classical density perturbations.
Although Inflation is rather fascinating and attractive, we actually do not know much about the underlying theory of such exponential expansion. There is no unique model of Inflation and, moreover, there may be alternatives to Inflation which, so far, observations have not ruled out.
Besides Inflation there are other pressing open questions in cosmology. The majority of the matter in the universe is "dark", and we actually know little about it. Also, the nature of the ingredient which produces the accelerated expansion is very obscure: we call it dark energy, and we are extremely far away from understanding it at a fundamental level. It is evident that, in order to make progress, we need to address these questions. Clearly, clues must come from the observational side and, next generation surveys like SKA [6], LSST [7] and the Euclid satellite [8] are planned exactly for this reason: they are supposed to improve the precision in measuring cosmological observables thereby constraining different cosmological parameters.

This work will consider forecasts on the performance of Euclid in measuring some cosmological parameters. Euclid will inspect the large-scale structure of the universe by measuring position and velocity of galaxies. It will measure about 2 billion photometric galaxy images and 30 million spectroscopic redshifts. It will range from $z \sim 0.7$

up to $z \sim 2$ and it will cover 15000 deg^2 of the sky. The investigation of the large-scale structure of the universe is extremely important: indeed from the large scales we can understand both the initial conditions (Inflation) and the development of the cosmic structures (dark energy). Gravitational instability is the main actor during structure formation and therefore we need a quantitative description of gravitational instability dynamics in order to be able to test theory against observations. Large-scale structure surveys can outdo CMB measurements in the number of Fourier modes present for observations and they can also probe the power spectrum to smaller scales. However, the principal obstacles in a smooth connection between models and data are nonlinearities. Such nonlinearities come from redshift space distorsions, nonlinear evolution of dark matter, galaxy and halo bias and so forth. We thus need a framework in which we can model nonlinear effects in order to extract the cosmological information present in observational data. Such a framework is represented by perturbation theory (PT), which has been strongly developed in the last decades. In this work we will approach the dynamics of gravitational instability from the linear to non-linear regime mainly in the Eulerian framework. Initially density perturbations at very large scales ($k \lesssim 0.5$) and $z \approx 0$ are small enough so that linear theory is valid. Considering higher redshifts ($z \gtrsim 1$) and smaller scales, in the so called weakly nonlinear regime, PT is successful in describing the evolution of perturbations. However, as we lower the redshift or we consider smaller scales, even PT fails to describe properly the dynamics; the standard tool used in this range is N-body simulations, although they are very expensive in terms of computational time. An alternative method, in this range, would be to broaden the knowledge of analytic methods grounded on perturbation theory. Keeping in mind the limitations of a fully PT approach, in this work we will limit ourselves to analytical results, which have the virtue of making the relevant conceptual points evident.

In this work we will focus on the Consistency Relations of the large scale structure (CR), which are relations between correlation functions at different order [9–11]. Since, as we have said, the large-scale structure of the universe is dominated by nonlinear effects, it is extremely remarkable that we are able to write exact relations beyond any approximation scheme.
By using a Fisher matrix approach, we will examine the possibility of measuring the bias parameter using the CR from the power spectrum and the bispectrum. Moreover we will investigate the possibility to use CR's to constrain primordial features, of inflationary origin, in these observables. The next generation of cosmological experiments, such as Euclid, will help us in understanding if we effectively see departures from the power-law power spectrum predicted by slow-roll Inflation. If so, it would be an exceptional result: not only it would enlarge the knowledge of primordial physics, but also it would discriminate among different models of Inflation. Obviously, the detection of these potential primordial features is extremely complex, as they are expected to be suppressed at late times, exactly as the Baryon Acoustic Oscillations (BAO) are.

This work is organized as follows.

In Chapter 1 we describe the standard cosmology. After a brief description of the basic notions of cosmology we go through the Hot Big Bang model and its results. Then, starting from the issues that arise from the Big Bang, we present Inflation in its simplest paradigm: slow-roll Inflation.

In Chapter 2 we review the cosmological perturbation theory. In the first part of the chapter we study the effects of perturbing, in the context of General Relativity, the inflaton field and the metric. We also introduce a fundamental tool used in cosmology, the power spectrum, and we study more in detail the cosmic microwave background. In the second part we analyze a very important feature of the universe, which is extremely important for this work: Baryon Acoustic Oscillations. In the third part the Newtonian treatment of perturbations is presented. From the Vlasov equation we derive the Continuity and the Euler equations, both in real and Fourier space. We then give more details of PT results for the Einstein-de Sitter universe and in more general cosmologies. Finally, in the last section, we introduce the Wick theorem, and derive the power spectrum up to first order in PT and the tree-level bispectrum.

In Chapter 3 we approach cosmology from a statistical point of view. In particular, after reviewing some basic statistical concepts, we analyze the Fisher matrix approach and we derive the Cramer-Rao inequality.

In Chapter 4 the large-scale structure consistency relations are derived and a check in perturbation theory is done. In the second section of the chapter we study the behavior of the BAO and understand why they are suppressed at late times.

In Chapter 5 using the consistency relations and the Fisher matrix approach, we forecast different cosmological parameters for a Euclid-like survey. In the first part we make a forecast on the bias parameter defined in the CR derivation. After, we repeat the calculation using suppressed baryon acoustic oscillations. In the second section we introduce the primordial oscillations which may be present in the power spectrum and study how the CR behave in the presence of this type of power spectrum. Finally, in the last section we perform a two-dimensional forecast on the parameters that are present in the power spectrum which exhibits primordial oscillations.

Chapter 1

Standard Cosmology

Cosmology is the study of the universe considered in its entirety. The aim of cosmology is to study the composition, the dynamics, the evolution and, more in general, the properties of the universe. Standard cosmology makes use of some assumptions, summarized in what is called Cosmological Principle, which have to be supported by experimental observations; the result of these assumptions is basically to reduce the number of degrees of freedom of a system in order to build a simpler model of the universe itself. We can state the cosmological principle as follows [12]: "Any comoving observer, at a fixed time in his reference system, at large scales sees the universe homogeneous and isotropic".
Homogeneity is related to what is also called Copernican Principle, and it simply is the fact the there is no privileged point of observation in the universe. Therefore we can say that the quantities that describe the universe must have properties of translational invariance. Isotropy, instead, is the characteristic that, in whatever direction an observer may observe, the universe always looks the same (on scales of order of ~ 100 Mpc) [13].
Already from the Hubble's discovery, see Fig. 1.1, in this past hundred years a lot of evidences of the expansion of the universe have been gathered: the light from distant galaxies is shifted towards the red end of the spectrum, the predictions of the Big Bang Nucleosynthesis are matched with the observed abundances of the light elements (such as H, He and Li) and a relic radiation of a very hot early universe is the only explanation for the presence of the Cosmic Microwave Background.

1.1 FLRW Spacetime

The background metric describing an universe with these properties is the Friedmann-Lemaître-Robertson-Walker metric, that is:

$$ds^2 = -dt^2 + a^2(t)\left[\frac{dr^2}{1-kr^2} + r^2(d\theta^2 + \sin^2\theta d\phi^2)\right]. \tag{1.1}$$

This metric describes a maximally simmetric universe, governed by the scale factor

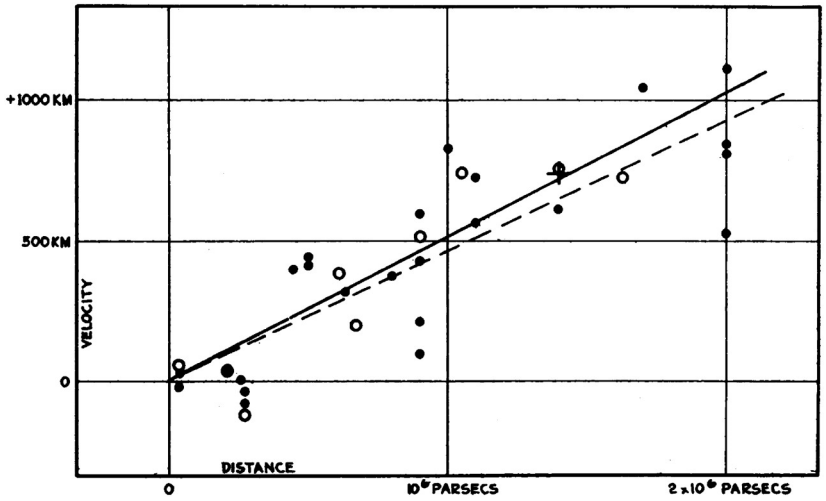

Figure 1.1: The originale graph, taken from [14], that showed the first evidences of a linear relation between the velocity and the distance of a given galaxy, giving a strong support to models that describe an expanding universe.

$a(t)$. It is written in polar coordinates and from a comoving observer point of view, i.e. an observer that is moving along with the source of the geometry of the universe; k is a constant that describes the Gaussian curvature of the space taken into account. By a coordinate transformation the metric (1.1) can be written as:

$$ds^2 = -dt^2 + a(t)^2 \left[d\chi^2 + \Phi_K(\chi^2)(d\theta^2 + \sin^2\theta d\phi^2)\right] \tag{1.2}$$

where

$$r^2 = \Phi_k(\chi^2) \equiv \begin{cases} \sinh^2\chi & k = -1 \\ \chi^2 & k = 0 \\ \sin^2\chi & k = 1 \end{cases} . \tag{1.3}$$

A really important quantity we need to introduce is the Hubble parameter:

$$H \equiv \frac{\dot{a}(t)}{a(t)}, \tag{1.4}$$

with $\dot{} \equiv \frac{\mathrm{d}}{\mathrm{d}t}$. The Hubble parameter is the FLRW spacetime expansion rate and it sets the fundamental scales for the spacetime, that is the characteristic time and lenght of FLRW spacetime ($c = 1$):

$$\begin{aligned} t &\sim H^{-1} \\ d &\sim H^{-1} \end{aligned} \tag{1.5}$$

1.2 Kinematics and Dynamics

Experimental observations constrain the universe to be almost (if not exactly) flat, as we will see in Sec. 1.3.1; for this reason we can assume k to be equal to 0, and consider simply a spatially flat background:

$$ds^2 = -dt^2 + a(t)^2 \left[d\chi^2 + \chi^2(d\theta^2 + \sin^2\theta d\phi^2)\right]. \tag{1.6}$$

We can also rewrite this equation using conformal time τ defined as

$$\tau = \int \frac{dt}{a(t)}, \tag{1.7}$$

obtaining the so called conformal metric:

$$ds^2 = a^2(\tau) \left[-d\tau^2 + d\chi^2 + \chi^2(d\theta^2 + \sin^2\theta d\phi^2)\right]. \tag{1.8}$$

In addition, we can take a brief look at the Einstein field equations. They have the form:

$$G_{\mu\nu} = 8\pi G T_{\mu\nu}, \tag{1.9}$$

where $G_{\mu\nu}$ is the Einstein tensor:

$$G_{\mu\nu} = R_{\mu\nu} - \frac{1}{2} R g_{\mu\nu}, \tag{1.10}$$

and $R_{\mu\nu}$ and R the Ricci tensor and scalar. The energy momentum tensor $T_{\mu\nu}$ represents the source of the geometry of the universe. Assuming an homogeneus and isotropic universe means to require the same for $T_{\mu\nu}$. In the case of a perfect fluid, for example, we obtain [12]:

$$T^{\mu}_{\ \nu} = [\rho(t) + p(t)]\, u^{\mu} u_{\nu} - p(t)\delta^{\mu}_{\ \nu} \tag{1.11}$$

where

$$u^{\mu} = \frac{dx^{\mu}}{d\tau} \tag{1.12}$$

is the four velocity of the fluid, $\rho(t)$ the energy density of the background matter whereas $p(t)$ is the isotropic pressure of the fluid. Let us note that they depend only on time because of the assumptions of homogeneity and isotropy.
Moreover, if we consider an observer comoving with the fluid, we may choose a null spatial velocity, i.e. $u^{\mu} = (1, 0, 0, 0)$, ending up with:

$$\begin{aligned} T_{00} &= \rho(t) \\ T_{0i} &= T_{i0} = 0 \\ T_{ij} &= -p(t)\delta^{i}_{\ j} \end{aligned} \tag{1.13}$$

and sobstituting equations (1.13) into (1.9) we obtain the first two (independent) Friedmann equations:

$$H^2 \equiv \left(\frac{\dot{a}}{a}\right)^2 = \frac{8\pi G}{3}\rho - \frac{k}{a^2}, \tag{1.14}$$

$$\frac{\ddot{a}}{a} = -\frac{4\pi G}{3}\left(\rho + 3p\right), \tag{1.15}$$

From the continuity equation

$$D_\mu T^{\mu\nu} = 0 \tag{1.16}$$

we derive the third Friedmann equation:

$$\dot{\rho} = -3H\left(\rho + p\right). \tag{1.17}$$

The three Friedmann equations are not independent. In fact, while (1.15) defines the dynamic of the system, equations (1.14) and (1.17) are just constraining equations. Thus, we find ourselves with three independent variables ($a(t)$, $p(t)$ and $\rho(t)$) but only two equations. The equation of state (which connects pressure with density) comes to the rescue and, as first good approximation, it may take the following form:

$$p(t) = w\rho(t). \tag{1.18}$$

We can therefore write eq. (1.17) as

$$\frac{\mathrm{d}\log\rho(t)}{\mathrm{d}\log a(t)} = -3(1+w) \tag{1.19}$$

and integrating it we obtain

$$\rho(t) \sim a(t)^{-3(1+w)}, \tag{1.20}$$

which, together with the Friedmann equation (1.14), it gives the evolution of the scale factor along with time:

$$a(t) \sim \begin{cases} t^{\frac{2}{3(1+w)}} & w \neq -1 \\ e^{Ht} & w = -1 \end{cases}. \tag{1.21}$$

The constant w takes different values depending on which kind of matter/energy we are considering. In particular we have $w = 0$ for ordinary **matter**, $w = 1/3$ for **radiation** and $w = -1$ when the universe is dominated by the **cosmological constant**. The solutions for the main variables of a flat ($k = 0$) FLRW universe in different moment of the evolution of the universe are summarized in Tab. 1.1.

	w	$\rho(a)$	$a(t)$	$a(\tau)$
MD	0	a^{-3}	$t^{2/3}$	τ^2
RD	$\frac{1}{3}$	a^{-4}	$t^{1/2}$	τ
Λ	-1	a^0	e^{Ht}	$-\tau^{-1}$

Table 1.1: Solutions of a flat FRW universe dominated by matter (MD), radiation (RD) or a cosmological constant (Λ). Table taken from [15].

1.3 Hot Big Bang

We now want to derive an explicit expression for $a(t), \rho(t), p(t)$. In order to do so, we take into account the equation of state, eq. (1.18), the Friedmann equations and the fact that, for what we have said so far, we can consider the universe flat, i.e. $k = 0$. We start from taking eq. (1.20) and write it in the following way:

$$\rho(t) = \rho_\star \left(\frac{a(t)}{a_\star}\right)^{-3(1+w)}. \tag{1.22}$$

Then, we take the first Friedmann equation, eq. (1.14) and write it in the following way:

$$\dot{a}(t)^2 = \frac{8\pi G}{3}\rho_\star a_\star^{3(1+w)} a^{2-3(1+w)} = A^2 a^{2-3(1+w)} \tag{1.23}$$

which becomes

$$a^{\frac{1+3w}{2}} da = \pm A dt. \tag{1.24}$$

We choose the positive solution and, integrating, we arrive to:

$$a(t) = a_\star \left[1 + \frac{3}{2}(1+w)H_\star(t - t_\star)\right]^{\frac{2}{3(1+w)}} \tag{1.25}$$

with

$$H_\star = \sqrt{\frac{8\pi G}{3}\rho_\star}. \tag{1.26}$$

Now we substitute eq. (1.25) into eq. (1.22), and obtain:

$$\rho(t) = \rho_\star \left[1 + \frac{3}{2}(1+w)H_\star(t - t_\star)\right]^{-2}. \tag{1.27}$$

Finally, since $H(t) = \dot{a}(t)/a(t)$ we also determine the Hubble parameter, that is:

$$H(t) = H_\star \left[1 + \frac{3}{2}(1+w)H_\star(t - t_\star)\right]^{-1}. \tag{1.28}$$

Therefore, looking at the expression of the scale factor, it is clear that at some time t_0 the expression in the square brackets goes to 0. This happens for:

$$t_0 = t_\star - \frac{2}{3}H_\star^{-1}(1+w)^{-1}. \tag{1.29}$$

We rescale the time

$$t \to t - t_0 \tag{1.30}$$

so that, for $t \to 0$, we have:

$$a(t \to 0) \to 0, \quad \rho(t \to 0) \to \infty, \quad H(t \to 0) \to \infty \tag{1.31}$$

This particular situation, which is effectively a singularity, it is usually called *Big Bang* and, because of the high energies involved, we refer to this model as the *Hot Big Bang Model*.

Let us suppose, then, we want to describe the different components of the universe at different times within the Hot Big Bang model. To know the thermal history of the universe means actually to understand its evolution along with time, that is how the scale factor $a(t)$ changes with time and temperature. In order to do so we need to define the thermodynamic quantities which are most important for the Hot Big Bang model. We start defining the particle numerical density

$$n(T,\mu) = \frac{g}{(2\pi)^3}\int f(\mathbf{q},T,\mu)d^3q \tag{1.32}$$

where $\mathbf{q}$ are the moments of the particles, g is the number of helicity state, μ is the chemical potential and $f(\mathbf{q},T,\mu)$ is the distribution function. If we assume to be at the thermodynamic equilibrium, f will just be the statistical distribution of the considered particle species, either fermionic or bosonic:

$$f(\mathbf{q},T,\mu) = \left[e^{\frac{E-\mu}{T}} \mp 1\right]^{-1} \tag{1.33}$$

where $-$ stands for bosons and $+$ for fermions. Note that E is the energy we are considering and it is given by $E = \sqrt{q^2 + m^2}$.

For the energy density we have instead:

$$\rho(T,\mu) = \frac{g}{(2\pi)^3}\int E(\mathbf{q})f(\mathbf{q},T,\mu)d^3q \tag{1.34}$$

whereas the pressure reads:

$$p(T,\mu) = \frac{g}{(2\pi)^3}\int \frac{q^2}{3E(\mathbf{q})} f(\mathbf{q},T,\mu)d^3q. \tag{1.35}$$

Solving these integrals in the relativistic case ($T \gg m$) we find:

$$n(T)\begin{cases} g\frac{\zeta(3)}{pi^2}T^3, & \text{Bosons} \\ \frac{3}{4}g\frac{\zeta(3)}{\pi^2}T^3, & \text{Fermions} \end{cases} \tag{1.36}$$

$$\rho(T)\begin{cases} g\frac{\pi^2}{30}T^4, & \text{Bosons} \\ \frac{7}{8}g\frac{\pi^2}{30}T^4, & \text{Fermions} \end{cases} \tag{1.37}$$

and $p(T) = \frac{1}{3}\rho(T)$ as we would expect for a perfect fluid.
Instead, in the non relativistic case ($T \ll m$) we find that the particle number density is actually suppressed:

$$n(T) \sim e^{-\frac{m}{T}} \tag{1.38}$$

and, since in this limit $\rho(T) = mn(T)$ and $p(T) = n(T)T$ we find the same behavior for the energy density and the pressure.

In Tab. 1.1 we can look at the a-dependence of the energy densities in the different epochs of the universe. In particular it is easy to understand that, during the early universe, the radiation was the dominant component; for this reason when we talk about primordial times we can simply consider an ultra-relativistic fluid. At the beginning the rate of interactions between particles was much greater than the rate of expansion of the Universe $H(t)$ meaning that the fluid was initially in a thermodynamic equilibrium. Considering the conservation of the entropy in an expanding universe one can find the following relation between the temperature and the scale factor [13]:

$$T \sim a^{-1}. \tag{1.39}$$

If we use the definition of cosmic redshift

$$1 + z = \frac{\lambda_o}{\lambda_e} = \frac{a_0}{a_e} = \frac{1}{a_e}, \tag{1.40}$$

where "e" stands for *emitted* and "o" for *observed*, i.e. present, we can easily see that

$$T \sim 1 + z. \tag{1.41}$$

These last equations tell us that the more we go backward, the more the universe becomes *hot*. This is why we can, in some way, describe the evolution of the universe through its thermal history, see Fig. 1.2.

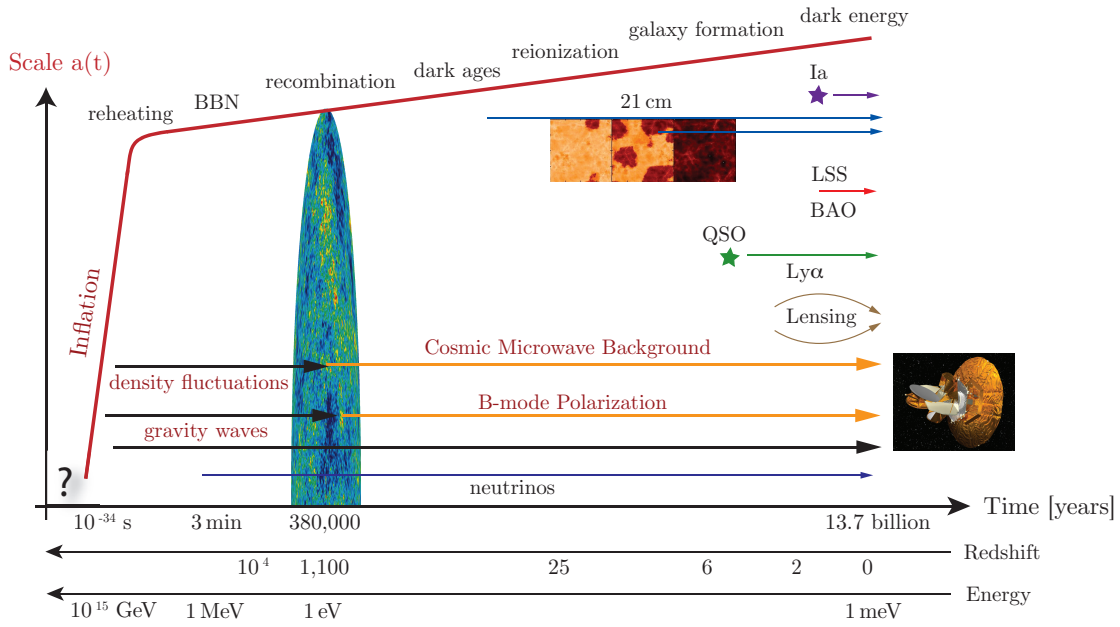

Figure 1.2: A schematic representation of the history of the universe. As we have said, we can relate the time with the redshift and the energy (i.e. the temperature). After a first exponential expansion due to inflation, we step into the Hot Big Bang model, starting from the Big Bang Nucleosynthesis and arriving to the present dark energy era. We also illustrate several cosmological probes that provide us with information about the structure and evolution of the universe, from the inflationary gravitational waves, passing through the CMB and arriving to the Large Scale Structure of the universe. This Figure was taken from [15].

At early epochs all the particle species were in thermal equilibrium. Therefore, for very high energies, we expect a phase where the symmetry between matter and anti-matter was broken. This era is called baryogenesis and, as the name suggests, it was the moment during which the matter we observe today was actually created. This happened thanks to a process of annihilation of baryons and antibaryons, present in the universe with a little initial asymmetry (around $10^9 + 1$ baryons for 10^9 antibaryons).
At very high energies, the weak interaction and the electromagnetic interaction were unified in the electroweak interaction. Then, as the universe expanded, around energies of order ~ 1 Mev, neutrinos ceased to interact with photons, meaning that neutrinos and radiation were not in thermodynamic equilibrium anymore.
At temperature of the order ~ 100 keV, i.e. around ~ 100 s after the Big Bang, the temperature of the radiation was so high that all the nuclear bonds were broken; all the nuclei were decomposed into protons and neutrons. However, as the temperature kept going dow, the universe reached a moment in which the binding nuclear energies were higher than the temperature of the nucleons. This is the moment of the formation of the first fundamental nuclei: this phase is called nucleosynthesis. This phase was described by Gamow [16] and it is a fundamental prediction of the Big Bang theory. It predicts an abundance of ^{4}He which is not justified considering only the elements produced in the stellar nuclear reactions. The observation of an abundance of chem-

ical elements in accordance with the nucleosynthesis prediction is one of the striking successes of the Big Bang theory.
As we have said before, the initial period was dominated by the presence of radiation, from here the name *radiation dominated era*. As the universe expanded, and temperature decreased, the matter became predominant, leading to the *matter dominated era*. During this epoch all the large scale structures that we observe in the universe, such as galaxies and clusters, started to form due to gravitational instability.
After the radiation-matter equivalence, one of the most important event in the universe history took place. When the universe was almost $\sim 10^6$ years old the temperature was higher than the binding energy of the Hydrogen, 13.6 eV, which translated to the fact that the Universe was ionized and therefore opaque to radiation. The photons were not free to stream as they interacted with the electron through Compton scattering. Then, as the temperature lowered below the binding energy of H, the electron could start interacting with the protons through the interaction

$$e^- + p^+ \rightarrow H + \gamma, \tag{1.42}$$

meaning that finally the first Hydrogen atoms were created. At this point the interaction between photons ad electrons stopped to be to dominant one and photons started to be free to travel. This point in time defines what is called *last scattering surface* and this epoch is called Hydrogen recombination. The radiation that left the last scattering surface was then cooled by the expansion of the Universe to the value of ~ 3 K, and now constitutes the Cosmic Microwave Background (CMB) we observe. The CMB is a fundamental prediction of the Big Bang model and it represents a milestone of the history of Cosmology: its discovery [17] opened the way to a more detailed study of the first moments of the Universe.

1.3.1 Constraints From Observations and ΛCDM Model

In this section we will briefly show results of constraints on cosmological parameters. All numerical results, which are given with 68% confidence level, come from the Planck mission [18].
Observations of the cosmic microwave background and the large-scale structure (which we will analyze in more detail in the following sections) show that the universe is flat (Fig. 1.3), i.e.

$$\Omega_k = 0.001 \pm 0.002, \tag{1.43}$$

and it is composed of 5% matter (or baryons), 26% cold dark matter and 69% dark energy (Fig. 1.3), i.e.

$$\Omega_m = 0.0490 \pm 0.0003, \qquad \Omega_{dm} = 0.2607 \pm 0.0020, \qquad \Omega_\Lambda = 0.6889 \pm 0.0056, \tag{1.44}$$

with $w_\Lambda = -1.03 \pm 0.03$.

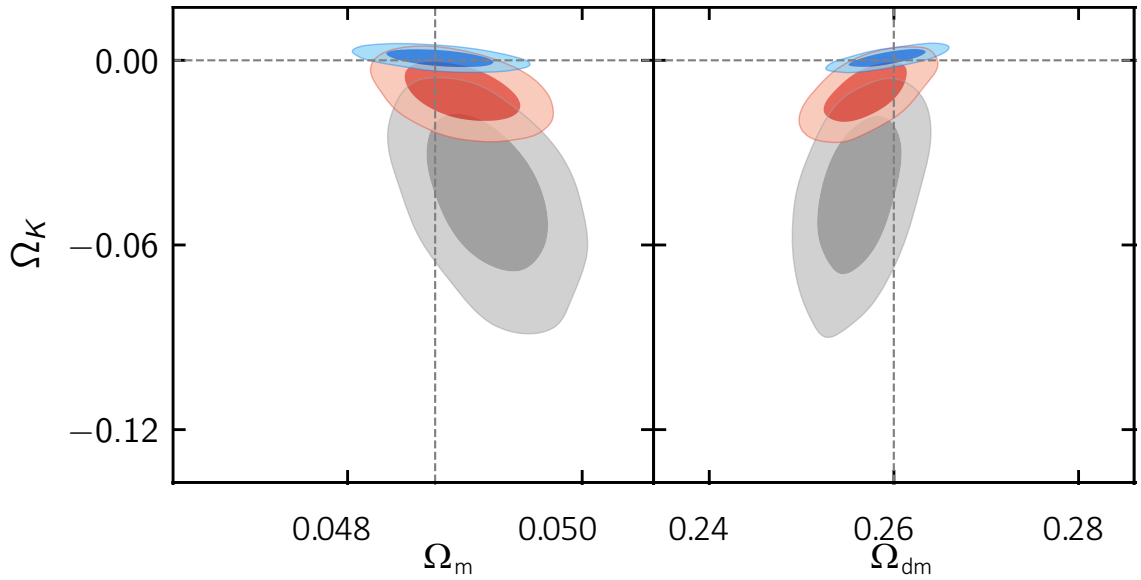

Figure 1.3: Constraints on ΛCDM parameters. Contours show 68% and 95% confidence regions for Planck TT,TE,EE+lowE (grey), Planck TT,TE,EE+lowE+lensing (red), and Planck TT,TE,EE+lowE+lensing+BAO (blue). Vertical lines show the mean posterior values in the base model for Planck TT,TE,EE+lowE+lensing whereas horizontal lines correspond to the parameter values assumed in the ΛCDM model. Figure taken from [18].

As we have explained above, at early times the Universe was dominated by its radiation component, then it passed through a matter-dominated era and, now, the dominant component is the dark energy. Also, we have just mentioned that the spatial curvature of the Universe is compatible with zero: a direct consequence of this measurement is that the actual density of the Universe is almost the critical one. The basic model which describes the cosmic evolution is the so-called ΛCDM model, partially summarized by eq. (1.44), that is dark energy (which is also responsable for the acceleration of the expansion of the universe) composes the 69% of the universe, dark matter 26% and baryons 5%. Note that we talk about *Cold* Dark Matter. Cold means that dark matter was non-relativistic at the time of decoupling: if the dark matter was hot, i.e. relativistic at the time of its decoupling, it would have had important consequences on the formation of the large scale structure of the Universe [19]. Furthermore, it is called dark because it does not emit light and we can measure its presence only by indirect observations (e.g. galaxies rotation curves, large scale structure measurements, CMB). The baryonic matter (galaxies, stars, planets and so on) is only a little percentage of the total composition of the Universe, meaning that the Universe we live in is almost dark. In Fig. 1.4 it is possible to see all the six fundamental parameters (the first six of the list) of the ΛCDM model. A striking characteristic of this model is that it describes the history of the universe just using 6 parameters. Although many of the ingredients of the model remain mysterious from a fundamental physics point of view, the ΛCDM model is one of the most successful phenomenological models in physics.

Parameter	TT+lowE 68% limits	TE+lowE 68% limits	EE+lowE 68% limits	TT,TE,EE+lowE 68% limits	TT,TE,EE+lowE+lensing 68% limits	TT,TE,EE+lowE+lensing+BAO 68% limits
$\Omega_b h^2$	0.02212 ± 0.00022	0.02249 ± 0.00025	0.0240 ± 0.0012	0.02236 ± 0.00015	0.02237 ± 0.00015	0.02242 ± 0.00014
$\Omega_c h^2$	0.1206 ± 0.0021	0.1177 ± 0.0020	0.1158 ± 0.0046	0.1202 ± 0.0014	0.1200 ± 0.0012	0.11933 ± 0.00091
$100\theta_{MC}$	1.04077 ± 0.00047	1.04139 ± 0.00049	1.03999 ± 0.00089	1.04090 ± 0.00031	1.04092 ± 0.00031	1.04101 ± 0.00029
τ	0.0522 ± 0.0080	0.0496 ± 0.0085	0.0527 ± 0.0090	$0.0544^{+0.0070}_{-0.0081}$	0.0544 ± 0.0073	0.0561 ± 0.0071
$\ln(10^{10} A_s)$	3.040 ± 0.016	$3.018^{+0.020}_{-0.018}$	3.052 ± 0.022	3.045 ± 0.016	3.044 ± 0.014	3.047 ± 0.014
n_s	0.9626 ± 0.0057	0.967 ± 0.011	0.980 ± 0.015	0.9649 ± 0.0044	0.9649 ± 0.0042	0.9665 ± 0.0038
H_0 [km s^{-1} Mpc^{-1}]	66.88 ± 0.92	68.44 ± 0.91	69.9 ± 2.7	67.27 ± 0.60	67.36 ± 0.54	67.66 ± 0.42
Ω_Λ	0.679 ± 0.013	0.699 ± 0.012	$0.711^{+0.033}_{-0.026}$	0.6834 ± 0.0084	0.6847 ± 0.0073	0.6889 ± 0.0056
Ω_m	0.321 ± 0.013	0.301 ± 0.012	$0.289^{+0.026}_{-0.033}$	0.3166 ± 0.0084	0.3153 ± 0.0073	0.3111 ± 0.0056
$\Omega_m h^2$	0.1434 ± 0.0020	0.1408 ± 0.0019	$0.1404^{+0.0034}_{-0.0039}$	0.1432 ± 0.0013	0.1430 ± 0.0011	0.14240 ± 0.00087
$\Omega_m h^3$	0.09589 ± 0.00046	0.09635 ± 0.00051	$0.0981^{+0.0016}_{-0.0018}$	0.09633 ± 0.00029	0.09633 ± 0.00030	0.09635 ± 0.00030
σ_8	0.8118 ± 0.0089	0.793 ± 0.011	0.796 ± 0.018	0.8120 ± 0.0073	0.8111 ± 0.0060	0.8102 ± 0.0060
$S_8 \equiv \sigma_8 (\Omega_m/0.3)^{0.5}$	0.840 ± 0.024	0.794 ± 0.024	$0.781^{+0.052}_{-0.060}$	0.834 ± 0.016	0.832 ± 0.013	0.825 ± 0.011
$\sigma_8 \Omega_m^{0.25}$	0.611 ± 0.012	0.587 ± 0.012	0.583 ± 0.027	0.6090 ± 0.0081	0.6078 ± 0.0064	0.6051 ± 0.0058
z_{re}	7.50 ± 0.82	$7.11^{+0.91}_{-0.75}$	$7.10^{+0.87}_{-0.73}$	7.68 ± 0.79	7.67 ± 0.73	7.82 ± 0.71
$10^9 A_s$	2.092 ± 0.034	2.045 ± 0.041	2.116 ± 0.047	$2.101^{+0.031}_{-0.034}$	2.100 ± 0.030	2.105 ± 0.030
$10^9 A_s e^{-2\tau}$	1.884 ± 0.014	1.851 ± 0.018	1.904 ± 0.024	1.884 ± 0.012	1.883 ± 0.011	1.881 ± 0.010
Age [Gyr]	13.830 ± 0.037	13.761 ± 0.038	$13.64^{+0.16}_{-0.14}$	13.800 ± 0.024	13.797 ± 0.023	13.787 ± 0.020
z_*	1090.30 ± 0.41	1089.57 ± 0.42	$1087.8^{+1.6}_{-1.7}$	1089.95 ± 0.27	1089.92 ± 0.25	1089.80 ± 0.21
r_* [Mpc]	144.46 ± 0.48	144.95 ± 0.48	144.29 ± 0.64	144.39 ± 0.30	144.43 ± 0.26	144.57 ± 0.22
$100\theta_*$	1.04097 ± 0.00046	1.04156 ± 0.00049	1.04001 ± 0.00086	1.04109 ± 0.00030	1.04110 ± 0.00031	1.04119 ± 0.00029
z_{drag}	1059.39 ± 0.46	1060.03 ± 0.54	1063.2 ± 2.4	1059.93 ± 0.30	1059.94 ± 0.30	1060.01 ± 0.29
r_{drag} [Mpc]	147.21 ± 0.48	147.59 ± 0.49	146.46 ± 0.70	147.05 ± 0.30	147.09 ± 0.26	147.21 ± 0.23
k_D [Mpc^{-1}]	0.14054 ± 0.00052	0.14043 ± 0.00057	0.1426 ± 0.0012	0.14090 ± 0.00032	0.14087 ± 0.00030	0.14078 ± 0.00028
z_{eq}	3411 ± 48	3349 ± 46	3340^{+81}_{-92}	3407 ± 31	3402 ± 26	3387 ± 21
k_{eq} [Mpc^{-1}]	0.01041 ± 0.00014	0.01022 ± 0.00014	$0.01019^{+0.00025}_{-0.00028}$	0.010398 ± 0.000094	0.010384 ± 0.000081	0.010339 ± 0.000063
$100\theta_{s,eq}$	0.4483 ± 0.0046	0.4547 ± 0.0045	0.4562 ± 0.0092	0.4490 ± 0.0030	0.4494 ± 0.0026	0.4509 ± 0.0020
f_{2000}^{143}	31.2 ± 3.0			29.5 ± 2.7	29.6 ± 2.8	29.4 ± 2.7
$f_{2000}^{143\times217}$	33.6 ± 2.0			32.2 ± 1.9	32.3 ± 1.9	32.1 ± 1.9
f_{2000}^{217}	108.2 ± 1.9			107.0 ± 1.8	107.1 ± 1.8	106.9 ± 1.8

Figure 1.4: All the fundamental parameters of the ΛCDM model as measured by the Planck mission. Figure taken from [18].

1.3.2 Issues of the Hot Big Bang Model and Inflationary Solution

As we have discussed, there are some fundamental predictions of the Big Bang (such as nucleosynthesis or the Cosmic Microwave Background) which are definitely great outcomes of the therory, confirmed by experimental results, which give strong support to the theory.
However, in the context of the model, some problematic issues arise: we will see that they are linked to the problem of the initial conditions of the universe.

To approach these issues, we first need to understand two important concepts: the Particle Horizon and the Hubble Horizon.

Particle Horizon If we set $ds^2 = 0$ in equation (1.1) we obtain the distance that light travels between two points of spacetime, namely:

$$0 = -dt^2 + a^2(t)\left[\frac{dr^2}{1-kr^2} + r^2 d\Omega\right] := -dt^2 + dl^2. \tag{1.45}$$

where we have used $d\Omega = d\theta^2 + \sin^2\theta d\phi$. We then define the comoving distance as:

$$d(t) = \int_0^{l(t)} dl'. \tag{1.46}$$

Exploiting the property of isotropy we can set $d\Omega = 0$, obtaining:

$$d(t) = \int_0^{r(t)} \frac{dr}{\sqrt{1-kr}} = \int_0^t \frac{dt'}{a(t')}. \tag{1.47}$$

The particle horizon, which is the physical distance traveled by light, is then:

$$d_H = a(t)\int_0^t \frac{dt'}{a(t')}. \tag{1.48}$$

Physically speaking, $d_H(t)$ defines the radius of a sphere, centered in the observer, that contains all the points of the spacetime that entered in causal connection with the observer within the time t. In particular this means that, if two points are further apart than $d_H(t)$, they never entered in causal connection with each other. In order to obtain the particle horizon we used the following relation that connects physical and comoving distances:

$$\lambda_{phys} = a(t)\lambda_{com} \tag{1.49}$$

Let us also note that, from the explicit form of a(t), eq. (1.25), and exploiting the second Friedmann equation, we obtain that $d_H(t)$ exists if $\ddot{a(t)} < 0$ (a decelerating universe) and its explicit form is:

$$d_H(t) = \frac{3(1+w)}{3w+1}. \tag{1.50}$$

Hubble horizon Since H is an expanding rate, we can define the Hubble time $\tau_H \equiv \frac{1}{H}$ as the characteristic time of expansion of the universe. Hence the Hubble radius is:

$$R_H(t) = c\tau_H. \tag{1.51}$$

The comoving Hubble radius is then:

$$r_H(t) = \frac{R_H(t)}{a(t)} = \frac{1}{\dot{a}(t)} \tag{1.52}$$

Also in this case, thinking of the region standing inside the sphere of radius r_H, we can define a comoving Hubble horizon. Let us point out that there is a substantial

difference between the Particle and the Hubble Horizon; in fact, the Particle Horizon takes into account the entire past history up to time t, whereas the Hubble Horizon considers only the interactions happened in a Hubble time H^{-1}.

We can now go through the issues that arise in the context of the Hot Big Bang model, and see how they are solved by what is called the inflationary model.
The first is the so called **horizon problem**. A portion of the universe, with characteristic length λ, can be all causal connected only if $\lambda < r_H$, that is the comoving Hubble horizon has to be greater than the characteristic length λ. We can think of this saying that, up to a certain time t_H a certain region will not be causally connected. When at time t_H we have that $\lambda = r_H$, then the region of length λ gets causally connected. According to this reasoning, there are some portions of the universe which entered in causal connection only recently (since the universe is expanding); however, from the CMB observation, this is not what we see. We do see, indeed, homogeneity and isotropy on the entire scale of the visible universe. How can this be possible if these regions never talked to each other?
The inflationary solution, in some sense, is actually fairly easy: we can just think that, in a moment previous to the radiation dominated epoch, it happened that $\dot{r_H}(t) < 0$, meaning that there is a period in which $r_H(t)$ decreased, as it is illustrated in Fig. 1.5.

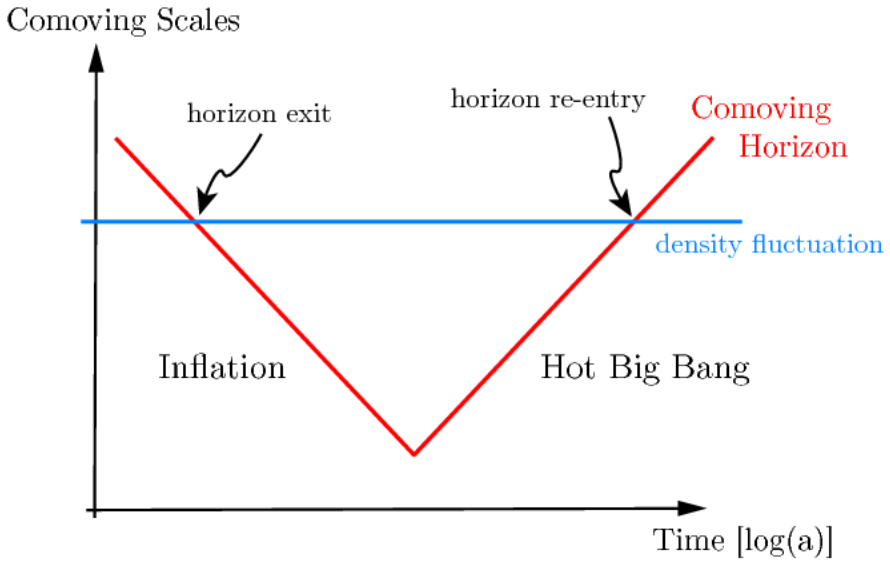

Figure 1.5: The comoving length of the region considered remains constant during the cosmological evolution. At a certain time it exits the horizon, while inflation occurs. Then it re-enters the horizon at later times. Figure from [15].

In this way regions entering for the first time in causal connection actually had a chance to exchange information in the very early period of the universe. In more quantitative terms we are saying:

$$\frac{d}{dt}r_H(t) < 0 \iff -\frac{\ddot{a}(t)}{(a(t))^2} < 0 \iff \ddot{a}(t) > 0. \tag{1.53}$$

Hence, in full generality, we will talk about inflationary solution when we have an accelerated expansion of the universe.
We have, though, also to impose a condition on the duration of the inflationary period, since we need that at least what we observe today has entered in causal connection during the inflationary period. Thus, we require:

$$r_H(t_i) \geq r_H(t_0). \tag{1.54}$$

Let us also note that, from eq. (1.15), in order to have $\ddot{a}(t) > 0$ we obtain $\rho + 3p > 0$, implying:

$$w < -\frac{1}{3}, \tag{1.55}$$

that is, negative pressure. One particular condition that is compatible with this condition is when $w = -1$. We are in this case saying (from eq. (1.17)):

$$\dot{\rho} = 0 \implies \rho = const. \tag{1.56}$$

namely, the density of this "exotic fluid" remains constant throughout the evolution of the universe (cosmological constant). Assuming $\rho = const$, from eq. (1.14), we also get that:

$$a(t) \propto e^{Ht}, \tag{1.57}$$

that is an exponential growth of the scale factor. This solution is also called De Sitter universe.

We want now to address the second issue of the Hot Big Bang model: **the flatness problem**. From the Friedmann equations we define the critical density as the density needed in order to have zero curvature:

$$\rho_c = \frac{3H^2}{8\pi G}. \tag{1.58}$$

Recalling the definition of the density parameter

$$\Omega = \frac{\rho}{\rho_c}, \tag{1.59}$$

from the first Friedmann equation we obtain:

$$\Omega(t) - 1 = \frac{k}{a^2H^2} = kr_H^2(t) \tag{1.60}$$

This equation gives us the evolution of the density parameter in FLRW models. In particular in these models the value of $r_H(t)$ grows with time. So, if the Universe is perfectly flat $k = 0$ and $\Omega = 1$ but, if $\Omega \neq 1$, then the difference between Ω and 1 will grow as fast as r_H does. This means that going backward in time we expect Ω to get closer and closer to 1. From the Plank mission Ω takes the value [18]:

$$|\Omega_0 - 1| = 0.0007 \pm 0.0019 \tag{1.61}$$

and taking as a reference time the Planck time $t_{Pl} = 10^{-44}$ we find that:

$$|\Omega(t_{Pl}) - 1| \leq 10^{-62}. \tag{1.62}$$

Basically we are saying that, in order to explain what we observe today, we must require that the spatial curvature of the universe at the beginning was significantly close to 1 (1 part over 10^{62}) but not exactly 1. To require such an exact initial condition seems very unnatural; this problem goes under the name of fine tuning problem.

Again, also in this case the problem is solved allowing r_H to decrease. In fact, from eq. (1.60), if r_H decreases, than also $|\Omega(t) - 1|$ decreases:

$$|\Omega(t) - 1| \propto r_H^2(t) = \frac{1}{a^2 H^2} \tag{1.63}$$

but if H is constant we have seen that $a(t) \propto e^{Ht}$, thus:

$$|\Omega(t) - 1| \propto e^{-Ht}. \tag{1.64}$$

It is an interesting approach, because no matter what deviation we have at the beginning, the inflation suppresses exponentially the deviation of Ω from 1: we say that inflation is an attractor solution.

The last issue of the Hot Big Bang model we briefly address is the so called **unwanted relics problem**. It is known that at very high temperature in the early universe, some very massive particles X may have been created. If created, these particle could have survived up to today, contributing with an $\Omega_{0X} \gg 1$, which is not what we observe today. Some examples of what are also called topological defects are magentic monopoles, cosmic strings, domain walls, textures and so on. The number density of these cosmic relics has the behavior $n_X \sim a^{-3}$. If we have a primordial era in which the expansion was exponential (or very close to be so) we have that $n_X \sim e^{-3Ht}$; therefore we have a mechanism that can explain the suppression of the cosmological relics [20].

1.4 Inflation

The strength of inflation is that it is a mechanism that solves the above-mentioned problems, providing in a dynamical way initial conditions in agreement with observations; hence, we do not have to assume some very precise and peculiar conditions of homogeneity and isotropy at the beginning of the universe.
In particular now we want to ask ourselves what allows the fact that $p < -\frac{1}{3}\rho$, eq. (1.55), and we will see that the answer is: a scalar field ϕ. How does a scalar field evolve in an expanding universe? Let us remind the fact that a De-Sitter expansion can be achieved in the presence of a cosmological constant Λ. The Einstein's equations with the cosmological constant are:

$$R_{\mu\nu} - \frac{1}{2}g_{\mu\nu} = 8\pi G T_{\mu\nu} - \Lambda g_{\mu\nu}. \tag{1.65}$$

We can write the right hand side as:

$$8\pi G T_{\mu\nu} - \Lambda g_{\mu\nu} = 8\pi G \left(T_{\mu\nu} - \frac{\Lambda}{8\pi G} g_{\mu\nu} \right) \tag{1.66}$$

and define $T^{\Lambda}_{\mu\nu} = -\frac{\Lambda}{8\pi G} g_{\mu\nu}$. If now we recall eq. (1.11), we can define $p_\Lambda = -\frac{\Lambda}{8\pi G} g_{\mu\nu}$ and $\rho_\Lambda = \frac{\Lambda}{8\pi G} g_{\mu\nu}$, which gives back exactly $T^{\Lambda}_{\mu\nu}$. Usually Λ gets the interpretation of the vacuum energy of the quantum state of the system, i.e.:

$$\langle 0 | \, T_{\mu\nu} \, | 0 \rangle = - \langle 0 | \, \rho \, | 0 \rangle \, g_{\mu\nu} \implies \Lambda = \langle 0 | \, \rho \, | 0 \rangle \, 8\pi G. \tag{1.67}$$

The vacuum describes the creation and annihilation of virtual particles with an associated energy. Why do we associate the behavior of a scalar field with the cosmological constant? Let us make an example. We can take the stress-energy tensor of a scalar field (which we derive in the next section):

$$T^{\phi}_{\mu\nu} = \partial_\mu \phi \partial_\nu \phi - g_{\mu\nu} \left(-\frac{1}{2} g^{\rho\sigma} \partial_\rho \phi \partial_\sigma \phi - V(\phi) \right)$$

and take the minimum of the potential of ϕ, which we may indicate as follows:

$$\langle \phi \rangle \equiv \langle 0 | \, \phi \, | 0 \rangle \, . \tag{1.68}$$

Now if we assume that $\langle \phi \rangle = const$ it follows that $\partial \langle \phi \rangle = 0$, and therefore we can compute the stress-energy tensor around the minimum of the scalar field potential, and obtain:

$$T^{\phi}_{\mu\nu}(\langle \phi \rangle) = -V(\langle \phi \rangle) g_{\mu\nu}. \tag{1.69}$$

Comparing eq. (1.67) to eq. (1.69) we clearly see that, in both cases, we have that

$$T_{\mu\nu} = const \cdot g_{\mu\nu} \tag{1.70}$$

and we can thus say that the scalar field ϕ mimics the cosmological constant behavior.

With that being said, we will now address the description of the dynamics of the so called standard slow-roll model of inflation: we will see the primordial (quantum) perturbations of the inflaton (the scalar field ϕ) and the perturbations of the metric tensor.

1.4.1 Slow-Roll Inflation

In the slow-roll paradigm we consider a very simple field description: only General Relativity and a scalar field (minimally coupled to gravity) are involved. The action we take into account is [12]:

$$S = \frac{M_{Pl}^2}{2}\int dx^4\sqrt{-g}R + \int dx^4\sqrt{-g}\mathcal{L}_\phi\left[\phi, g_{\mu\nu}\right] + S_M. \tag{1.71}$$

While the first term is the classic Hilbert-Einstein action, the second term contains the dependence on the scalar field ϕ through the presence of the Lagrangian $\mathcal{L}_\phi$; moreover S_M represents the action of other fields (gauge bosons, fermionic fields and so on) and their possible interactions with the scalar field. The lagrangian takes the form:

$$\mathcal{L}_\phi = -\frac{1}{2}g^{\mu\nu}\partial_\mu\phi\partial_\nu\phi - V(\phi). \tag{1.72}$$

$V(\phi)$ is the potential term, and it includes the mass term and self interaction terms. From General Relativity we know we can build a symmetric stress-energy tensor associated to the scalar field:

$$T_{\mu\nu} \equiv -\frac{2}{\sqrt{-g}}\frac{\delta\sqrt{-g}\mathcal{L}}{\delta g^{\mu\nu}} \tag{1.73}$$

In the case of a minimally coupled scalar field, after some calculations, we obtain [21]:

$$T^\phi_{\mu\nu} = \partial_\mu\phi\partial_\nu\phi - g_{\mu\nu}\left(-\frac{1}{2}g^{\rho\sigma}\partial_\rho\phi\partial_\sigma\phi - V(\phi)\right). \tag{1.74}$$

Because of homogeneity and isotropy, regarding the metric tensor, we can assume invariance under spatial traslations and rotations, that is $g_{\mu\nu} = g_{\mu\nu}(t)$. In the same manner, the background value ϕ_0 depends only on time. We can then proceed in writing the scalar field and the metric tensor as a sum of a background value and a perturbation term:

$$\phi(\mathbf{x}, t) = \phi_0(t) + \delta\phi(\mathbf{x}, t) \tag{1.75}$$

$$g_{\mu\nu}(\mathbf{x}, t) = g^{(0)}_{\mu\nu}(t) + \delta g_{\mu\nu}(\mathbf{x}, t). \tag{1.76}$$

Note that this is a good approximation if the perturbation is much smaller than the background value, e.g. $\langle\delta\phi^2\rangle \ll \phi_0^2(t)$, and in general it seems to be the case since experimentally we observe temperature anisotropies in the CMB of the order of $\Delta T/T \sim 10^{-5}$.

1.4.2 Background Dynamics and Slow-Roll Conditions

In order to understand the inflationary models we will need to study the quantum perturbations. But as a first step we will go through the background dynamics, which describes the accelerated expansion during the inflationary period. To describe the background metric we will make use, in the following, of the FLRW metric with null spatial curvature, namely equation (1.6). The scalar field has the same properties of homogeneity and isotropy, so its stress-energy tensor is:

$$T^{\phi}_{00} = \rho_{\phi_0}, \tag{1.77}$$

$$T^{\phi}_{ij} = \rho_{\phi_0} g_{ij}. \tag{1.78}$$

Therefore, comparing these last two equation with (1.74) we obtain:

$$\rho_{\phi_0} = \frac{1}{2}\dot{\phi}_0^2 + V(\phi_0) \tag{1.79}$$

$$p_{\phi_0} = \frac{1}{2}\dot{\phi}_0^2 - V(\phi_0) \tag{1.80}$$

The remarkable fact is that it is possible to realize the inflationary epoch, that is to have negative pressure (see eq. (1.55)) thanks to the presence of the -V term in eq. (1.80). The condition (1.55) translates into:

$$V > \dot{\phi}_0^2 \tag{1.81}$$

Then, if we consider the kinetic term negligible with respect to the potential one

$$\frac{1}{2}\dot{\phi}_0^2 \ll V \tag{1.82}$$

from equations (1.77) and (1.78) we obtain:

$$p_{\phi_0} \simeq -\rho_{\phi_0}. \tag{1.83}$$

Equation (1.83) represents a quasi-De Sitter universe with accelerated and (nearly) exponential expansion $a(t) \simeq a_0 e^{Ht}$. Let us look better into eq. (1.82). This condition is telling us that the field is moving very slowly with respect to the potential: this condition is called slow-roll of the scalar field. Substituting eq. (1.82) into (1.15) we learn that, in this case, we have an alomst flat potential for the entire duration of inflation:

$$H^2 = \frac{8}{3}\pi G \rho_\phi \simeq \frac{8}{3}\pi G V(\phi) \simeq const \tag{1.84}$$

where the last equality holds for a quasi-De Sitter universe.

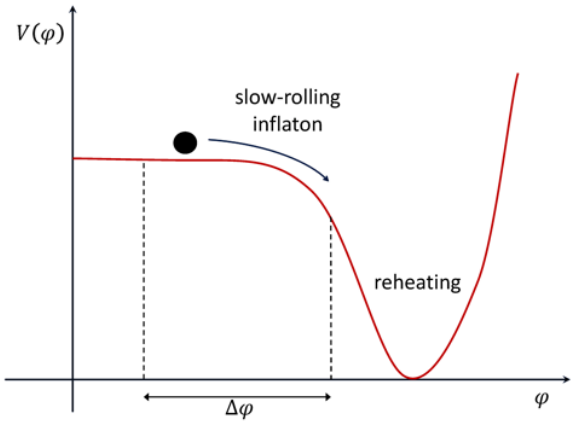

Figure 1.6: This in an example of an inflationary potential with a flat region. After the slow-roll of the field ends, a new phase starts, the so called reheating phase. Figure taken from [21].

Let us take a look to the evolution of the background of the scalar field. In general the equation of motion for a scalar field with a potential term is described by the Klein-Gordon equation:

$$\Box\phi = \frac{\partial V}{\partial \phi} \tag{1.85}$$

where the box operator is defined as [22]:

$$\Box\phi = \frac{1}{\sqrt{-g}}\partial_\mu\left(\sqrt{-g}g^{\mu\nu}\partial_\nu\phi\right). \tag{1.86}$$

We thus obtain the equation of motion for ϕ_0:

$$\ddot{\phi}_0 + 3\frac{\dot{a}}{a}\dot{\phi}_0 = -\frac{\partial V}{\partial \phi}. \tag{1.87}$$

Note that the second term in eq. (1.87) represents a sort of friction term and it is the real difference between the Minkowski and FRW metric.

Let us now define some important model-independent parameters that are useful to describe different models of inflation. We have already seen the condition expressed in eq. (1.82) and, from eq. (1.84), we also note that it is extremely important to have a potential that is *almost* constant; only in this way inflation will have an end. The variation of a generic quantity g in an expanding universe with scale factor $a(t)$ can be estimated by the parameter

$$\epsilon_g = \frac{\mathrm{d}\log g}{\mathrm{d}\log a} = \frac{\dot{g}}{Hg} \tag{1.88}$$

which gives a measure of the variation of g with respect to the expansion of the universe.

Thus, it is possible to make the same exact definition for the Hubble parameter, obtaining:

$$\epsilon = -\frac{\dot{H}}{H^2}, \tag{1.89}$$

being ϵ the **first slow-roll parameter**. Let us note that:

$$\dot{H} = \frac{\ddot{a}}{a} - \left(\frac{\dot{a}}{a}\right)^2 = \frac{\ddot{a}}{a} - H^2$$

therefore

$$\ddot{a} = aH^2\left(1 + \frac{\dot{H}}{H^2}\right).$$

Since, in the case of an accelerated expansion, we have $\ddot{a} > 0$, then

$$-\frac{\dot{H}}{H^2} < 1.$$

The physical meaning is that the Hubble parameter must vary slower than its squared valued and, for a quasi-De Sitter universe we actually require that

$$-\frac{\dot{H}}{H^2} \ll 1$$

i.e.

$$\epsilon \ll 1. \tag{1.90}$$

This condition has been found without any constraint on the theory of inflation, nor on the potential. Actually the condition (1.90) can be translated into the potential of the scalar field using the Friedmann equations. In fact deriving w.r.t. time equation (1.14), using eq. (1.79) and (1.87) we see that the condition $\epsilon \ll 1$ corresponds to $\frac{1}{2}\dot{\phi}_0^2 \ll V$.

The other important topic we need to address is the duration of inflation. In order to solve the horizon and the flatness problem, it can be shown that the number of e-folds N must be around $N \sim 60 - 70$ [13]. Furthermore, the Hubble parameter must, during this period, remains almost constant. This is equivalent to ask that ϵ varies vary slowly. Let us define $dN = d\ln a = Hdt$, then we can define the **second slow-roll parameter** we are looking for as:

$$\eta \equiv \frac{\mathrm{d}ln\epsilon}{\mathrm{d}N} = \frac{\dot{\epsilon}}{H\epsilon} \tag{1.91}$$

asking again that it holds:

$$\eta \ll 1. \tag{1.92}$$

This condition corresponds to [22]

$$\ddot{\phi} \ll 3H\dot{\phi}. \tag{1.93}$$

We can furthermore introduce two more parameters, ϵ_V and η_V, which take into account also the form of the potential:

$$\epsilon_V = \frac{M_{Pl}^2}{2}\left(\frac{V'}{V}\right)^2, \tag{1.94}$$

$$\eta_V = M_{Pl}^2\frac{V''}{V}, \tag{1.95}$$

where M_{Pl} is the Planck mass. This last condition can be rewritten as

$$\eta_V = \frac{1}{3}\frac{V''}{H^2} \tag{1.96}$$

where $V' \equiv \frac{\partial V}{\partial \phi}$.
Let us note that, in the slow-roll approximation, it is easy to demonstrate that

$$\begin{aligned} \epsilon &\simeq \epsilon_V, \\ \eta &\simeq \eta_V - \epsilon_V. \end{aligned} \tag{1.97}$$

So far we do not have measurements of the slow-roll parameters; however, through the Planck measurements, we are able to set bounds on their value [18]:

$$\epsilon_V < 0.0097, \tag{1.98}$$

$$\eta_V = -0.010^{+0.0078}_{-0.0072}. \tag{1.99}$$

1.4.3 Reheating Phase

Surely inflation cannot proceed forever as it has to stop at some time. The great successes of the Hot Big Bang model (such as primordial nucleosynthesis and the origin of the CMB) require a mechanism that allows the transition from the inflationary period to the standard FLRW universe dominated first by radiation and then by matter. This process is called reheating. Since the condition we asked to have inflation is $\epsilon, |\eta| \ll 1$, when $\epsilon, |\eta| \to 1$ the potential that drives inflation is not flat as it was before, and inflation can come to an end. Let us take a simple example. If the potential is of the form given in Fig. (1.6), then, expanding the potential around its minimum at the point σ, we see that the scalar field acquires a mass and starts oscillating

$$V'(\phi) \simeq V'(\sigma) + V''(\sigma)\phi = 0, \tag{1.100}$$

with $V'(\sigma) = 0$.

The equation of motion for the scalar field becomes

$$\ddot{\phi} + 3H\dot{\phi} + V''(\sigma) = 0. \tag{1.101}$$

This is the standard evolution equation for an oscillating field in an expanding universe. In this example one possible mechanism of reheating is that, while oscillating, the fields starts decaying into light and relativistic particles, giving rise to the radiation dominated epoch. To take into account this effect we add a new term in the equation of motion:

$$\ddot{\phi} + (3H + \Gamma_\phi)\,\dot{\phi} + V'(\phi) = 0 \tag{1.102}$$

where Γ_ϕ stands for the decay rate of the inflaton. We can rearrange this expression and obtain [20]

$$\dot{\rho}_\phi + (3H + \Gamma_\phi)\,\rho_\phi = 0. \tag{1.103}$$

Chapter 2

Cosmological Perturbation Theory

2.1 Cosmic Microwave Background and Cosmological Perturbations

In the previous chapter we have illustrated a universe described by the FLRW metric, eq. (1.1). This metric, however, holds only as a first approximation, as we do see inhomogeneities both in the CMB and in the matter distribution of the present universe. One of the most powerful predictions of models of inflation is the production of perturbations due to quantum oscillations of the scalar field around the background value. Therefore we are now interested to see what happens, in the context of General Relativity, in perturbing the scalar field and the metric.

2.1.1 Quantum Fluctuations During Inflation

From the Einstein equations we know that to perturb the metric tensor means also to perturbe the stress-energy tensor and vice versa. This is why, besides the perturbation of the scalar field, we are interested in the perturbation of the metric. Let us point out the fact that we are assuming the universe isotropic and homogeneous in a FLRW spacetime. This means that the scalar field and the metric tensor can be decomposed into a homogeneous background and inhomogeneous perturbation. Hence, we can write:

$$T(t, \mathbf{x}) = T_0(t) + \delta T(t, \mathbf{x}). \tag{2.1}$$

We may also want to expand the perturbation as a power series in the following way:

$$\delta T(t, \mathbf{x}) = \sum_{n=1}^{\infty} \frac{\lambda^n}{n!} \delta T_n(t, \mathbf{x}), \tag{2.2}$$

where we introduced the small parameter λ and the subscript n that indicates the order of the perturbation.

Since the perturbations are small, namely $|\delta T| \ll |T_0|$, expanding the Einstein equations at linear order in perturbations is already a good approximation of the full non-linear solution:

$$\delta G_{\mu\nu} = 8\pi G \delta T_{\mu\nu}. \tag{2.3}$$

Metric Perturbations We will start by perturbing the left hand side of equation (2.3), and we are interested in what happens to the metric. We can perturbe the metric (FRW) using the following decomposition (note that we are using conformal time τ) [15]:

$$g_{00} = -a^2(\tau)\left[1 + 2\Psi(\tau, \mathbf{x})\right] = -a^2(\tau)\left[1 + 2\sum_{r=1}^{\infty} \Psi^{(r)}(\tau, \mathbf{x})\right], \tag{2.4}$$

$$g_{0i} = g_{i0} = a^2(\tau)\omega_i(\tau, \mathbf{x}) = a^2(\tau)\sum_{r=1}^{\infty} \frac{\omega_i^{(r)}(\tau, \mathbf{x})}{r!}, \tag{2.5}$$

$$\begin{aligned} g_{ij} &= a^2(\tau)\left[(1 - 2\Psi(\tau, \mathbf{x}))\delta_{ij} + h_{ij}(\tau, \mathbf{x})\right] \\ &= a^2(\tau)\left\{\left[1 - 2\sum_{r=1}^{\infty} \frac{\Phi_i^{(r)}(\tau, \mathbf{x})}{r!}\right]\delta_{ij} + \sum_{r=1}^{\infty} \frac{h_{ij}^{(r)}(\tau, \mathbf{x})}{r!}\right\} \end{aligned} \tag{2.6}$$

The functions $\Psi^{(r)}$, $\omega^{(r)}$, $\Phi^{(r)}$ and $h_{ij}^{(r)}$ are the rth-order perturbations of the metric; $h_{ij}^{(r)}$ is a transverse and traceless tensor:

$$\partial^i h_{ij} = 0, \tag{2.7}$$

$$h_i^i = 0. \tag{2.8}$$

We will consider, from now on, only the linear case, that is $r = 1$. We can decompose the metric and the stress-energy perturbations into independent scalar, vector and tensor degrees of freedom, i.e. into objects that have well-defined transformations under spatial rotations [15]. This is useful because, at the linear order, the dynamics of the different degrees of freedom is uncoupled.
We can exploit the Helmoltz theorem; each vector can be decomposed into a solenoidal and a longitudinal part:

$$\omega_i = \partial_i \omega^{||} + \omega_i^{\perp}. \tag{2.9}$$

$\omega_i^{\perp}$ is called solenoidal because $\partial^i \omega_i^{\perp} = 0$.

The traceless perturbation of g_{ij} can be decomposed in a similar fashion:

$$h_{ij} = D_{ij}h^{||} + \partial_i h_j^{\perp} + \partial_j h_i^{\perp} + h_{ij}^T \tag{2.10}$$

where $h^{||}$ is a scalar function, $h_i^{\perp}$ is a solenoidal vector field and the tensor part h_{ij}^T is symmetric, solenoidal and traceless; D instead is $D_{ij} = \partial_i\partial_j - \delta_{ij}\nabla^2/3$.

Matter Perturbations Now we take a look at the right hand side of eq. (2.3), the matter perturbations. It can be shown that, for a generic fluid, the stress-energy tensor can be written in the following way [12]:

$$T_{\mu\nu} = (\rho + p_0)\, u_\mu u_\nu + p_0 g_{\mu\nu} + \Pi_{\mu\nu} \tag{2.11}$$

which is a generalization of eq. (1.11). It is important to note that it has been added a new term, $\Pi_{\mu\nu}$, the anisotropic stress tensor, constrained as $u^\nu\Pi_{\mu\nu} = \Pi^\mu_\mu = 0$. In the cases of a minimally coupled field or a perfect fluid such a term vanishes. Perturbing eq. (2.11) and decomposing each physical quantity according to its transformation properties, the first-order components of the stress-energy tensor can be written as [21]:

$$T_0^0 = -\rho_0 + \delta\rho, \tag{2.12}$$

$$T_i^i = 3(p_0 + \delta p) = 3p_0(1 + \Pi_L), \tag{2.13}$$

$$T_i^0 = T_0^i = 0, \tag{2.14}$$

$$T_j^i = p_0\left[(1 + \Pi_L)\delta_j^i + \Pi_{T,j}^i\right], \tag{2.15}$$

where we have neglected vector perturbations. We interpret Π_L as the amplitude of an isotropic pressure perturbation and therefore Π_T is interpreted as the amplitude of an anisotropic stress perturbation, practically imperfections of the fluid.

Scalar Field Perturbations We consider now the perturbation of the scalar field, given in eq. (1.75), on a FRW background metric. Let us point out the fact that, rigorously, we should perturb, besides the scalar field, the background metric as well. We will see this later on.

Since the field has explicit dependence on space coordinates, the equation of motion (1.85) now becomes:

$$\ddot{\phi}(\mathbf{x}, t) + 3H\dot{\phi}(\mathbf{x}, t) - a^{-2}\nabla^2\phi(\mathbf{x}, t) = -\frac{\partial V}{\partial\phi} \tag{2.16}$$

Now we perturb it to the first order and we assume eq. (1.87) still valid for the background, thus obtaining the equation of motion for the perturbation $\delta\phi(\mathbf{x}, t)$:

$$\delta\ddot{\phi} + 3H\delta\dot{\phi} - \frac{\nabla^2\delta\phi}{a^2} = -\frac{\partial^2 V}{\partial\phi^2}\delta\phi \tag{2.17}$$

To find a general solution of eq. (2.17) we perform a Fourier transform of $\delta\phi(\mathbf{x}, t)$:

$$\delta\phi(\mathbf{x}, t) = \int d^3k e^{i\mathbf{kx}}\delta\phi_{\mathbf{k}}, \tag{2.18}$$

where $\delta\phi_{\mathbf{k}} = \tilde{\delta\phi}(\mathbf{k}, t)$. In the Fourier space the equation becomes:

$$\delta\ddot{\phi}_{\mathbf{k}} + 3H\dot{\phi}_{\mathbf{k}} + \frac{k^2\delta\phi_{\mathbf{k}}}{a^2} = -V''\delta\phi_{\mathbf{k}} \tag{2.19}$$

Equation (1.96) is equivalent to say that the mass of the field is negligible: $m_\phi^2 = V'' \simeq 0$. Therefore eq. (2.19) now is:

$$\delta\ddot{\phi}_{\mathbf{k}} + 3H\dot{\phi}_{\mathbf{k}} + \frac{k^2\delta\phi_{\mathbf{k}}}{a^2} = 0. \tag{2.20}$$

It is interesting to see the behavior of this equation in two different regimes.
In the **small-scale regime**, $\lambda_{phys} \ll H^{-1}$, the wavelenght is much smaller than the hubble radius ($k^2 \gg a^2H^2$), so that the second term is negligible:

$$\delta\ddot{\phi}_{\mathbf{k}} + \frac{k^2\delta\phi_{\mathbf{k}}}{a^2} = 0. \tag{2.21}$$

Equation (2.21) is the equation of an harmonic oscillator with frequency amplitude

$$\omega_a = \frac{k^2}{a^2}$$

that decreases with time. This means that, on small scale, the field fluctuates around its vacuum value ϕ_0.
In the **large-scale regime**, $\lambda_{phys} \gg H^{-1}$, we have:

$$\delta\ddot{\phi} + 3H\delta\dot{\phi} = 0 \tag{2.22}$$

which has exact solution:

$$\delta\phi = ae^{-3Ht} + b$$

where a and b are constants. Thus, after a short time ($t \simeq (3H)^{-1}$), the perturbation stays constant; the perturbation is said to be frozen at the value it has while crossing the Hubble horizon.

2.1.2 Power Spectrum

Now we want to introduce an important tool used in cosmology, the Power Spectrum. In order to do so, we consider a cosmic scalar field such as the cosmic density field ($\delta(\mathbf{x})$) or the velocity divergence field ($\theta(\mathbf{x})$) or the cosmic gravitational potential ($\Phi(\mathbf{x})$) and so on (see Sec. 2.3.1 for definitions of these fields).
We will assume that cosmic fields are statistically homogeneous and isotropic, as predicted by most cosmological theories. This means that all the probability distribution functions of the field of interest stay the same under translation of coordinates and under spatial rotations.
First thing to do, we define the Fourier transform. The convention we will adopt in this work for the Fourier transform of a field $A(\mathbf{x}, \tau)$ is the following:

$$\tilde{A}(\mathbf{k}, \tau) = \int \frac{d^3\mathbf{x}}{(2\pi)^3} e^{-i\mathbf{k}\cdot\mathbf{x}} A(\mathbf{x}, \tau). \tag{2.23}$$

The *two-point correlation function*, instead, is defined as the joint ensemble average of the density at two different locations, i.e.

$$\xi(r) = \langle \delta(\mathbf{x})\delta(\mathbf{x}+\mathbf{r}) \rangle \tag{2.24}$$

which depends only on the absolute value of $\mathbf{r}$ because of statistical homogeneity and isotropy. Here we use $\langle\cdot\rangle$ to indicate ensamble average (this concept will be better explained in Chapter 3). The density contrast $\delta(\mathbf{x})$ is usually written in terms of its Fourier components,

$$\delta(\mathbf{x}) = \int d^3\mathbf{k} \delta(\mathbf{k}) e^{i\mathbf{k}\cdot\mathbf{x}} \tag{2.25}$$

the quantities $\delta(\mathbf{k})$, then, are complex random variables. Since $\delta(\mathbf{x})$ is real, it follows that

$$\delta(\mathbf{k}) = \delta^\star(-\mathbf{k}). \tag{2.26}$$

Thus, the density field is determined entirely by the statistical properties of the random variable $\delta(\mathbf{k})$ and we can compute the correlator in Fourier space,

$$\begin{aligned}
\langle \delta(\mathbf{k})\delta(\mathbf{k}') \rangle &= \langle \int \frac{d^3\mathbf{x}}{(2\pi)^3} \delta(\mathbf{x}+\mathbf{r}) e^{-i\mathbf{k}\cdot(\mathbf{x}+\mathbf{r})} \int \frac{d^3\mathbf{r}}{(2\pi)^3} \delta(\mathbf{x}) e^{-i\mathbf{k}'\cdot\mathbf{x}} \rangle \\
&= \int \frac{d^3\mathbf{x}}{(2\pi)^3} \int \frac{d^3\mathbf{r}}{(2\pi)^3} \langle \delta(\mathbf{x})\delta(\mathbf{x}+\mathbf{r}) \rangle e^{-i(\mathbf{k}+\mathbf{k}')\cdot\mathbf{x} - i\mathbf{k}\cdot\mathbf{r}} \\
&= \int \frac{d^3\mathbf{x}}{(2\pi)^3} \int \frac{d^3\mathbf{r}}{(2\pi)^3} \xi(r) e^{-i(\mathbf{k}+\mathbf{k}')\cdot\mathbf{x} - i\mathbf{k}\cdot\mathbf{r}} \\
&= \delta_D(\mathbf{k}+\mathbf{k}') \int \frac{d^3\mathbf{r}}{(2\pi)^3} \xi(r) e^{-i\mathbf{k}\cdot\mathbf{r}}
\end{aligned} \tag{2.27}$$

leading to

$$\langle \delta(\mathbf{k})\delta(\mathbf{k}')\rangle = \delta_D(\mathbf{k}+\mathbf{k}')P(k) \tag{2.28}$$

where we have defined the density **Power Spectrum**

$$P(k) = \int \frac{d^3\mathbf{r}}{(2\pi)^3}\xi(r)e^{-i\mathbf{k}\cdot\mathbf{r}} \tag{2.29}$$

which is, indeed, an essential and efficient tool used in cosmology to characterize the properties of field perturbations. The inverse relation between the two-point correlation function and the power spectrum thus is

$$\xi(r) = \int d^3\mathbf{k}P(k)e^{i\mathbf{k}\cdot\mathbf{r}} \tag{2.30}$$

meaning that, basically, the Power Spectrum is the Fourier transform of the two-point correlation function.
Additionally, we can define the dimensionless power spectrum $\Delta(k)$ in the following way:

$$\langle \delta(\mathbf{k})\delta(\mathbf{k}')\rangle = \frac{1}{4\pi k^3}\delta_D(\mathbf{k}+\mathbf{k}')\Delta(k). \tag{2.31}$$

The Δ power spectrum measures the amplitude of the fluctuations at a given mode k. We see, indeed, that $P(k)$ and $\Delta(k)$ are correlated:

$$\Delta(k) = 4\pi k^3 P(k). \tag{2.32}$$

Furthermore we can easily see that:

$$\langle \delta^2(\mathbf{x})\rangle = \int \frac{dk}{k}\Delta(k) = \int d(\log k)\Delta(k). \tag{2.33}$$

What eq. (2.33) is telling us is that $\Delta(k)$ is the contribution to the variance per unit logarithmic interval in wave number k.
A new physical quantity we now introduce is the spectral index:

$$n_s(k) - 1 = \frac{d\log\Delta(k)}{d\log k} \tag{2.34}$$

which is useful to describe the slope of the power spectrum. In general n_s depends on the considered scale ($n_s = n_s(k)$); if it is constant, then:

$$\Delta(k) = \Delta(k_0)\left(\frac{k}{k_0}\right)^{n_s-1}. \tag{2.35}$$

We call k_0 pivot scale; moreover, when the spectral index is exactly equal to unity the power spectrum of the field is scale invariant and gets the name of Harrison-Zel'dovich power spectrum.

Now we proceed in quantizing the scalar field with the standard second quantization procedure. We do this because we are interested to specify the form the power spectrum assumes in a general case, when the stochastic field is a canonically quantized scalar field that lives in a curved space time, as the inflaton is. We introduce the physical perturbation $\hat{\delta\phi} = a\delta\phi$ and promote the field into an operator:

$$\hat{\delta\phi}(\tau, \mathbf{x}) = \frac{1}{(2\pi)^3} \int d^3k \left[u_k(\tau) a_{\mathbf{k}} e^{i\mathbf{kx}} + u_k^*(\tau) a_{\mathbf{k}}^\dagger e^{-i\mathbf{kx}} \right] \tag{2.36}$$

where $u_{\mathbf{k}}$ and $u_{\mathbf{k}}^*$ satisfy the canonical commutation relations $u_k^* u_k' - u_k u_k'^* = -i$ by

$$[a_{\mathbf{k}}, a_{\mathbf{k'}}] = 0, \qquad \left[a_{\mathbf{k}}, a_{-\mathbf{k}'}^\dagger \right] = \delta_D(\mathbf{k} + \mathbf{k}'). \tag{2.37}$$

From eq. (2.36) and (2.37) we get:

$$\langle \delta_{\phi_{\mathbf{k}_1}} \delta_{\phi_{\mathbf{k}_2}} \rangle = \frac{|u_k|^2}{a^2} \delta_D(\mathbf{k}_1 + \mathbf{k}_2) \tag{2.38}$$

which leads to the following dimensionless power spectrum

$$\Delta_{\delta\phi}(k) = 4\pi k^3 |\delta\phi_k|^2. \tag{2.39}$$

2.1.3 Scalar Perturbations in Curved Spacetime

Now we will deal with scalar perturbations in curved space time, namely we will perturb not only the scalar field but also the background metric. We will just present some brief results, following [21] and references therein. For a detailed study see [23]. We need a gauge-invariant quantity which univocally describes scalar perturbations. We work in a space time described by the metric (2.4) perturbed at first order. Hence, let us consider the intrinsic spatial curvature on hyper-surfaces of constant conformal time at linear order, namely:

$${}^{(3)}R = \frac{4}{a^2} \nabla^2 \hat{\Phi} \quad \text{where} \quad \hat{\Phi} \equiv \Phi + \frac{1}{6} \nabla^2 \chi^{||}. \tag{2.40}$$

$\hat{\Phi}$ is usually referred to as the curvature perturbation, however it is not a gauge-invariant quantity [21]. So we need a gauge-invariant combination that reduces to the curvature perturbation choosing a particular gauge. Thus, let us consider the following expression ($\mathcal{H} \equiv d \log a / d\tau$):

$$-\zeta \equiv \hat{\Phi} + \mathcal{H} \frac{\delta\rho}{\rho'}. \tag{2.41}$$

The quantity (2.41), considering the $\hat{\Phi}$ transformation and the gauge transformation for scalars, is gauge-invariant and it is referred to as the gauge-invariant curvature perturbation of the uniform energy-density hyper-surfaces.

It is possible to keep track of the evolution of ζ exploiting the perturbed Kleing-Gordon equation for the field ϕ from the action (1.71):

$$\delta\phi'' + 2\mathcal{H}\delta\phi' - \nabla^2\delta\phi + a^2\delta\phi\frac{\partial^2 V}{\partial\phi^2}a^2 + 2\Psi\frac{\partial V}{\partial\phi} - \phi_0''\left(\Psi' + 3\Phi' + \nabla^2\omega^{||}\right) = 0. \quad (2.42)$$

To simplify the equation of motion it is useful to introduce a new variable, the so called Sasaki-Mukhanov gauge-invariant variable:

$$\mathcal{Q}_\phi \equiv \delta\phi + \frac{\phi'}{\mathcal{H}}\Phi. \quad (2.43)$$

It can be shown that ζ and $\mathcal{Q}_\phi$ are linked. Thus, solving equation of motion for $\mathcal{Q}_\phi$ means to solve it for ζ and to find its power spectrum. In fact, let us introduce the field $\hat{\mathcal{Q}}_\phi = a\mathcal{Q}_\phi$, then the Klein-Gordon equation reads:

$$\hat{\mathcal{Q}}_\phi'' + \left(k^2 - \frac{a''}{a} + \mathcal{M}_\phi^2 a^2\right)\hat{\mathcal{Q}}_\phi = 0 \quad (2.44)$$

where

$$\mathcal{M}_\phi^2 = \frac{\partial^2 V}{\partial\phi^2} - \frac{8\pi G}{a^3}\left(\frac{a^3}{H}\phi^2\right). \quad (2.45)$$

In the slow-roll approximation the latter expression reduces to $\mathcal{M}_\phi^2/H^2 = 3\eta - 6\epsilon$. Moving to Fourier space, the solution of (2.44) is a combination of the Hankel functions of the first and the second order which, at the lowest order in the slow-roll parameters and for super-horizon scales, are approximated by:

$$|\mathcal{Q}_\phi(k)| = \frac{H}{\sqrt{2k^3}}\left(\frac{k}{aH}\right)^{3/2-\nu_\phi}, \quad (2.46)$$

where $\nu_\phi \simeq \frac{3}{2} + 3\epsilon - \eta$. In order to obtain the ζ power-spectrum we consider the gauge-invariant curvature perturbationon comoving hyper-surfaces which, in the case of a stress-energy tensor of a single scalar field, is:

$$\mathcal{R} \equiv \hat{\Phi} + \frac{\mathcal{H}}{\phi'}\delta\phi. \quad (2.47)$$

From eq. (2.43) we derive $\mathcal{R} = \mathcal{H}\mathcal{Q}_\phi/\phi'$. Also, $\mathcal{R}$ is related to the curvature perturbation ζ by

$$-\zeta = \mathcal{R} + \frac{2\rho}{9(\rho + P)}\left(\frac{k}{aH}\right)^2\Psi. \quad (2.48)$$

On large scales ($k \ll aH$) we can approximate this relation to $\mathcal{R} \simeq -\zeta$.

Therefore, putting eq. (2.46) and the expression of $\mathcal{R}$ into the expression (2.39), we finally obtain the power spectrum for ζ on large scales:

$$\Delta_\zeta = 2\pi \left(\frac{H^2}{\dot{\phi}}\right)^2 \left(\frac{k}{aH}\right)^{3-2\nu_\phi} \simeq 2\pi \left(\frac{H^2}{\dot{\phi}}\right)^2_* \tag{2.49}$$

where the star denotes quantities evaluated at $k = aH$, namely the epoch at which a given mode leaves the horizon. Equation (2.49) tells us that curvature perturbations remain time-independent on super horizon scales. This means that the solution obtained for ζ is valid throughout different evolution eras of the universe until the mode remains super horizon. As we shall see, the same behavior occurs for tensor perturbations. At the lowest order in slow-roll approximation, the spectral index is:

$$n_\zeta - 1 = 3 - 2\nu_\phi = -6\epsilon + 2\eta. \tag{2.50}$$

2.1.4 Inflationary Consistency Relations

Let us define the spectral index for the tensor perturbation as

$$n_h = \frac{\mathrm{d}\log \Delta_h(k)}{\mathrm{d}\log k} \tag{2.51}$$

which we know it holds that $n_h = -2\epsilon < 0$. In this case the power spectrum is called red, whereas in the case of $n_h > 0$ it is called blue.
There is an interesting relation that holds in this inflationary scenario. As we have already seen we can write the scalar and tensor power spectra as follows:

$$\begin{aligned} \Delta_\zeta(k) &= A_S \left(\frac{k}{k_0}\right)^{n_\zeta - 1} \\ \Delta_h(k) &= A_T \left(\frac{k}{k_0}\right)^{n_h} \end{aligned} \quad . \tag{2.52}$$

A_S and A_T are the amplitudes of the power spectra at the pivot scale k_0. We define the tensor-to-scalar ratio as:

$$r \equiv \frac{A_T}{A_S}. \tag{2.53}$$

During inflation it holds that $\dot{H} = -4\pi G\dot{\phi}^2$ and also that $\epsilon = -\dot{H}/H^2$ (eq. (1.89)). Moreover we know:

$$A_S = 2\pi \left(\frac{H^2}{\dot{\phi}}\right)^2 \quad \text{and} \quad A_T = 32 \left(\frac{2\pi H}{M_{Pl}}\right)^2.$$

Hence, we obtain:

$$r = 16\epsilon \tag{2.54}$$

which is a general prediction of the inflationary models. We can equivalently re-write it in the following way:

$$r = -8n_h. \tag{2.55}$$

These relations are called (inflationary) consistency relations because they connect three different parameters and hold for each single field slow-roll model of inflation. In order to probe this equality it is necessary to perform a measurement of the tensor power spectrum (both the amplitude and the spectral index). Moreover, if this relation holds, it means that it would be hard to measure any scale dependance of the tensors, since a large spectral index would invalidate the consistency relation. Right now we only have an upper bound on the tensor-to-scalar ratio [18]: $r_{0.002} < 0.07$ at 95% CL, assuming the consistency relations, where the subscript stands for the pivot scale, equal to 0.002 Mpc^{-1}.

2.1.5 CMB Power Spectrum

Let us introduce a formalism useful to link together the primordial matter perturbations and the anisotropies of the CMB. As a general process, what we can do is to parametrize the temperature field, which depends on conformal time, position and direction of the photon momentum:

$$T(\tau, \mathbf{x}, \hat{\mathbf{p}}) = T_0(\tau) + \Delta T(\tau, \mathbf{x}, \hat{\mathbf{p}}) = T_0(\tau)(1 + \Theta(\tau, \mathbf{x}, \hat{\mathbf{p}})), \tag{2.56}$$

where T_0 represents the black-body temperature of the background, whereas $\Theta \equiv \Delta T/T$ is the temperature perturbation field. The only fundamental dependence of the perturbation field is the momentum direction $\hat{\mathbf{p}}$. Therefore, we need to study the evolution of the photon distribution function in an expanding universe by means of the Boltzmann equation

$$\mathbb{L}[f] = \mathbb{C}[f] \tag{2.57}$$

where the Liouville operator, in a general metric, reads [20]:

$$\mathbb{L} = p^\mu \frac{\partial}{\partial x^\mu} - \Gamma^\rho_{\mu\nu} p^\mu p^\nu \frac{\partial}{\partial p^\rho}. \tag{2.58}$$

The right hand side of eq. (2.57) is the collision operator, which contains all possible collision terms of the particle species we are considering. Since, as far as it concerns this particular section, we are interested in photons, we need to understand all the possible interactions among photons and all the other components of the universe. It is known that CMB radiation is a black-body radiation, that leads to a one-to-one relation between temperature and momentum of the photon. Thus, using the temperature perturbation field, we can describe the variation in energy for the photons.

We introduce the multipole expansion of the temperature perturbation

$$\Theta(\mathbf{k},\hat{\mathbf{p}}) = \sum_{l=1}^{\infty}(-i)^l(2l+1)\mathcal{P}_l(\hat{\mathbf{p}})\Theta_l(\mathbf{k}) \tag{2.59}$$

where $\mathcal{P}_l$ are the solutions of the Legendre differential equation, i.e. Legendre polynomials. If we invert the latter relation we obtain the definition of each multipole:

$$\Theta_l \equiv \frac{1}{(-i)^l}\int_{-1}^{1}\frac{d\mu}{2}\mathcal{P}_l(\mu)\Theta(\mu). \tag{2.60}$$

It is clear, then, what the various l-values mean: $l = 0$ stands for the monopole (a constant pertubation), $l = 1$ the dipole perturbation, $l = 2$ the quadrupole, and so forth.

We proceed now in briefly sketching the connection between theoretical multipoles (Θ_l) and the observation of the CMB. First, we decompose the temperature perturbation field throughout spherical harmonics:

$$\Theta(\tau,\mathbf{x},\hat{\mathbf{p}}) = \sum_{l=1}^{\infty}\sum_{m=-l}^{+l} a_{lm}(\tau,\mathbf{x})Y_{lm}(\hat{\mathbf{p}}). \tag{2.61}$$

Eq. (2.61) is equivalent to a Fourier transform on the surface of a sphere: l,m are the conjugate to the real space of $\hat{\mathbf{p}}$ and $Y_{lm}(\hat{\mathbf{p}})$ are the complete set of eigenfunctions for the expansion on the surface of a sphere. Moreover, the coefficients a_{lm} play a key role in cosmology, since they contain information about the temperature perturbation field. What is the connection between a_{lm} and Θ_l?
Using the orthogonality property of spherical harmonics

$$\int_{\Omega} d\Omega Y_{lm}(\hat{\mathbf{p}})Y^*_{l'm'}(\hat{\mathbf{p}}) = \delta_{ll'}\delta_{mm'}, \tag{2.62}$$

we can invert relation (2.61) multiplying it by $Y^*_{lm}(\hat{\mathbf{p}})$ and integrating over the solid angle

$$a_{lm}(\tau,\mathbf{x}) = \int d\Omega Y^*_{lm}(\hat{\mathbf{p}})\Theta(\tau,\mathbf{x},\hat{\mathbf{p}}) = \int d^3\mathbf{k}e^{i\mathbf{kx}}\int d\Omega Y^*_{lm}(\hat{\mathbf{p}})\Theta(\tau,\mathbf{k},\hat{\mathbf{p}}) \tag{2.63}$$

where in the second equality we have used the Fourier transform of the temperature perturbation field, since all the solution are in momentum space. Considering that a_{lm} is a stochastic field, it holds that $\langle a_{lm}\rangle = 0$ and we define the variance:

$$\langle a_{lm}a^*_{l'm'}\rangle = \delta_{ll'}\delta_{mm'}C_l. \tag{2.64}$$

Let us note that, given a certain l, each a_{lm} has the same variance. This means that, for large l, when we measure all the possible a_{lm} coefficients we are sampling the distribution, i.e. this much information will give a good handle on the underlying

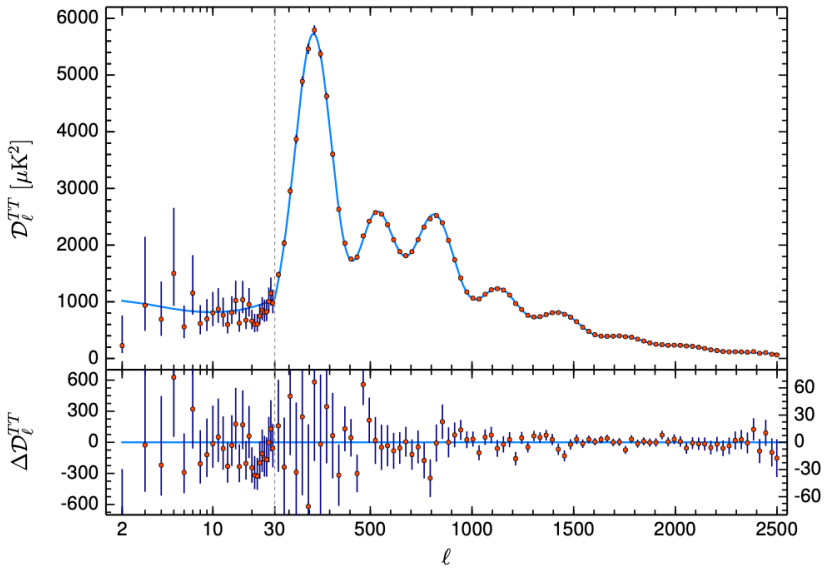

Figure 2.1: Angular power spectrum of CMB temperature fluctuations, taken from [18]. In the figure it is plotted $D_l^{TT} \equiv l(l+1)C_l/(2\pi)$, because at large scales (small l) the dominant effect is the so called Sachs-Wolfe effect [13], which predicts $l(l+1)C_l \simeq const$.

variance of the distribution. For low l, instead, we do not have much information about the variance. This fundamental uncertainty in the low-l variances is called cosmic variance.
Finally, following [13] we can find the expression of C_l in terms of Θ_l:

$$C_l = \frac{2}{\pi}\int_0^\infty dk k^2 P_{dm}(k)\left|\frac{\Theta_l(k)}{\delta_{dm}(k)}\right|^2. \tag{2.65}$$

where P_{DM} is the dark matter power spectrum and δ_{dm} the Dark Matter overdensity. Therefore, using the Boltzmann equation, it is possible to plot the anisotropy spectrum today, as depicted in fig. (2.1).

2.2 Baryon Acoustic Oscillations

In this section we will analyze a very important feature of the universe which comes directly from the fluctuations mechanism: the Baryon Acoustic Oscillations (BAO). The BAO's are frozen relics left over from the pre-decoupling universe [24]. As we have already mentioned in Sec. 1.3, before recombination and decoupling the universe consisted of a hot plasma of photons and baryons which were tightly coupled via Thomson scattering. The plasma was almost homogeneous, but there were slight over- and under-densities spread throughout. These small density variations, because of competing forces of radiation pressure and gravity, caused pressure variations in the radiation field and this made sound waves propagate across the photon fluid.
Now we consider just a single, spherical density perturbation in the tightly coupled baryon-photon plasma of a very early universe; this perturbation will propagate outwards as, indeed, an acoustic wave with a speed

$$c_s = \frac{c}{\sqrt{3(1+R)}} \tag{2.66}$$

where [25]

$$R \equiv \frac{3\rho_b}{4\rho_\gamma} \propto \frac{\Omega_b}{1+z}. \tag{2.67}$$

Up until recombination ($z \sim 1200$), the baryons and the photons rush away from the center of the density perturbation together, precisely because they are tightly coupled together. Meanwhile, the dark matter spreads out much more slowly. This is because it is not electromagnetically coupled to the photons. It only interacts gravitationally, and so it only follows slowly behind in response to the gravitational drag of the photon-baryon component. Then, the cosmos becomes neutral and the pressure on the baryons is removed. The baryon wave stalls while the photons freely propagate away forming the Cosmic Microwave Background. The characteristic radius of the spherical shell formed when the baryon wave stalled is imprinted on the distribution of the baryons as a density excess. The baryons and dark matter interact through gravity, and so the dark matter also gathers on this scale. Therefore, there is an increased probability that a galaxy will form somewhere in the higher density remains of the stalled baryon wave than either side of the shell. This entire process is well depicted in Fig. (2.2).
If a galaxy had formed at the center of the initial density perturbation there would be a higher probability of finding two galaxies separated by the distance r_s, with r_s the radius of our spherical cell. This translates into a bump in the two-point correlation function at the radius r_s. The scale r_s is close to the sound horizon, the comoving distance a sound wave could have traveled in the photon-baryon fluid by the time of decoupling, and depends on the baryon and matter densities via [26]:

$$r_s = \int_{z_{rec}}^{\infty} \frac{c_s}{H(z)} dz = \frac{1}{\sqrt{\Omega_m H_0^2}} \frac{2c}{3 z_{eq} R_{eq}} \log \left[\frac{\sqrt{1+R_{rec}} + \sqrt{R_{rec}+R_{eq}}}{1+\sqrt{R_{eq}}} \right] \tag{2.68}$$

where

$$z_{eq} = \frac{\Omega_m}{\Omega_{rad}} \tag{2.69}$$

is the redshift of matter-radiation equality and "rec" refers to recombination. The CMB strongly constrains the matter and baryon densities at decoupling and hence the sound horizon [27]:

$$r_s = 146.8 \pm 1.8 \text{ Mpc}. \tag{2.70}$$

Obviously, the universe did not begin with a single point-like over-density but actually variations in the density existed everywhere. Thus, from each point of space, a spherical shell of BAO started growing, each one with a different amplitude. Therefore, the final density distribution is a linear superposition which, in real space approach to cosmic perturbations based on Green's functions, can be made rigorous, see [28]. We show this in Fig. (2.3).
Hence, also looking at Fig. (2.3), it is clear that there is a preferred scale, that is the sound horizon r_s. This, incidentally, is the reason why the BAO matter clustering provides a standard ruler for lenght scale.
As we have already said, one method of extracting a statistical scale from the clustering of galaxies is using the two-point correlation function, $\xi(r)$, which quantifies the excess clustering on a given scale relative to a uniform distribution with the same mean density [24].

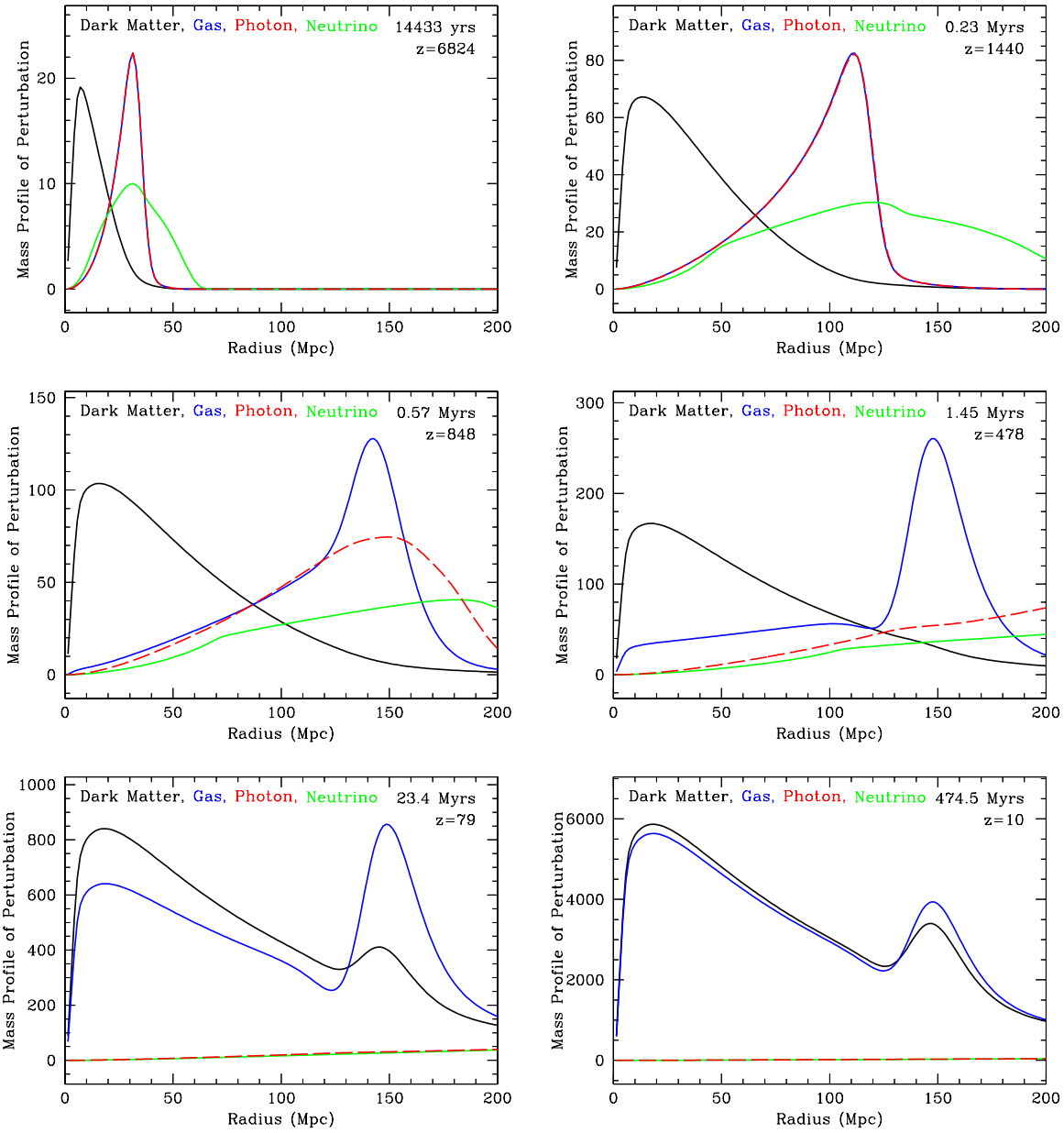

Figure 2.2: We show snapshots of an evolving spherical density perturbation. We have located at the origin an initially point-like overdensity, and the radial mass profile as a function of comoving radius is depicted. The perturbation grows from very early times ($z = 6824$, top left) to more recent time ($z = 10$, bottom right). At the beginning ($z = 6824$), the density perturbation propagates through the photons and baryons all together dragging along the dark matter distribution ($z = 1440$). During recombination, however, the photons start to stream away from the baryons ($z = 848$). As recombination is completed ($z = 470$) the photons freely stream away leaving only a density perturbation in the baryons around 150 Mpc, and a dark matter perturbation near the origin. Finally, we see how the gravitational interaction between dark matter and baryons affects the peak: dark matter pulls the baryons to the peak in the density near zero radius, while the baryons continue to drag the dark matter overdensity towards the 150 Mpc peak ($z = 79$). In the very last snapshot we see that dark matter and baryons finally have come to equilibrium, with neutrinos and photons that have almost "disappeared". Figure taken from [25].

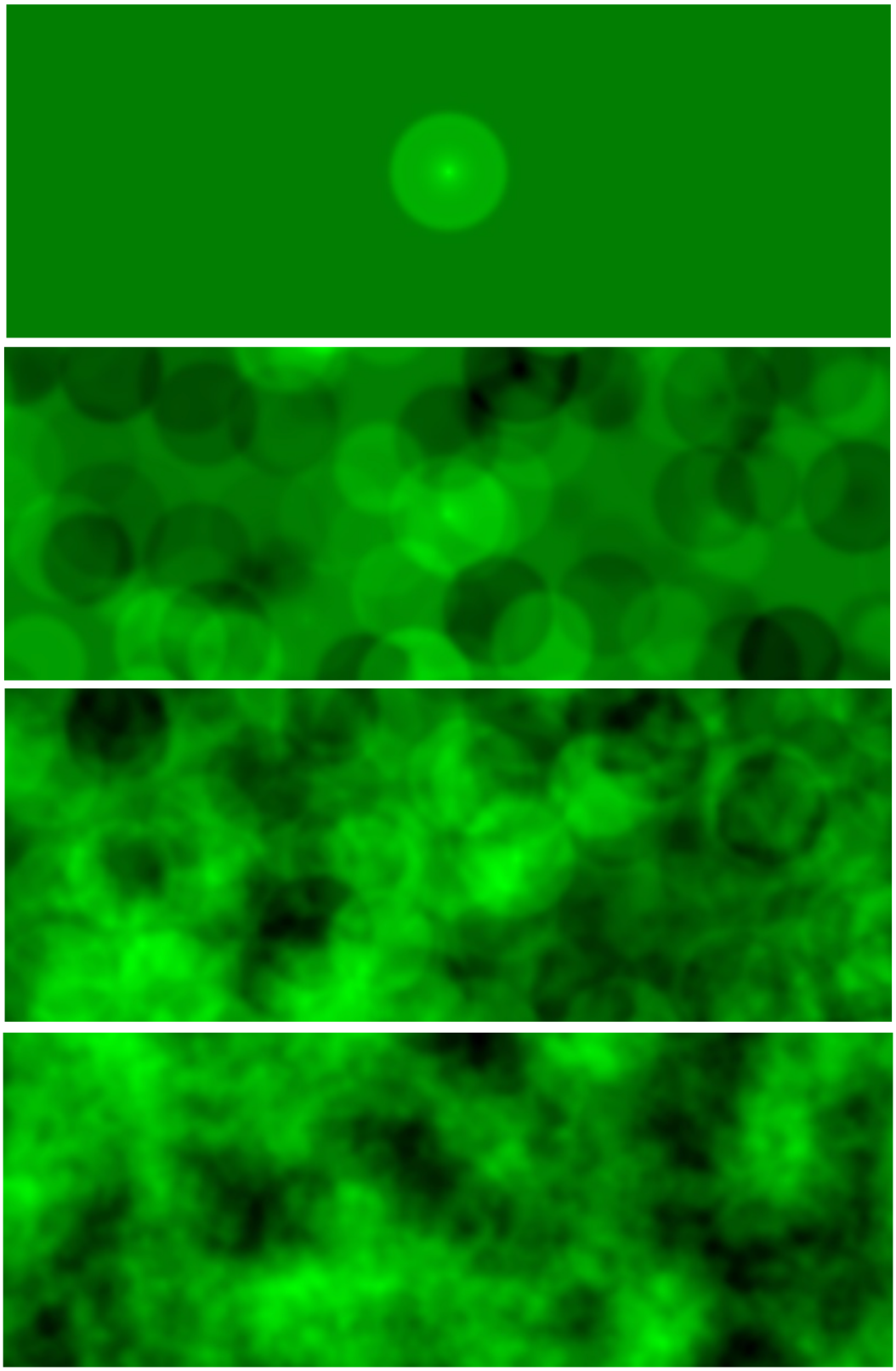

Figure 2.3: Expanding over- and under-densities shells, around time of recombination. Only photon densities are shown, without the dark matter or baryons. In the first panel only one perturbation is present whereas 150 shells are present in the second panel and 1000 in the third. As the number of shells becomes appreciable (490000 shells in the last panel), no single shell can be distinguished, but the resulting patterns do have a size that is roughly the size of the 150 Mpc shells. Figure taken from [29].

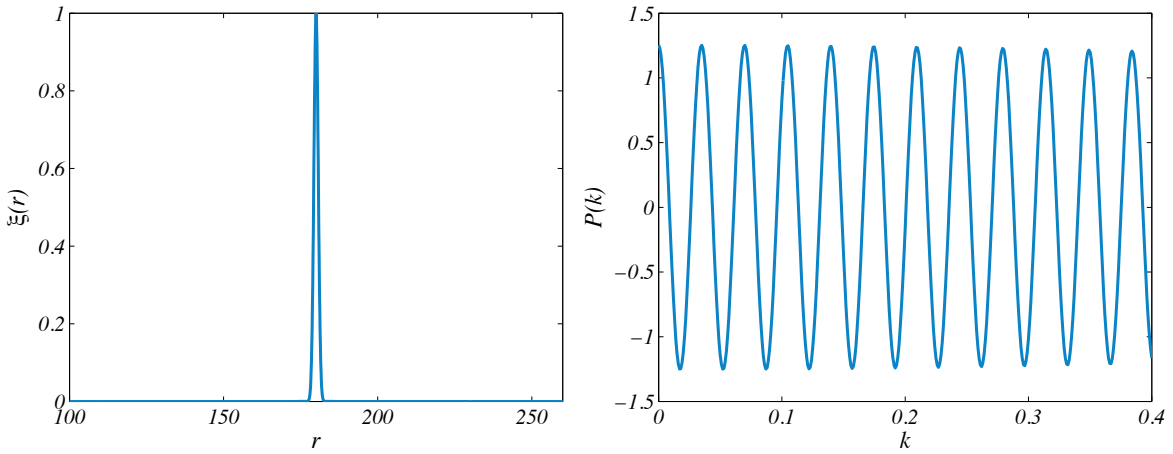

Figure 2.4: Schematic illustration of the Fourier pairs $\xi(r)$, $P(k)$. A sharp peak in the correlation function (left panel) corresponds to a series of oscillations in $P(k)$ (right panel). The Baryon Acoustic Peak in the correlation function will induce characteristic Baryon Acoustic Oscillations in the power spectrum. Figure taken from [24].

The correlation function of galaxies is approximately described by a power law [30],

$$\xi(r) \propto \left(\frac{r_0}{r}\right)^{\gamma} \tag{2.71}$$

with $r_0 \sim 5h^{-1}\mathrm{Mpc}^{-1}$.
A characteristic scale in the clustering of galaxies will appear as a peak (or a dip) in the correlation function, depending on whether there is an excess or a lack of clustering at that given scale. What is also important is that any characteristic feature will also be present in the power spectrum, since, as we can tell from eq. (2.29)

$$P(k) = \int \frac{d^3\mathbf{r}}{(2\pi)^3}\xi(r)e^{-i\mathbf{k}\cdot\mathbf{r}}$$

the correlation function and power spectrum are a Fourier pair. Thus, we are interested in the power spectrum as well, because features in the two functions are related. A δ_D function at a characteristic scale, say $r_\star$, in $\xi(r)$ will result in power spectrum oscillations, $P(k) \propto e^{-ikr_\star}$, as can be seen in Fig. (2.4). These kind of oscillations, which come from the preferred scale at the sound horizon, are the Baryon Acoustic Oscillations.
Figures (2.5) and (2.6) show the original evidence for the acoustic signature in the correlation function and power spectrum respectively.
On general grounds, galaxies tend to form where the density of hydrogen and helium is higher, because these locations gravitationally attract surrounding material, which collapses until it starts forming stars, and this happened somewhere around $z = 7 - 8$, i.e., looking at the last plot of Fig. (2.2), when the density distribution of baryons and dark matter are roughly coincident. This means that, around that redshift, the BAO feature is still present.

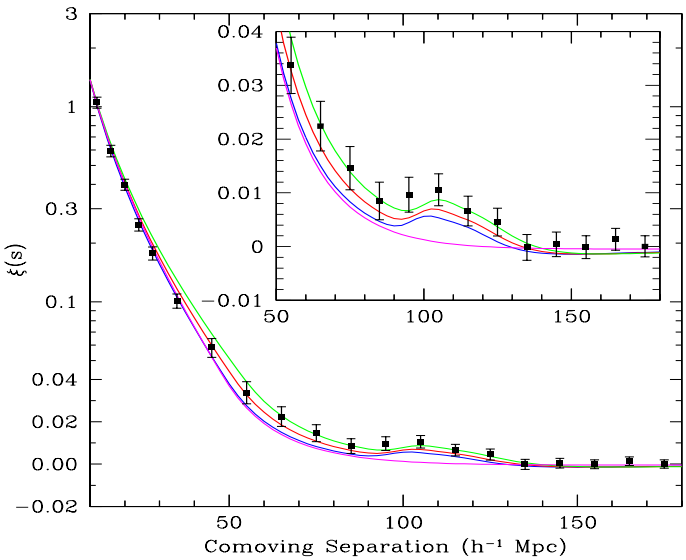

Figure 2.5: The Baryon Acoustic Peak (BAP) in the correlation function, from Sloan Digital Sky Survey (SDSS) LRG galaxy sample. Note that the BAP is sensitive to the matter density (shown are models with $\Omega_m h^2 = 0.12$ (top), 0.13 (second) and 0.14 (third), all with $\Omega_b h^2 = 0.024$). In fact, the bottom line without a BAP is the correlation function in the pure CDM model, with $\Omega_b = 0$: in the absence of baryons we would not have any peak. Figure taken from [31].

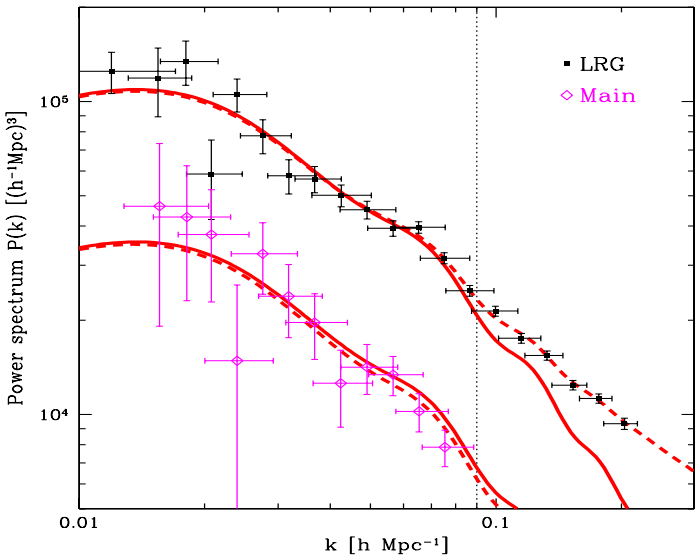

Figure 2.6: Baryon Acoustic Oscillations in the SDSS power spectra – the BAP of figure (2.5) now becomes a series of oscillations in the matter power spectrum of the SDSS sample. In this graph, the power spectrum is computed for both the main SDSS sample (bottom curve) and the Luminous Red Galaxy (LRG) sample (top curve), illustrating how LRGs are significantly more biased than average galaxies. The solid lines show the ΛCDM fits to the WMAP3 data [32], while the dashed lines include nonlinear corrections. Figure taken from [33].

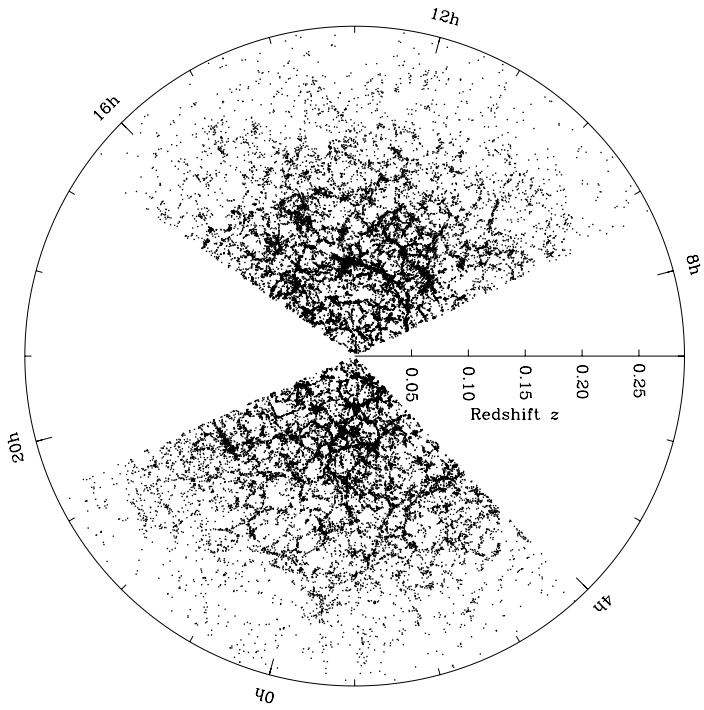

Figure 2.7: A two-dimensional slice of the map of the Universe obtained by the Sloan Digital Sky Survey, only galaxies within ±1.25 deg of the celestial equator are shown. Figure taken from [34].

Let us point out, however, that the typical length-scale of a galaxy is around 0.03 Mpc, much smaller than the BAO scale (150 Mpc). Thus, the structure within individual galaxies is not affected at all by BAO but, on very large scales, the clustering of galaxies is influenced by the BAO scale.
In Fig. (2.7) is shown the large-scale distribution of galaxies today. We can, therefore, combine this image with Fig. (2.5) and see how the BAO feature is present when looking at the correlation of the position of galaxies, therefore connecting the early stages of the universe with the large-scale structure of the present-day universe.

2.3 Newtonian Treatment of Perturbations

Understanding the large-scale structure of the universe has become a central issue of cosmology. Gravitational instability surely plays a central role in forming the structures we see in galaxy survey. Therefore, we need to learn a quantitative understanding of the dynamics of gravitational instability in order to extract all the information stored in galaxy clustering.
In this section, following [35], we will study the non-linear cosmological perturbation theory, useful in interpreting results from galaxy surveys; this happens to be so because density fluctuations become small enough at large scales (weakly non-linear regime) that a perturbative approach can be adopted to understand their evolution.
As we have said numerous times, we are assuming a universe that is isotropic and homogeneous. The framework of Perturbation Theory, and therefore gravitation instability, is based on the fact that gravity, at large scales, is the only agent responsible for the structure formation in universe with density fluctuations dominated by dark matter. This assumption is in very good agreement with observations of galaxy clustering. In particular, the non-gravitational effects associated with galaxy formation may alter the distribution of luminous matter compared to the dark matter one, especially at small scales. This is called "galaxy biasing", and can be probed with statistical techniques we will use in this work.

The most natural explanation for the large-scale structures (superclusters, walls, filaments and so on) seen in galaxy surveys, is that they are the result of gravitational amplification of small primordial fluctuations due to the gravitational interaction of collisionless cold dark matter (CDM) particles in an expanding universe [36].
Even if the nature of dark matter is not entirely clear, all candidates for CDM particles are extremely light compared to the mass scale of typical galaxies. The expected number densities are around 10^{50} particles/Mpc^3 [20]. In this limit the number of particles is $N \gg 1$, therefore discreteness effects are negligible, and collisionless dark matter obeys the Vlasov equation for the distribution function in phase space. Since CDM particles are non-relativistic, at small scales, smaller than the Hubble radius, the equations of motion reduce essentially to those of Newtonian gravity.

2.3.1 The Vlasov Equation

Now we consider a collection of particles of mass m interacting in an expanding universe via gravitational interaction. The equation of motion for a particle of velocity $\mathbf{v}$ at position $\mathbf{r}$ reads:

$$\frac{\mathrm{d}\mathbf{v}}{\mathrm{d}t} = Gm \sum_i \frac{\mathbf{r}_i - \mathbf{r}}{|\mathbf{r}_i - \mathbf{r}|^3}. \tag{2.72}$$

If we consider the limit of a large number of particles, we can recast the latter equation in terms of a smooth gravitational potential caused by the particle distribution,

$$\frac{\mathrm{d}\mathbf{v}}{\mathrm{d}t} = -\frac{\partial\phi}{\partial\mathbf{r}}, \tag{2.73}$$

where we are indicating with ϕ the Newtonian potential generated by the mass density, i.e.

$$\phi(\mathbf{r}) = G\int d^3\mathbf{r}'\frac{\rho(\mathbf{r}')}{|\mathbf{r}'-\mathbf{r}|}. \tag{2.74}$$

We can write the Friedmann equation in terms of conformal time τ, and recast them in the following way:

$$(\Omega_{tot}-1)\,\mathcal{H}^2(\tau) = k \tag{2.75}$$

$$\frac{\partial\mathcal{H}(\tau)}{\partial\tau} = -\frac{\Omega_m(\tau)}{2}\mathcal{H}^2(\tau) + \frac{\Lambda}{3}a^2(\tau) \equiv \left(\Omega_\Lambda - \frac{\Omega_m(\tau)}{2}\right)\mathcal{H}^2 \tag{2.76}$$

where let us remember that:

$$\mathcal{H}(\tau) \equiv \frac{1}{a(\tau)}\frac{\mathrm{d}a(\tau)}{\mathrm{d}\tau}. \tag{2.77}$$

We proceed with the definition of the density contrast $\delta(\mathbf{x})$, which is

$$\rho(\mathbf{x},\tau) \equiv \bar{\rho}(\tau)\,[1+\delta(\mathbf{x},\tau)] \tag{2.78}$$

and where $\bar{\rho}(\tau)$ indicates the background density. We also define the peculiar velocity analogously

$$\mathbf{v}(\mathbf{x},\tau) \equiv \mathcal{H}\mathbf{x} + \mathbf{u}(\mathbf{x},\tau) \tag{2.79}$$

and the cosmological gravitational potential Φ as well:

$$\phi(\mathbf{x},\tau) \equiv -\frac{1}{2}\frac{\partial\mathcal{H}}{\partial\tau}x^2 - \Phi(\mathbf{x},\tau) \tag{2.80}$$

In particular, with this last definition, we can see that the only source of the gravitational potential are the density fluctuations, meaning, in fact, that the Poisson equation is:

$$\nabla^2\Phi(\mathbf{x},\tau) = \frac{3}{2}\Omega_m(\tau)\mathcal{H}^2(\tau)\delta(\mathbf{x},\tau). \tag{2.81}$$

If now we choose

$$\mathbf{p} = am\mathbf{u} \tag{2.82}$$

we can rewrite eq. (2.73) in the following way:

$$\frac{\mathrm{d}\mathbf{p}}{\mathrm{d}\tau} = -am\nabla\Phi(\mathbf{x}) \tag{2.83}$$

Next, we define the particle number density in phase space by $f(\mathbf{x}, \mathbf{p}, \tau)$; phase-space conservation implies:

$$\frac{\mathrm{d}f}{\mathrm{d}\tau} = \frac{\partial f}{\partial \tau} + \frac{\partial \mathbf{x}}{\partial \tau}\frac{\partial f}{\partial \mathbf{x}} + \frac{\partial \mathbf{p}}{\partial \tau}\frac{\partial f}{\partial \mathbf{p}} = 0 \tag{2.84}$$

that is, the Vlasov Equation:

$$\frac{\mathrm{d}f}{\mathrm{d}\tau} = \frac{\partial f}{\partial \tau} + \frac{\mathbf{p}}{ma}\nabla f - am\frac{\partial f}{\partial \mathbf{p}} = 0. \tag{2.85}$$

This is the master equation from which all subsequent calculations of gravitational instability are derived.

2.3.2 The Continuity and Euler Equations

Now, we want to solve the evolution of the spatial distribution. To this end we can take the momentum moments of the distribution function. The zeroth-order moment of the distribution function relates the phase space density to the local mass density field,

$$\int d^3\mathbf{p} f(\mathbf{x}, \mathbf{p}, \tau) \equiv \rho(\mathbf{x}, \tau). \tag{2.86}$$

The first and the second-order moment of f are:

$$\int d^3\mathbf{p} \frac{\mathbf{p}}{am} f(\mathbf{x}, \mathbf{p}, \tau) \equiv \rho(\mathbf{x}, \tau)\mathbf{u}(\mathbf{x}, \tau), \tag{2.87}$$

$$\int d^3\mathbf{p} \frac{p_i p_j}{a^2 m^2} f(\mathbf{x}, \mathbf{p}, \tau) \equiv \rho(\mathbf{x}, \tau) u_i(\mathbf{x}, \tau) u_j(\mathbf{x}, \tau) + \sigma_{ij}(\mathbf{x}, \tau). \tag{2.88}$$

They define the peculiar velocity flow $\mathbf{u}(\mathbf{x}, \tau)$ and the stess tensor σ_{ij}.
We can derive the continuity equation from the zeroth moment of the Vlasov equation. In fact:

$$\begin{aligned} 0 = \int d^3\mathbf{p} \frac{\mathrm{d}f(\mathbf{x}, \mathbf{p}, \tau)}{\mathrm{d}t} &= \int d^3\mathbf{p} \left(\frac{\partial f}{\partial \tau} + \frac{\mathbf{p}}{am} \cdot \nabla f - am\nabla\Phi \cdot \frac{\partial f}{\partial \mathbf{p}} \right) \\ &= \frac{\partial}{\partial \tau} \left(\int d^3\mathbf{p} f \right) + \int d^3\mathbf{p} \left(\frac{\mathbf{p}}{am} \cdot \nabla f - am\nabla\Phi \cdot \frac{\partial f}{\partial \mathbf{p}} \right) \end{aligned} \tag{2.89}$$

which leads to:

$$\frac{\partial}{\partial\tau}[(1+\delta(\mathbf{x},\tau)] + \nabla\cdot\int d^3\mathbf{p}\frac{\mathbf{p}}{am}\cdot f - am\nabla\Phi\cdot\int d^3\mathbf{p}\frac{\partial f}{\partial\mathbf{p}} = 0. \tag{2.90}$$

The last term vanishes due to boundary conditions and, using eq. (2.87), we recover the **continuity equation**:

$$\frac{\partial\delta(\mathbf{x},\tau)}{\partial\tau} + \nabla\cdot[(1+\delta(\mathbf{x},\tau))\mathbf{u}(\mathbf{x},\tau)] = 0, \tag{2.91}$$

which describes conservation of mass. We can also derive the Euler equation, which is a little bit more complicated. Let us start again from the first moment of the Vlasov equation,

$$\int d^3\mathbf{p}\frac{\mathbf{p}}{am}\left(\frac{\partial f}{\partial\tau} + \frac{\mathbf{p}}{am}\cdot\nabla f - am\nabla\Phi\cdot\frac{\partial f}{\partial\mathbf{p}}\right) = 0 \tag{2.92}$$

which in turn gives three terms:

$$\underbrace{\int d^3\mathbf{p}\frac{\mathbf{p}}{am}\frac{\partial f}{\partial\tau}}_{\mathbf{A}} + \underbrace{\int d^3\mathbf{p}\frac{\mathbf{p}}{am}\left(\frac{\mathbf{p}}{am}\cdot\nabla f\right)}_{\mathbf{B}} - \underbrace{\int d^3\mathbf{p}\frac{\mathbf{p}}{am}\left(am\nabla\Phi\cdot\frac{\partial f}{\partial\mathbf{p}}\right)}_{\mathbf{C}} = 0. \tag{2.93}$$

We start with the **A** term.

$$\begin{aligned}
\mathbf{A} &= \frac{\partial}{\partial\tau}\left(\int d^3\mathbf{p}\frac{\mathbf{p}}{am}f\right) - \int d^3\mathbf{p}\frac{\partial}{\partial\tau}\left(\frac{\mathbf{p}}{am}\right) \\
&= \frac{\partial}{\partial\tau}\left[\rho_0(1+\delta)\mathbf{u}\right] - \int d^3\mathbf{p}\left[\frac{\partial\mathbf{p}}{\partial\tau}\frac{1}{am} + \frac{\partial}{\partial\tau}\left(\frac{1}{a}\right)\frac{\mathbf{p}}{m}\right] \\
&= \frac{\partial}{\partial\tau}\left[\rho_0\mathbf{u} + \rho_0\delta\mathbf{u}\right] + \int d^3\mathbf{p}\frac{a'}{a}\left(\frac{\mathbf{p}}{am}\right)f \\
&= \rho_0\frac{\partial\mathbf{u}}{\partial\tau} + \rho_0\delta\frac{\partial\mathbf{u}}{\partial\tau} + \rho_0\frac{\partial\delta}{\partial\tau}\mathbf{u} + \mathcal{H}\left[\rho_0(1+\delta)\mathbf{u}\right] \\
&= \rho_0\frac{\partial\mathbf{u}}{\partial\tau} + \rho_0\delta\frac{\partial\mathbf{u}}{\partial\tau} - (\nabla\cdot\mathbf{u})\,\mathbf{u}(1+\delta)\rho_0 - (\mathbf{u}\cdot\nabla)\left[\mathbf{u}(1+\delta)\rho_0\right] + \mathcal{H}\left[\rho_0(1+\delta)\mathbf{u}\right] \\
&= \rho_0(1+\delta)\left[\frac{\partial\mathbf{u}}{\partial\tau} - \mathbf{u}\,(\nabla\cdot\mathbf{u}) + \mathcal{H}\mathbf{u}\right] - (\mathbf{u}\cdot\nabla)\left[\rho_0(1+\delta)\mathbf{u}\right]
\end{aligned} \tag{2.94}$$

Let us proceed with the **B** term:

$$\begin{aligned}
\mathrm{B}_i &= \int d^3\mathbf{p}\frac{p_i}{am}\frac{p_j}{am}\frac{\partial f}{\partial x^j} = \frac{\partial}{\partial x^j}\int d^3\mathbf{p}\frac{p_i}{am}\frac{p_j}{am}f \\
&= \frac{\partial}{\partial x^j}\left[\rho_0(1+\delta)u_iu_j + \rho_0(1+\delta)\sigma_{ij}\right] \\
&= \frac{\partial}{\partial x^j}\left[\rho_0(1+\delta)\right]u_iu_j + \rho_0(1+\delta)\left[\frac{\partial u_i}{\partial x^j}u_j + u_i\frac{\partial u_j}{\partial x^j}\right] + \frac{\partial}{\partial x^j}\left[\rho_0(1+\delta)\sigma_{ij}\right] \\
&= (\mathbf{u}\cdot\nabla)\left[\rho_0(1+\delta)u_i\right] + \rho_0(1+\delta)\left[(\mathbf{u}\cdot\nabla)u_i + u_i(\nabla\cdot\mathbf{u})\right] + \nabla_j\left[\rho_0(1+\delta)\sigma_{ij}\right],
\end{aligned} \tag{2.95}$$

leading to:

$$\mathbf{B} = (\mathbf{u}\cdot\nabla)\left[\rho_0(1+\delta)\mathbf{u}\right] + \rho_0(1+\delta)\left[(\mathbf{u}\cdot\nabla)\mathbf{u} + \mathbf{u}(\nabla\cdot\mathbf{u})\right] + \nabla_j\left[\rho_0(1+\delta)\sigma_{ij}\right]. \tag{2.96}$$

The C_i term reads:

$$\begin{aligned}
\mathrm{C}_i &= \int d^3\mathbf{p}\frac{\partial\Phi}{\partial x^j}\frac{\partial f}{\partial p_j}p_i = \frac{\partial\Phi}{\partial x^j}\int d^3\mathbf{p}\frac{\partial f}{\partial p_j}p_i \\
&= -\frac{\partial\Phi}{\partial x^j}\int d^3\mathbf{p}f\frac{\partial p_i}{\partial x^j} = -\frac{\partial\Phi}{\partial x^i}\rho_0(1+\delta)
\end{aligned} \tag{2.97}$$

Thus we can write **C** as:

$$\mathbf{C} = -\nabla\Phi\rho_0(1+\delta). \tag{2.98}$$

Then, summing up equations (2.94), (2.96) and (2.98) we finally arrive to the **Euler equation**,

$$\frac{\partial\mathbf{u}(\mathbf{x},\tau)}{\partial\tau} + \mathcal{H}(\tau)\mathbf{u}(\mathbf{x},\tau) + \mathbf{u}(\mathbf{x},\tau)\cdot\nabla\mathbf{u}(\mathbf{x},\tau) = -\nabla\Phi(\mathbf{x},\tau) - \frac{1}{\rho}\nabla_j\left(\rho\sigma_{ij}\right) \tag{2.99}$$

which describes conservation of momentum. Let us point out that the continuity equation (eq. (2.91)) couples the zeroth moment of the distribution function (ρ) to the first ($\mathbf{u}$). Intstead, the Euler equation couples the first moment ($\mathbf{u}$) to the second (σ_{ij}). Nevertheless, since we have integrated out the phase-space information, we can rely on phenomenological models to close the hierarchy by postulating an assumption for the stress tensor σ_{ij} [35], i.e. the equation of state of the cosmological fluid. For example, standard fluid dynamics [37] gives $\sigma_{ij} = -p\delta_{ij} + \eta(\nabla_i u_j + \nabla_j u_i - \frac{2}{3}\delta_{ij}\nabla\cdot\mathbf{u}) + \zeta\delta_{ij}\nabla\cdot\mathbf{u}$, where p indicates the pressure and ζ and η are viscosity coefficients.
In fact, the equation of state relies on the hypothesis that cosmological structure formation is driven by Cold Dark matter, which is, indeed, matter with negligible pressure. Let us point out that the stress tensor σ_{ij} characterizes the deviation of particle motions from a single coherent flow (single stream). Thus, it is a good approximation to

put $\sigma_{ij} \approx 0$, at least in the first moments of gravitational instability when structures did not have time to collapse. As time goes on, this approximation will break down at progressively larger scales [35].
We can now investigate the solutions of the Poisson Equation, the continuity and the Euler equation in the case of a vanishing stress tensor, i.e. $\sigma_{ij} = 0$.

2.3.3 Linear and Non-Linear Perturbation Theory

At large scales, the fluctuation fields $\delta(\mathbf{x}, \tau)$, $\mathbf{u}(\mathbf{x}, \tau)$ and $\Phi(\mathbf{x}, \tau)$ in eqs. (2.78)-(2.80) can be assumed to be small compared to the homogeneous contribution described by the first terms. Thus we can linearize the Poisson equation (2.81), the continuity equation (2.91) and the Euler equation (2.99) in order to obtain the equations of motion in the linear regime:

$$\frac{\partial \delta(\mathbf{x}, \tau)}{\partial \tau} + \theta(\mathbf{x}, \tau) = 0 \tag{2.100}$$

$$\frac{\partial \mathbf{u}(\mathbf{x}, \tau)}{\partial \tau} + \mathcal{H}(\tau)\mathbf{u}(\mathbf{x}, \tau) = -\nabla\Phi(\mathbf{x}, \tau) \tag{2.101}$$

where we have used:

$$\theta(\mathbf{x}, \tau) \equiv \nabla \cdot \mathbf{u}(\mathbf{x}, \tau). \tag{2.102}$$

Note that in eq. (2.100) we have neglected the term with $\delta(\mathbf{x}, \tau)$, as well as for the term $\mathbf{u}(\mathbf{x}, \tau) \cdot \nabla\mathbf{u}(\mathbf{x}, \tau)$ in eq. (2.101). Moreover, as we have said, we have assumed $\sigma_{ij} \approx 0$, that is the single stream approximation. We are basically saying that, during the collapse, we can treat dark matter as a fluid. In other words, we are assuming that the velocities of the fluid particles entering the considered shell have all the same value. These equations are now easy to solve.
Let us first say that the velocity field, as any vector field, can be described by its divergence $\theta(\mathbf{x}, \tau)$ and its vorticity $\mathbf{w}(\mathbf{x}, \tau) \equiv \nabla \times \mathbf{u}(\mathbf{x}, \tau)$, whose equation of motion can be derived from eq. (2.101). In fact, taking the divergence of the linearized Euler equation we obtain:

$$\frac{\partial \theta(\mathbf{x}, \tau)}{\partial \tau} + \mathcal{H}(\tau)\theta(\mathbf{x}, \tau) + \frac{3}{2}\Omega_m(\tau)\mathcal{H}^2(\tau)\delta(\mathbf{x}, \tau) = 0 \tag{2.103}$$

and, similarly, through its curl we arrive to:

$$\frac{\partial \mathbf{w}(\mathbf{x}, \tau)}{\partial \tau} + \mathcal{H}(\tau)\mathbf{w}(\mathbf{x}, \tau) = 0. \tag{2.104}$$

From the last equation we see that in the linear regime any initial vorticity decays away due to the expansion of the universe, i.e.

$$\mathbf{w}(\tau) \sim a(\tau)^{-1}. \tag{2.105}$$

Instead, the density contrast evolution follows by taking the time derivative of eq. (2.103) and replacing in eq. (2.100):

$$\frac{\mathrm{d}^2 D_1(\tau)}{\mathrm{d}\tau^2} + \mathcal{H}(\tau)\frac{\mathrm{d}D_1(\tau)}{\mathrm{d}\tau} = \frac{3}{2}\Omega_m(\tau)\mathcal{H}^2(\tau)D_1(\tau) \tag{2.106}$$

where we have defined the linear growth factor $D_1(\tau)$ as:

$$\delta(\mathbf{x},\tau) = D_1(\tau)\delta(\mathbf{x},0). \tag{2.107}$$

This equation, together with the Friedmann equations (2.75, 2.76), determines the growth of density perturbations in the linear regime. Since it is a second-order differential equation, it has two independent solutions. Let us denote the fastest growing mode $D_1^{(+)}(\tau)$ and the slowest one $D_1^{(-)}(\tau)$. The evolution of the density is then

$$\delta(\mathbf{x},\tau) = D_1^{(+)}(\tau)A(\mathbf{x}) + D_1^{(-)}(\tau)B(\mathbf{x}) \tag{2.108}$$

where $A(\mathbf{x})$ and $B(\mathbf{x})$ are two arbitrary functions of position describing the initial density field configuration.
For the velocity divergence we can use eq. (2.100) and obtain:

$$\theta(\mathbf{x},\tau) = -\mathcal{H}(\tau)\left[f(\Omega_m,\Omega_\Lambda)A(\mathbf{x}) + g(\Omega_m,\Omega_\Lambda)B(\mathbf{x})\right] \tag{2.109}$$

where

$$f(\Omega_m,\Omega_\Lambda) \equiv \frac{\mathrm{d}\log D_1^{(+)}}{\mathrm{d}\log a} = \frac{1}{\mathcal{H}}\frac{\mathrm{d}\log D_1^{(+)}}{\mathrm{d}\tau}, \tag{2.110}$$

$$g(\Omega_m,\Omega_\Lambda) \equiv \frac{\mathrm{d}\log D_1^{(-)}}{\mathrm{d}\log a} = \frac{1}{\mathcal{H}}\frac{\mathrm{d}\log D_1^{(-)}}{\mathrm{d}\tau}. \tag{2.111}$$

We can take, as an example, the case of an Einstein-de Sitter universe, in which $\Omega_m = 1$ and $\Omega_\Lambda = 0$. In this situation we have

$$D_1^{(+)} = a \quad D_1^{(-)} = a^{-3/2} \quad f(1,0) = 1, \tag{2.112}$$

hence, the density fluctuations grow as the scale factor.

We will now consider the evolution of density and velocity fields beyond the linear approximation. In order to do so, we will first make an approximation: we will characterize the velocity field by its divergence, and neglect the vorticity degrees of freedom. We can justify this choice in the following way: eq. (2.99) can be written as

$$\frac{\partial \mathbf{w}(\mathbf{x},\tau)}{\partial\tau} + \mathcal{H}(\tau)\mathbf{w}(\mathbf{x},\tau) - \nabla\times[\mathbf{u}(\mathbf{x},\tau)\times\mathbf{w}(\mathbf{x},\tau)] = \nabla\times\left(\frac{1}{\rho}\nabla\cdot\vec{\sigma}\right) \tag{2.113}$$

We see that if $\sigma_{ij} \approx 0$, as in the case of a pressureless perfect fluid, if the primordial vorticity vanishes, it remains zero at all times. On the other hand, if the initial vorticity

is non-zero, eq. (2.105) tells us that in the linear regime vorticity decays due to the expansion of the universe; however, looking at the third term of eq. (2.113) we see that the voriticity can be amplified non-linearly.
We will assume that the initial vorticity vanishes, thus eq. (2.113) together with the equation of state $\sigma_{ij} \approx 0$ guarantees that vorticity remains zero throughout the evolution. Note, however, that only as long as the condition $\sigma_{ij} \approx 0$ stays valid this assumption is self-consistent; actually multi-streaming and shocks can generate vorticity [38] and we expect this to occur at small scales when, in fact, perturbation theory breaks down.
The main assumption of PT is to expand the density and velocity fields around the linear solutions, treating the variance of the linear fluctuations as a small parameter (and assuming no vorticity in the velocity field):

$$\delta(\mathbf{x},\tau) = \sum_{n=1}^{\infty} \delta^{(n)}(\mathbf{x},\tau), \tag{2.114}$$

$$\theta(\mathbf{x},\tau) = \sum_{n=1}^{\infty} \theta^{(n)}(\mathbf{x},\tau). \tag{2.115}$$

2.3.4 Fourier Representation

When we are at large scales, fluctuations are small, therefore linear PT provides an adequate description of cosmological fields. In this regime, different Fourier modes evolve independently conserving the primordial statistics. Thus, we want to Fourier transform eqs. (2.81), (2.91) and (2.99) and work in Fourier space.

To begin with, we first perform the Fourier transform of $\theta(\mathbf{x},\tau)$, the divergence of the peculiar velocity (eq. (2.102)):

$$\begin{aligned}
\tilde{\theta}(\mathbf{k},\tau) &= \int \frac{d^3\mathbf{x}}{(2\pi)^3} e^{-i\mathbf{k}\cdot\mathbf{x}} \left(\nabla \cdot \mathbf{u}(\mathbf{x},\tau)\right) \\
&= \int \frac{d^3\mathbf{x}}{(2\pi)^3} e^{-i\mathbf{k}\cdot\mathbf{x}} \nabla \cdot \int d^3\mathbf{p} e^{i\mathbf{p}\cdot\mathbf{x}} \tilde{\mathbf{u}}(\mathbf{p},\tau) \\
&= \int \frac{d^3\mathbf{x}}{(2\pi)^3} e^{-i\mathbf{k}\cdot\mathbf{x}} \int d^3\mathbf{p} e^{i\mathbf{p}\cdot\mathbf{x}} \left(i\mathbf{p}\cdot\tilde{\mathbf{u}}(\mathbf{p},\tau)\right) \\
&= i \int d^3\mathbf{p} \delta_D(\mathbf{k}-\mathbf{p}) \mathbf{p}\cdot\tilde{\mathbf{u}}(\mathbf{p},\tau) \\
&= i\mathbf{k}\cdot\tilde{\mathbf{u}}(\mathbf{k},\tau)
\end{aligned} \tag{2.116}$$

where we have used the definition of the Dirac delta:

$$\delta_D = \int \frac{d^3\mathbf{x}}{(2\pi)^3} e^{-i\mathbf{k}\cdot\mathbf{x}} \tag{2.117}$$

and, from equation (2.116), we have

$$\tilde{\mathbf{u}}(\mathbf{k},\tau) = -i\frac{\mathbf{k}}{k^2}\tilde{\theta}(\mathbf{k},\tau). \tag{2.118}$$

Hence, we take eq. (2.91) and we apply a Fourier transformation. The only non-trivial term is the non linear one, that is, $\nabla \cdot \delta(\mathbf{x},\tau)\mathbf{u}(\mathbf{x},\tau)$. If we Fourier transform it we obtain:

$$\begin{aligned}
&\int \frac{d^3\mathbf{x}}{(2\pi)^3} e^{-i\mathbf{k}\cdot\mathbf{x}} \nabla \cdot (\delta(\mathbf{x},\tau)\mathbf{u}(\mathbf{x},\tau)) = \int \frac{d^3\mathbf{x}}{(2\pi)^3} e^{-i\mathbf{k}\cdot\mathbf{x}} \times \\
&\qquad \times \nabla \cdot \int d^3\mathbf{k}_1 e^{i\mathbf{x}\cdot\mathbf{k}_1} \tilde{\delta}(\mathbf{k}_1,\tau) \int d^3\mathbf{k}_2 e^{i\mathbf{x}\cdot\mathbf{k}_2} \tilde{\delta}(\mathbf{k}_2,\tau) \\
&= \int\int\int \frac{d^3\mathbf{x}}{(2\pi)^3} d^3\mathbf{k}_1 d^3\mathbf{k}_2 e^{-i\mathbf{k}\cdot\mathbf{x}} \times \\
&\qquad \times \left[i\mathbf{k}_1 e^{i\mathbf{k}_1\cdot\mathbf{x}} e^{i\mathbf{k}_2\cdot\mathbf{x}} + i\mathbf{k}_2 e^{i\mathbf{k}_1\cdot\mathbf{x}} e^{i\mathbf{k}_2\cdot\mathbf{x}} \right] \tilde{\delta}(\mathbf{k}_1,\tau)\tilde{\mathbf{u}}(\mathbf{k}_2,\tau) \\
&= \int\int\int \frac{d^3\mathbf{x}}{(2\pi)^3} d^3\mathbf{k}_1 d^3\mathbf{k}_2 e^{-i\mathbf{x}(\mathbf{k}-\mathbf{k}_1-\mathbf{k}_2)} \left[\frac{\mathbf{k}_1\cdot\mathbf{k}_2}{k_2^2} + \frac{\mathbf{k}_2\cdot\mathbf{k}_2}{k_2^2} \right] \tilde{\delta}(\mathbf{k}_1,\tau)\tilde{\theta}(\mathbf{k}_2,\tau) \\
&= \int\int d^3\mathbf{k}_1 d^3\mathbf{k}_2 \delta_D\left(\mathbf{k}-\mathbf{k}_1-\mathbf{k}_2\right) \left[\frac{(\mathbf{k}_1+\mathbf{k}_2)\cdot\mathbf{k}_2}{k_2^2} \right] \tilde{\delta}(\mathbf{k}_1,\tau)\tilde{\theta}(\mathbf{k}_2,\tau)
\end{aligned} \tag{2.119}$$

where we have used eq. (2.118).
Now putting all the pieces together we obtain the Fourier transform of the **continuity equation**, that is:

$$\frac{\partial\tilde{\delta}(\mathbf{k},\tau)}{\partial\tau} + \tilde{\theta}(\mathbf{k},\tau) = -\int d^3\mathbf{k}_1 \int d^3\mathbf{k}_2 \delta_D\left(\mathbf{k}-\mathbf{k}_1-\mathbf{k}_2\right) \alpha(\mathbf{k}_1,\mathbf{k}_2)\tilde{\delta}(\mathbf{k}_1,\tau)\tilde{\theta}(\mathbf{k}_2,\tau) \tag{2.120}$$

where the function

$$\alpha(\mathbf{k}_1,\mathbf{k}_2) \equiv \frac{(\mathbf{k}_1+\mathbf{k}_2)\cdot\mathbf{k}_2}{k_2^2} \tag{2.121}$$

encodes the non-linearity of the evolution (mode coupling) and comes from the non-linear term in eq. (2.91). From eq. (2.120) we see that the evolution of $\tilde{\delta}(\mathbf{k},\tau)$ is determined by the mode coupling of the fields at all pair vectors $\mathbf{k}_1$ and $\mathbf{k}_2$ with sum equal to $\mathbf{k}$. This constraint comes from the property of translation invariance in a spatially homogeneous universe.

Now we can continue applying a Fourier transform to the Euler equation, that is eq. (2.99). First thing to do, we apply the divergence to the Euler equation and obtain:

$$\frac{\partial\theta(\mathbf{x},\tau)}{\partial\tau} + \mathcal{H}\theta(\mathbf{x},\tau) + \nabla^2\Phi = -\nabla\cdot\left[(\mathbf{u}\cdot\nabla)\,\mathbf{u}\right] \tag{2.122}$$

where, again, we are assuming to deal with a pressurless perfect fluid, that is $\sigma_{ij} \approx 0$. We recognize right away the Poisson equation:

$$\nabla^2\Phi = \frac{3}{2}\Omega_m(\tau)\mathcal{H}^2(\tau)\delta(\mathbf{x},\tau) \tag{2.123}$$

and therefore the only non trivial term we have to work out is the right hand side one. We apply the Fourier transform, the inverse Fourier transform and use eq. (2.118). We then come to:

$$\begin{aligned}
&-\int \frac{d^3\mathbf{x}}{(2\pi)^3} e^{-i\mathbf{k}\cdot\mathbf{x}} \nabla \left[-\left(\int d^3\mathbf{k}_1 e^{i\mathbf{k}_1\cdot\mathbf{x}} \frac{\mathbf{k}_1}{k_1^2}\tilde{\theta}(\mathbf{k}_1)\cdot\nabla \right) \left(\int d^3\mathbf{k}_2 e^{i\mathbf{k}_2\cdot\mathbf{x}} \frac{\mathbf{k}_2}{k_2^2}\tilde{\theta}(\mathbf{k}_2) \right) \right] \\
&= \int \frac{d^3\mathbf{x}}{(2\pi)^3} e^{-i\mathbf{k}\cdot\mathbf{x}} \nabla \left[\int d^3\mathbf{k}_1 \int d^3\mathbf{k}_2 e^{i\mathbf{k}_1\cdot\mathbf{x}} \frac{1}{k_1^2}\tilde{\theta}(\mathbf{k}_1) i\mathbf{k}_1\cdot\mathbf{k}_2 e^{i\mathbf{k}_2\cdot\mathbf{x}} \frac{\mathbf{k}_2}{k_2^2}\tilde{\theta}(\mathbf{k}_2) \right] \\
&= \int \frac{d^3\mathbf{x}}{(2\pi)^3} e^{-i\mathbf{k}\cdot\mathbf{x}} \nabla \left[i \int d^3\mathbf{k}_1 \int d^3\mathbf{k}_2 e^{i(\mathbf{k}_1+\mathbf{k}_2)\cdot\mathbf{x}} \frac{(\mathbf{k}_1\cdot\mathbf{k}_2)\,\mathbf{k}_2}{k_1^2 k_2^2}\tilde{\theta}(\mathbf{k}_1)\tilde{\theta}(\mathbf{k}_2) \right] \\
&= -\int \frac{d^3\mathbf{x}}{(2\pi)^3} e^{-i\mathbf{k}\cdot\mathbf{x}} \times \\
&\qquad \times \left[\int d^3\mathbf{k}_1 \int d^3\mathbf{k}_2 \frac{(\mathbf{k}_1+\mathbf{k}_2)\cdot(\mathbf{k}_1\cdot\mathbf{k}_2)\,\mathbf{k}_2}{k_1^2 k_2^2}\tilde{\theta}(\mathbf{k}_1)\tilde{\theta}(\mathbf{k}_2) e^{i(\mathbf{k}_1+\mathbf{k}_2)\cdot\mathbf{x}} \right]
\end{aligned} \tag{2.124}$$

Now we can take a closer look to the first line of eq. (2.124); we see that it is not symmetric under the change of the wave vectors $\mathbf{k}_1$ and $\mathbf{k}_2$ but, since this comes from the Fourier transform of the right hand side of eq. (2.122), which, under change of wave vectors, stays the same, we must find a way to make the first line of eq. (2.124) symmetric under change of wave vectors pairs. This is easily achieved simply summing to the first line the same exact term but with $\mathbf{k}_1$ and $\mathbf{k}_2$ changed, all divided by 2. By doing this we arrive exactly at the last term of eq. (2.124); the only thing we have left to do is to sum the following terms:

$$\frac{1}{2}\left(\frac{(\mathbf{k}_1+\mathbf{k}_2)\cdot(\mathbf{k}_1\cdot\mathbf{k}_2)\,\mathbf{k}_2}{k_1^2 k_2^2} + \frac{(\mathbf{k}_2+\mathbf{k}_1)\cdot(\mathbf{k}_2\cdot\mathbf{k}_1)\,\mathbf{k}_1}{k_1^2 k_2^2} \right) \tag{2.125}$$

which actually lead to a symmetric term:

$$\frac{(\mathbf{k}_1+\mathbf{k}_2)^2\,(\mathbf{k}_1\cdot\mathbf{k}_2)}{2k_1^2 k_2^2} \equiv \beta(\mathbf{k}_1,\mathbf{k}_2). \tag{2.126}$$

We thus obtain:

$$\begin{aligned}
&-\int \frac{d^3\mathbf{x}}{(2\pi)^3} e^{i(\mathbf{k}_1+\mathbf{k}_2-\mathbf{k})\cdot\mathbf{x}} \int d^3\mathbf{k}_1 \int d^3\mathbf{k}_2 \beta(\mathbf{k}_1,\mathbf{k}_2)\tilde{\theta}(\mathbf{k}_1)\tilde{\theta}(\mathbf{k}_2) \\
&\qquad = -\int d^3\mathbf{k}_1 \int d^3\mathbf{k}_2 \delta_D(\mathbf{k}-\mathbf{k}_1-\mathbf{k}_2)\beta(\mathbf{k}_1,\mathbf{k}_2)\tilde{\theta}(\mathbf{k}_1)\tilde{\theta}(\mathbf{k}_2).
\end{aligned} \tag{2.127}$$

Therefore the final form of the Fourier transform of the **Euler equation** is:

$$\frac{\partial\tilde{\theta}(\mathbf{k},\tau)}{\partial\tau}+\mathcal{H}(\tau)\tilde{\theta}(\mathbf{k},\tau)+\frac{3}{2}\Omega_m(\tau)\mathcal{H}^2(\tau)\tilde{\delta}(\mathbf{x},\tau)= \\ -\int d^3\mathbf{k}_1\int d^3\mathbf{k}_2\delta_D(\mathbf{k}-\mathbf{k}_1-\mathbf{k}_2)\beta(\mathbf{k}_1,\mathbf{k}_2)\tilde{\theta}(\mathbf{k}_1)\tilde{\theta}(\mathbf{k}_2). \tag{2.128}$$

2.3.5 Einstein-de Sitter Cosmology

Let us now consider an Einstein-de Sitter universe, for which $\Omega_m = 1$ and $\Omega_\Lambda = 0$. From the Friedmann equation (2.76) we have that $a(\tau) \sim \tau^2$ and $\mathcal{H}(\tau) = 2/\tau$ and scaling out an overall factor of $\mathcal{H}$ from the velocity field brings eqs. (2.120) and (2.128) into homogeneous form in τ or, equivalently, in $a(\tau)$ [35]. Therefore, the continuity and the Euler equation in Fourier space can formally be solved with the following perturbative expansion [39]:

$$\tilde{\delta}(\mathbf{k},\tau)=\sum_{n=1}^{\infty}a^n(\tau)\delta_n(\mathbf{k}) \tag{2.129}$$

$$\tilde{\theta}(\mathbf{k},\tau)=-\mathcal{H}(\tau)\sum_{n=1}^{\infty}a^n(\tau)\delta_n(\mathbf{k}) \tag{2.130}$$

where only the fastest growing mode is taken into account. At small a, the series are dominated by their first term, and since $\theta_1(\mathbf{k}) = \delta_1(\mathbf{k})$ from the continuity equation, $\delta_1(\mathbf{k})$ completely characterizes the linear fluctuations.
Equations (2.129) and (2.130) must satisfy eqs. (2.120) and (2.128). This lead to the following form for $\delta_n(\mathbf{k})$ and $\theta_n(\mathbf{k})$ in terms of the linear fluctuations:

$$\delta_n(\mathbf{k})=\int d^3\mathbf{q}_1\cdots\int d^3\mathbf{q}_n\delta_D(\mathbf{k}-\mathbf{q}_{1\cdots n})F_n(\mathbf{q}_1,\cdots,\mathbf{q}_n)\delta_1(\mathbf{q}_1)\cdots\delta_1(\mathbf{q}_n) \tag{2.131}$$

$$\theta_n(\mathbf{k})=\int d^3\mathbf{q}_1\cdots\int d^3\mathbf{q}_n\delta_D(\mathbf{k}-\mathbf{q}_{1\cdots n})G_n(\mathbf{q}_1,\cdots,\mathbf{q}_n)\delta_1(\mathbf{q}_1)\cdots\delta_1(\mathbf{q}_n) \tag{2.132}$$

where the PT kernels F_n and G_n are homogeneous functions of the wave vectors and are constructed according to the recursion relations ($n \geq 2$) [40]:

$$F_n(\mathbf{q}_1,\cdots,\mathbf{q}_n)=\sum_{m=1}^{n-1}\frac{G_m(\mathbf{q}_1,\cdots,\mathbf{q}_m)}{(2n+3)(n-1)}\Big[(2n+1)\alpha(\mathbf{k}_1,\mathbf{k}_2)F_{n-m}(\mathbf{q}_{m+1},\cdots,\mathbf{q}_n) \\ +2\beta(\mathbf{k}_1,\mathbf{k}_2)G_{n-m}(\mathbf{q}_{m+1},\cdots,\mathbf{q}_n)\Big], \tag{2.133}$$

$$G_n(\mathbf{q}_1,\cdots,\mathbf{q}_n)=\sum_{m=1}^{n-1}\frac{G_m(\mathbf{q}_1,\cdots,\mathbf{q}_m)}{(2n+3)(n-1)}\Big[3\alpha(\mathbf{k}_1,\mathbf{k}_2)F_{n-m}(\mathbf{q}_{m+1},\cdots,\mathbf{q}_n) + 2n\beta(\mathbf{k}_1,\mathbf{k}_2)G_{n-m}(\mathbf{q}_{m+1},\cdots,\mathbf{q}_n)\Big] \tag{2.134}$$

where $\mathbf{k}_1\equiv\mathbf{q}_1+\cdots+\mathbf{q}_m$, $\mathbf{k}_2\equiv\mathbf{q}_{m+1}+\cdots+\mathbf{q}_n$, $\mathbf{k}\equiv\mathbf{k}_1+\mathbf{k}_2$ and $F_1=G_1\equiv 1$. For $n=2$, if we symmetrize the expressions with respect to $\mathbf{q}_1$ and $\mathbf{q}_2$, we get:

$$F_2^{(s)}(\mathbf{q}_1,\mathbf{q}_2)=\frac{5}{7}+\frac{1}{2}\frac{\mathbf{q}_1\cdot\mathbf{q}_2}{q_1q_2}\left(\frac{q_1}{q_2}+\frac{q_2}{q_1}\right)+\frac{2}{7}\frac{(\mathbf{q}_1\cdot\mathbf{q}_2)^2}{q_1^2q_2^2}, \tag{2.135}$$

$$G_2^{(s)}(\mathbf{q}_1,\mathbf{q}_2)=\frac{3}{7}+\frac{1}{2}\frac{\mathbf{q}_1\cdot\mathbf{q}_2}{q_1q_2}\left(\frac{q_1}{q_2}+\frac{q_2}{q_1}\right)+\frac{4}{7}\frac{(\mathbf{q}_1\cdot\mathbf{q}_2)^2}{q_1^2q_2^2}. \tag{2.136}$$

Since it will be useful for future calculations of this work, we will list here also the (not symmetrized) explicit expression for $F_3(\mathbf{q}_1,\mathbf{q}_2,\mathbf{q}_3)$ [40]:

$$\begin{aligned}F_3(\mathbf{q}_1,\mathbf{q}_2,\mathbf{q}_3)=&\frac{1}{3q_1^2q_2^2q_3^2|\mathbf{q}_1+\mathbf{q}_2|^2}\left[\frac{1}{21}\mathbf{q}_1\cdot\mathbf{q}_2|\mathbf{q}_1+\mathbf{q}_2|^2+\frac{1}{14}q_2^2\mathbf{q}_1\cdot(\mathbf{q}_1+\mathbf{q}_2)\right]\\&\times\left[7q_3^2(\mathbf{q}_1+\mathbf{q}_2)\cdot(\mathbf{q}_1+\mathbf{q}_2+\mathbf{q}_3)+\mathbf{q}_3\cdot(\mathbf{q}_1+\mathbf{q}_2)|\mathbf{q}_1+\mathbf{q}_2+\mathbf{q}_3|^2\right]\\&+\frac{\mathbf{q}_1\cdot(\mathbf{q}_2+\mathbf{q}_3)|\mathbf{q}_1+\mathbf{q}_2+\mathbf{q}_3|^2}{3q_1^2q_2^2q_3^2|\mathbf{q}_2+\mathbf{q}_3|^2}\left[\frac{1}{21}\mathbf{q}_2\cdot\mathbf{q}_3|\mathbf{q}_2+\mathbf{q}_3|^2+\frac{1}{14}q_3^2\mathbf{q}_2\cdot(\mathbf{q}_2+\mathbf{q}_3)\right]\\&+\frac{\mathbf{q}_1\cdot(\mathbf{q}_1+\mathbf{q}_2+\mathbf{q}_3)}{18q_1^2q_2^2q_3^2}\Big[\mathbf{q}_2\cdot\mathbf{q}_3|\mathbf{q}_2+\mathbf{q}_3|^2+5q_3^2\mathbf{q}_2\cdot(\mathbf{q}_2+\mathbf{q}_3)\Big].\end{aligned} \tag{2.137}$$

In order to symmetrize eq. (2.137) we just do the following:

$$\begin{aligned}F_3^{(s)}(\mathbf{q}_1,\mathbf{q}_2,\mathbf{q}_3)=&\frac{1}{6}\Big[F_3(\mathbf{q}_1,\mathbf{q}_2,\mathbf{q}_3)+F_3(\mathbf{q}_1,\mathbf{q}_3,\mathbf{q}_2)+F_3(\mathbf{q}_2,\mathbf{q}_1,\mathbf{q}_3)\\&+F_3(\mathbf{q}_2,\mathbf{q}_3,\mathbf{q}_1)+F_3(\mathbf{q}_3,\mathbf{q}_2,\mathbf{q}_1)+F_3(\mathbf{q}_3,\mathbf{q}_1,\mathbf{q}_2)\Big]\end{aligned} \tag{2.138}$$

We can now derive the corresponding recursion relations for vertices ν_n and μ_n which are defined as follows:

$$\nu_n\equiv n!\int\frac{d\Omega_1}{4\pi}\cdots\frac{d\Omega_n}{4\pi}F_n(\mathbf{k}_1,\ldots,\mathbf{k}_n), \tag{2.139}$$

$$\mu_n\equiv n!\int\frac{d\Omega_1}{4\pi}\cdots\frac{d\Omega_n}{4\pi}G_n(\mathbf{k}_1,\ldots,\mathbf{k}_n). \tag{2.140}$$

The vertices ν_n and μ_n therefore are the spherical average of the PT kernels.

The angle integrations can be done recursively and we come to [35]:

$$\nu_n = \sum_{m=1}^{n-1} \binom{n}{m} \frac{\mu_m}{(2n+3)(n-1)} \left[(2n+1)\nu_{n-m} + \frac{2}{3}\mu_{n-m} \right], \tag{2.141}$$

$$\mu_n = \sum_{m=1}^{n-1} \binom{n}{m} \frac{\mu_m}{(2n+3)(n-1)} \left[3\nu_{n-m} + \frac{2}{3}n\mu_{n-m} \right]. \tag{2.142}$$

Thus, for each step in perturbation theory, the vertices are pure numbers. For example we have:

$$\nu_1 = 1, \quad \mu_1 = 1, \quad \nu_2 = \frac{34}{21}, \quad \mu_2 = -\frac{26}{21}. \tag{2.143}$$

The vertices recursion relations, i.e. eq. (2.141) and (2.142) are directly related to the spherical collapse dynamics [41]. In this context, the Fourier transform of the linear density field $\delta_1(\mathbf{k})$ depends only on the norm of $\mathbf{k}$, and this property is valid throughout the entire collapse. Therefore, the central density for such initial conditions can be written as:

$$\delta_{sc} = (a) \sum_n a^n \int d^3\mathbf{q}_1 \cdots \int d^3\mathbf{q}_n F_n(\mathbf{q}_1, \cdots, \mathbf{q}_n)\delta_1(|\mathbf{q}_1|) \cdots \delta_1(|\mathbf{q}_n|) \tag{2.144}$$

where we have used eq. (2.129) and eq. (2.131); moreover, we have assumed $\Omega_m = 1$ and "sc" stands for spherical collapse. Integrating over the angles one obtains:

$$\delta_{sc}(a) = \sum_n \frac{\nu_n}{n!} a^n \xi^n \tag{2.145}$$

where

$$\xi = \int d^3\mathbf{q}\delta_1(|\mathbf{q}|). \tag{2.146}$$

Analogously, the velocity divergence for the spherical collapse can be expanded in terms of the μ_n parameters. Therefore, we reach an important result, valid for any cosmology: the angular average of the PT kernels is strictly related to the dynamics of the spherical collapse.

2.3.6 Beyond Einstein-de Sitter Cosmology

We have found, in the last section, the symmetrized PT kernels, which come from the recursion relations, eq. (2.133) and eq. (2.134). It is important to note that we will use these results in the rest of this work, in particular in Sec. (2.4) when obtaining the analytic form of the perturbed power spectrum and bispectrum.
However, we have obtained eq. (2.131) and eq. (2.132), which are the solutions of the

equation of motions of the density and the divergence field, and the PT kernels in the frame of an Einstein-de Sitter universe. Why are we allowed to use these solutions also in an arbitrary cosmology?
In a more general cosmology, the PT expansion is more complicated because the solutions at each order become non-separable functions of τ and $\mathbf{k}$ [42].
However, what happens is that we can write, in the spherical collapse approximation, the PT kernels order by order using the solutions found with the recursion relations of the vertices, i.e.:

$$\delta(\tau) = \sum_{n}^{\infty} \frac{\nu_n(\tau)}{n!} [D_1(\tau)\xi]^n, \tag{2.147}$$

$$\theta(\tau) = -\mathcal{H}(\tau) f(\Omega_m, \Omega_\Lambda) \sum_{n}^{\infty} \frac{\mu_n(\tau)}{n!} [D_1(\tau)\xi]^n. \tag{2.148}$$

Following [35], from eqs. (2.120) and (2.128), we obtain

$$\frac{\mathrm{d}\nu_n}{\mathrm{d}\log D_1} + n\nu_n - \mu_n = \sum_{m=1}^{n-1} \binom{n}{m} \nu_{n-m}\mu_m \tag{2.149}$$

$$\frac{\mathrm{d}\mu_n}{\mathrm{d}\log D_1} + n\mu_n + \left(\frac{3\Omega_m}{2f^2} - 1\right)\mu_n - \frac{3\Omega_m}{2f^2}\nu_n = \frac{1}{3}\sum_{m=1}^{n-1} \binom{n}{m} \mu_{n-m}\mu_m \tag{2.150}$$

These differential equations can be solved numerically at each order and [43] the results for $n = 2$ and $n = 3$ show that indeed the dependence of the vertices (which are, as we have said, simply the spherical average of the PT kernels) on cosmological parameters is a few percent effect at most.
This, as [44] shows, means that performing a simple approximation to the equations of motion for general Ω_m and Ω_Λ leads to separable solutions to arbitrary order in PT and the same recursion relations as in the Einstein–de Sitter case; moreover, all the information on the dependence of the PT solutions on Ω_m and Ω_Λ is retained in $D_1(\tau)$, the linear growth factor.
In perturbation theory, in the linear case, the growing-mode solution to the equations of motion (2.120) and (2.128) is:

$$\delta(\mathbf{k}, \tau) = D_1(\tau)\delta_1(\mathbf{k}), \tag{2.151}$$

$$\theta(\mathbf{k}, \tau) = -\mathcal{H}(\tau) f(\Omega_m, \Omega_\Lambda) D_1(\tau)\delta_1(\mathbf{k}). \tag{2.152}$$

We proceed as in the Einstein-de Sitter case, and we look for separable solutions as eqs. (2.129) and (2.130); we can write:

$$\delta(\mathbf{k}, \tau) = \sum_{n=1}^{\infty} D_n(\tau)\delta_n(\mathbf{k}), \tag{2.153}$$

$$\theta(\mathbf{k},\tau) = -\mathcal{H}(\tau) f(\Omega_m,\Omega_\Lambda) \sum_{n=1}^{\infty} E_n(\tau)\theta_n(\mathbf{k}). \tag{2.154}$$

Inserting them into the equations of motion leads to:

$$\frac{\mathrm{d}D_n}{\mathrm{d}\log D_1}\delta_n - E_n\theta_n = \int d^3\mathbf{k}_1 d^3\mathbf{k}_2 \delta_D(\mathbf{k}-\mathbf{k}_{12})\alpha(\mathbf{k},\mathbf{k}_1)\sum_{m=1}^{n-1} D_{n-m}E_m\theta_m(\mathbf{k}_1)\delta_{n-m}(\mathbf{k}_2) \tag{2.155}$$

$$\begin{aligned}\frac{\mathrm{d}E_n}{\mathrm{d}\log D_1}\theta_n + \left(\frac{3\Omega_m}{2f^2}\right)E_n\theta_n - \frac{3\Omega_m}{2f^2}D_n\delta_n \\ = \int d^3\mathbf{k}_1 d^3\mathbf{k}_2 \delta_D(\mathbf{k}-\mathbf{k}_{12})\beta(\mathbf{k},\mathbf{k}_1,\mathbf{k}_2)\sum_{m=1}^{n-1} E_{n-m}E_m\theta_m(\mathbf{k}_1)\theta_{n-m}(\mathbf{k}_2).\end{aligned} \tag{2.156}$$

It is interesting to note that if we put $f(\Omega_m,\Omega_\Lambda) = \Omega_m^{1/2}$ then the system of equations becomes separable, with $D_n = E_n = D_1^n$. This means that these relations reduce to the recursion relation of the Einstein-de Sitter case ($\Omega_m = 1$ and $\Omega_\Lambda = 0$), leading to same PT kernels. Obviously, we need to understand if $f(\Omega_m,\Omega_\Lambda) = \Omega_m^{1/2}$ is a good choice to describe an arbitrary cosmology. The answer is yes. In fact, we have already seen in eq. (2.112) that, when $\Omega_m = 1$ and $\Omega_\Lambda = 0$, $f(\Omega_m,\Omega_\Lambda) = 1$. However, for generic values of Ω_m and Ω_Λ the linear growth factor admits the following integral representation [45]:

$$D_1^{(+)} = a^3 H(a)\frac{5\Omega_m}{2}\int_0^a \frac{da}{a^3H^3(a)} \tag{2.157}$$

where

$$H(a) = \sqrt{\Omega_m^0 a^{-3} + (1-\Omega_m^0-\Omega_\Lambda^0)a^{-2} + \Omega_\Lambda^0}. \tag{2.158}$$

Furthermore, we can make the following approximation [46]:

$$D_1^{(+)} \approx \left(\frac{5}{2}\right)\frac{a\Omega_m}{\Omega_m^{4/7} - \Omega_\Lambda + (1+\Omega_m/2)(1+\Omega_\Lambda/70)} \tag{2.159}$$

$$D_1^{(-)} = \frac{\mathcal{H}}{a} \tag{2.160}$$

$$f(\Omega_m,\Omega_\Lambda) \approx \frac{1}{[1-(\Omega_0-\Omega_\Lambda^0-1)a+\Omega_\Lambda^0 a^3]^{0.6}}. \tag{2.161}$$

Finally, When $\Omega_m + \Omega_\Lambda = 1$ we have

$$f(\Omega_m,\Omega_\Lambda) = f(\Omega_m, 1-\Omega_m) \approx \Omega_m^{5/9}. \tag{2.162}$$

Therefore, setting $f(\Omega_m,\Omega_\Lambda) = \Omega_m^{1/2}$ is indeed a good approximation.

2.4 Wick Theorem and Perturbed Power Spectra

We have already introduced the concept of the power spectrum in Sec. 2.1.2. In particular, equation (2.28) holds, namely:

$$\langle \delta(\mathbf{k})\delta(\mathbf{k}')\rangle = \delta_D(\mathbf{k}+\mathbf{k}')P(k). \tag{2.163}$$

Moreover, being the field Gaussian, i.e. when any joint distribution of local densities is Gaussian distributed, we also have that any property of the field can be fully described by its mean value and it covariance (the two-point correlation function ξ). We can generalize this by saying that any ensemble average of product of variables can then be obtained by product of ensemble averages of pairs [35]. We write explicitly this property for the Fourier modes as follows:

$$\begin{aligned} \langle \delta(\mathbf{k}_1)\cdots\delta(\mathbf{k}_{2p+1})\rangle &= 0 \\ \langle \delta(\mathbf{k}_1)\cdots\delta(\mathbf{k}_{2p})\rangle &= \sum_p \prod_{\text{pairs (i,j)}} \langle \delta(\mathbf{k}_i)\delta(\mathbf{k}_j)\rangle \end{aligned} \tag{2.164}$$

where the sum is made over p, which stands for all possible pair associations. This fundamental result is called **Wick theorem**. Eq. (2.164) is telling us that the statistical properties of the random variables $\delta(\mathbf{k})$ are entirely determined by the shape and normalization of $P(k)$. As we have mentioned before, in the inflationary scenario the initial energy fluctuations are supposed to be Gaussian [47]. This means that the relations in eq. (2.164) are verified for all modes that exit the Hubble radius and long afterwards come back into the horizon as classical stochastic perturbations.
In general, it is possible to define higher-order correlation functions. They are defined as the connected part (denoted with subscript c) of the joint ensemble average of the density in an arbitrarily number of locations. We can formally write these correlation functions as [35]:

$$\begin{aligned} \xi_N(\mathbf{x}_1,\ldots,\mathbf{x}_N) &= \langle \delta(\mathbf{x}_1),\ldots,\delta(\mathbf{x}_N)_c\rangle \\ &= \langle \delta(\mathbf{x}_1),\ldots,\delta(\mathbf{x}_N)\rangle - \sum_{\mathcal{C}\in\mathcal{P}}\prod_{s_i\in\mathcal{C}} \xi_{\#s_i}(\mathbf{x}_{s_i(1)},\ldots,\mathbf{x}_{s_i(\#s_i)}) \end{aligned} \tag{2.165}$$

where the sum is made over the proper partitions (any partition except the set itself) of $\mathcal{P}(\{\mathbf{x}_1,\cdots,\mathbf{x}_N\})$ and s_i is thus a subset of $\{\mathbf{x}_1,\cdots,\mathbf{x}_N\}$ contained in partition $\mathcal{C}$. When the average of $\delta(\mathbf{x})$ is defined as zero, only partitions that contain no singlets contribute.
We can visualize the decomposition of connected and not-connected part in Fig. 2.8.
As we have already said, when treating Gaussian fields, as a consequence of Wick theorem, all connected correlation functions are zero except ξ_2. As a result, the only non-zero connected part is the two-point correlation function. Therefore the statistical properties of any Gaussian field can be written in terms of combinations of two-point functions of δ.

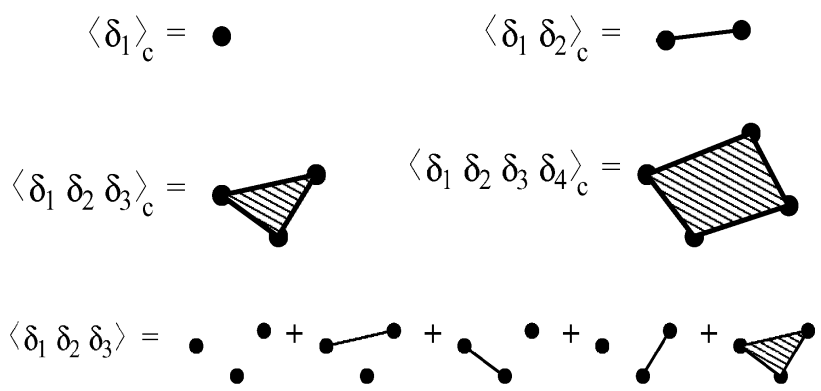

Figure 2.8: The figure shows the decomoposition in connected and not conneceted part of ensemble avarages. In particular, the first two lines represent connected part of moments. In the last line, instead, the three-point moment is "written" in terms of connected parts. Figure taken from [35].

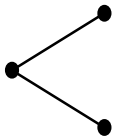

Figure 2.9: Tree-level diagram for the three-point function or Bispectrum. Figure taken from [35].

In Fourier space these definitions are extremely useful. Because of homogeneity of space, we have that $\langle \delta(\mathbf{k}_1) \cdots \delta(\mathbf{k}_N) \rangle_c$ is always proportional to the Dirac delta. Thus we can write

$$\langle \delta(\mathbf{k}_1) \cdots \delta(\mathbf{k}_N) \rangle_c = \delta_D(\mathbf{k}_1 + \cdots + \mathbf{k}_N) P_N(\mathbf{k}_1, \ldots, \mathbf{k}_N). \tag{2.166}$$

However, as we have previously said, the dynamics of gravitational instability is non-linear, hence non-linear evolution unavoidably leads to the development of non-Gaussian features. The statistical characterization of non-Gaussian fields is definitely a non-trivial subject and, as already mentioned, the problem is that in principle all N-point correlation functions are needed to specify the statistical properties of cosmic fields. In order to help us in this characterization, we continue in implementing a figurative way to approach this problem. We thus show in Fig. 2.9 the tree-diagram describing the three-point function induced by gravity. Let us remind that the lines coming out of a specific vertex describe the order in perturbation theory needed to construct that given diagram. In this way, the tree-diagram of the bispectrum (Fig. 2.9) is:

$$\langle \delta_2(1)\delta_1(2)\delta_1(3) \rangle + \langle \delta_1(1)\delta_2(2)\delta_1(3) \rangle + \langle \delta_1(1)\delta_1(2)\delta_2(3) \rangle \tag{2.167}$$

where the subscripts indeed represent the order in perturbation theory which gives rise to that diagram. Let us note, also, that eq. (2.167) is composed of three terms because we have to take into account all the possible permutations of Fig. 2.9.
In general, a consistent calculation of the connected p-point function induced by gravity

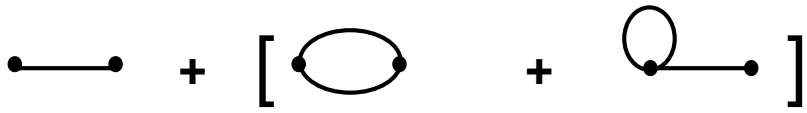

Figure 2.10: One-loop diagram for the two point function or Power Spectrum. Figure taken from [35].

to leading order, what we have called "tree-level", requires from first to $(p-1)$th order in PT [48]. At small scales corrections to tree-level PT are needed. These are naturally described in terms of diagrams as well, in particular, the next to leading order contributions, the so called "one-loop" corrections, which require from first to $(p+1)$th order in PT. These are represented by one-loop diagrams, i.e. connected diagrams where there is one closed loop (Fig. 2.10). In this case the one-loop diagram for the power spectrum is:

$$\langle\delta_1(1)\delta_1(2)\rangle + \langle\delta_2(1)\delta_2(2)\rangle + \langle\delta_3(1)\delta_1(2)\rangle + \langle\delta_1(1)\delta_3(2)\rangle \tag{2.168}$$

where, as well as for the bispectrum, we have to take into account all possible permutations of Fig. 2.10, thus explaining why eq. (2.168) is made out of four terms. The one-loop corrections to the power spectrum describe the non-linear corrections to the linear evolution, that is, the effects of mode coupling and the beginning of non-linear structure growth. Recall that each line in a diagram represents the power spectrum $P^{(0)}(k)$ (or two-point function) of the linear density field.

2.4.1 Tree-Level Bispectrum

We can now proceed in calculating the bispectrum (induced by gravity) at tree level. The bispectrum $B(k_1, k_2, k_3, \tau)$ is defined by

$$\langle\tilde{\delta}(\mathbf{k}_1,\tau)\tilde{\delta}(\mathbf{k}_2,\tau)\tilde{\delta}(\mathbf{k}_3,\tau)\rangle = \delta_D(\mathbf{k}_1+\mathbf{k}_2+\mathbf{k}_3)B(k_1,k_2,k_3,\tau). \tag{2.169}$$

As shown in eq. (2.167) the Bispectrum at tree level is made up of three terms:

$$\begin{aligned}\langle\tilde{\delta}(\mathbf{k}_1,\tau)\tilde{\delta}(\mathbf{k}_2,\tau)\tilde{\delta}(\mathbf{k}_3,\tau)\rangle &= \langle\delta_2(\mathbf{k}_1,\tau)\delta_1(\mathbf{k}_2,\tau)\delta_1(\mathbf{k}_3,\tau)\rangle \\ &+ \langle\delta_1(\mathbf{k}_1,\tau)\delta_2(\mathbf{k}_2,\tau)\delta_1(\mathbf{k}_3,\tau)\rangle + \langle\delta_1(\mathbf{k}_1,\tau)\delta_1(\mathbf{k}_2,\tau)\delta_2(\mathbf{k}_3,\tau)\rangle.\end{aligned} \tag{2.170}$$

Let us calculate the first term explicitly. Using eq. (2.131) and (2.132) we have that:

$$\begin{aligned}\langle\delta_2(\mathbf{k}_1,\tau)\delta_1(\mathbf{k}_2,\tau)\delta_1(\mathbf{k}_3,\tau)\rangle &= \\ &\langle\int d^3\mathbf{q}\int d^3\mathbf{p}\,\delta_D(\mathbf{k}_1-\mathbf{q}-\mathbf{p})F_2(\mathbf{q},\mathbf{p})\delta(\mathbf{q})\delta(\mathbf{p})\delta(\mathbf{k}_2)\delta(\mathbf{k}_3)\rangle \\ &= \int d^3\mathbf{q}\int d^3\mathbf{p}\,\delta_D(\mathbf{k}_1-\mathbf{q}-\mathbf{p})F_2(\mathbf{q},\mathbf{p})\langle\delta(\mathbf{q})\delta(\mathbf{p})\delta(\mathbf{k}_2)\delta(\mathbf{k}_3)\rangle.\end{aligned} \tag{2.171}$$

Now, due to the Wick theorem, eq. (2.164), we can arrange the term in brackets as follows:

$$\begin{aligned}\langle\delta(\mathbf{q})\delta(\mathbf{p})\delta(\mathbf{k}_2)\delta(\mathbf{k}_3)\rangle =&\langle\delta(\mathbf{q})\delta(\mathbf{p})\rangle\langle\delta(\mathbf{k}_2)\delta(\mathbf{k}_3)\rangle + \langle\delta(\mathbf{q})\delta(\mathbf{k}_2)\rangle\langle\delta(\mathbf{p})\delta(\mathbf{k}_3)\rangle \\ &+ \langle\delta(\mathbf{q})\delta(\mathbf{k}_3)\rangle\langle\delta(\mathbf{p})\delta(\mathbf{k}_2)\rangle.\end{aligned} \tag{2.172}$$

Therefore, eq. (2.171) becomes:

$$\begin{aligned}&= \int d^3\mathbf{q}\int d^3\mathbf{p}\,\delta_D(\mathbf{k}_1-\mathbf{q}-\mathbf{p})F_2(\mathbf{q},\mathbf{p})\Big[\langle\delta(\mathbf{q})\delta(\mathbf{p})\rangle\langle\delta(\mathbf{k}_2)\delta(\mathbf{k}_3)\rangle \\ &\qquad + \langle\delta(\mathbf{q})\delta(\mathbf{k}_2)\rangle\langle\delta(\mathbf{p})\delta(\mathbf{k}_3)\rangle + \langle\delta(\mathbf{q})\delta(\mathbf{k}_3)\rangle\langle\delta(\mathbf{p})\delta(\mathbf{k}_2)\rangle\Big] \\ &= \int d^3\mathbf{q}F_2(\mathbf{q},\mathbf{k}_1-\mathbf{q})\Big[\delta_D(\mathbf{k}_1)\delta_D(\mathbf{k}_2+\mathbf{k}_3)P^{(0)}(q)P^{(0)}(k_2) \\ &\qquad + \delta_D(\mathbf{q}+\mathbf{k}_2)\delta_D(\mathbf{k}_1+\mathbf{k}_3-\mathbf{q})P^{(0)}(k_2)P^{(0)}(k_3) \\ &\qquad + \delta_D(\mathbf{q}+\mathbf{k}_3)\delta_D(\mathbf{k}_1+\mathbf{k}_2-\mathbf{q})P^{(0)}(k_3)P^{(0)}(k_2)\Big],\end{aligned}$$

where in the last passage we have used the definition of the power spectrum, eq. (2.28). Moreover, since the first term in square brackets vanishes, we obtain:

$$\langle\delta_2(\mathbf{k}_1,\tau)\delta_1(\mathbf{k}_2,\tau)\delta_1(\mathbf{k}_3,\tau)\rangle = 2\delta_D(\mathbf{k}_1+\mathbf{k}_2+\mathbf{k}_3)F_2(\mathbf{k}_2,\mathbf{k}_3)P^{(0)}(k_2)P^{(0)}(k_3). \tag{2.173}$$

Finally, considering all terms of eq. (2.170) we arrive to:

$$\begin{aligned}\langle\tilde{\delta}(\mathbf{k}_1,\tau)\tilde{\delta}(\mathbf{k}_2,\tau)\tilde{\delta}(\mathbf{k}_3,\tau)\rangle = \delta_D(\mathbf{k}_1+\mathbf{k}_2+\mathbf{k}_3)\times \\ \Big[2F_2(\mathbf{k}_2,\mathbf{k}_3)P^{(0)}(k_2)P^{(0)}(k_3) \\ + 2F_2(\mathbf{k}_1,\mathbf{k}_3)P^{(0)}(k_1)P^{(0)}(k_3) \\ + 2F_2(\mathbf{k}_1,\mathbf{k}_2)P^{(0)}(k_1)P^{(0)}(k_2)\Big],\end{aligned} \tag{2.174}$$

obtaining a final form for the bispectrum computed at tree level:

$$B(k_1,k_2,k_3) = 2F_2(\mathbf{k}_1,\mathbf{k}_2)P^{(0)}(k_1)P^{(0)}(k_2) + cycl. \tag{2.175}$$

where, since we have calculated equal time correlators, we have omitted the time dependence.

2.4.2 One-Loop Power Spectrum

Now we proceed in calculating the power spectrum at one-loop in perturbation theory. As we can see from eq. (2.168) the one-loop power spectrum is made up of four terms:

$$\begin{aligned}\langle\tilde{\delta}(\mathbf{k}_1,\tau)\tilde{\delta}(\mathbf{k}_2,\tau)\rangle = \langle\delta_1(\mathbf{k}_1,\tau)\delta_1(\mathbf{k}_2,\tau)\rangle + \langle\delta_2(\mathbf{k}_1,\tau)\delta_2(\mathbf{k}_2,\tau)\rangle \\ + \langle\delta_3(\mathbf{k}_1,\tau)\delta_1(\mathbf{k}_2,\tau)\rangle + \langle\delta_1(\mathbf{k}_1,\tau)\delta_3(\mathbf{k}_2,\tau)\rangle.\end{aligned} \tag{2.176}$$

The first term is just:

$$\langle\delta_1(\mathbf{k}_1)\delta_1(\mathbf{k}_2)\rangle = \delta_D(\mathbf{k}_1+\mathbf{k}_2)P^{(0)}(k_1). \tag{2.177}$$

The second term is, instead, a little bit more complicated.

$$\begin{aligned}\langle\delta_2(\mathbf{k}_1)\delta_2(\mathbf{k}_2)\rangle &= \langle\int d^3\mathbf{q}_1\int d^3\mathbf{q}_2\delta_D(\mathbf{k}_1-\mathbf{q}_1-\mathbf{q}_2)F_2(\mathbf{q}_1,\mathbf{q}_2)\delta(\mathbf{q}_1)\delta(\mathbf{q}_2) \\ &\quad\times\int d^3\mathbf{p}_1\int d^3\mathbf{p}_2\delta_D(\mathbf{k}_1-\mathbf{p}_1-\mathbf{p}_2)F_2(\mathbf{p}_1,\mathbf{p}_2)\delta(\mathbf{p}_1)\delta(\mathbf{p}_2)\rangle \\ &= \langle\int d^3\mathbf{q}_1F_2(\mathbf{q}_1,\mathbf{k}_1-\mathbf{q}_1)\delta(\mathbf{q}_1)\delta(\mathbf{k}_1-\mathbf{q}_1) \\ &\quad\times\int d^3\mathbf{p}_1F_2(\mathbf{p}_1,\mathbf{k}_2-\mathbf{p}_1)\delta(\mathbf{p}_1)\delta(\mathbf{k}_2-\mathbf{p}_1)\rangle \\ &= \int d^3\mathbf{q}_1\int d^3\mathbf{p}_1F_2(\mathbf{q}_1,\mathbf{k}_1-\mathbf{q}_1)F_2(\mathbf{p}_1,\mathbf{k}_2-\mathbf{p}_1) \\ &\quad\times\langle\delta(\mathbf{q}_1)\delta(\mathbf{k}_1-\mathbf{q}_1)\delta(\mathbf{p}_1)\delta(\mathbf{k}_2-\mathbf{p}_1)\rangle.\end{aligned} \tag{2.178}$$

Then, thanks to the Wick theorem, eq. (2.164), we can arrange the last line of eq. (2.178) as follows:

$$
\begin{aligned}
&= \int d^3\mathbf{q}_1 \int d^3\mathbf{p}_1 F_2(\mathbf{q}_1, \mathbf{k}_1 - \mathbf{q}_1) F_2(\mathbf{p}_1, \mathbf{k}_2 - \mathbf{p}_1) \times \\
&\qquad \Big[\langle \delta(\mathbf{q}_1)\delta(\mathbf{k}_1 - \mathbf{q}_1)\rangle \langle \delta(\mathbf{p}_1)\delta(\mathbf{k}_2 - \mathbf{p}_1)\rangle \\
&\qquad + \langle \delta(\mathbf{q}_1)\delta(\mathbf{p}_1)\rangle \langle \delta(\mathbf{k}_1 - \mathbf{q}_1)\delta(\mathbf{k}_2 - \mathbf{p}_1)\rangle \\
&\qquad + \langle \delta(\mathbf{q}_1)\delta(\mathbf{k}_2 - \mathbf{p}_1)\rangle \langle \delta(\mathbf{k}_1 - \mathbf{q}_1)\delta(\mathbf{p}_1)\rangle \Big] \\
&= \int d^3\mathbf{q}_1 \int d^3\mathbf{p}_1 F_2(\mathbf{q}_1, \mathbf{k}_1 - \mathbf{q}_1) F_2(\mathbf{p}_1, \mathbf{k}_2 - \mathbf{p}_1) \times \\
&\qquad \Big[\delta_D(\mathbf{k}_1)\delta_D(\mathbf{k}_2) P^{(0)}(|\mathbf{k}_1 - \mathbf{q}_1|) P^{(0)}(|\mathbf{k}_2 - \mathbf{p}_1|) \\
&\qquad + \delta_D(\mathbf{q}_1 + \mathbf{p}_1)\delta_D(\mathbf{k}_1 + \mathbf{k}_2 - \mathbf{q}_1 - \mathbf{p}_1) P^{(0)}(q_1) P^{(0)}(|\mathbf{k}_1 - \mathbf{q}_1|) \\
&\qquad + \delta_D(\mathbf{q}_1 + \mathbf{k}_2 - \mathbf{p}_1)\delta_D(\mathbf{k}_1 + \mathbf{p}_1 - \mathbf{q}_1) P^{(0)}(q_1) P^{(0)}(|\mathbf{k}_1 - \mathbf{q}_1|) \Big] \\
&= \int d^3\mathbf{q}_1 F_2(\mathbf{q}_1, \mathbf{k}_1 - \mathbf{q}_1) F_2(\mathbf{q}_1 - \mathbf{k}_1, -\mathbf{q}_1) \Big[\delta_D(\mathbf{k}_1 + \mathbf{k}_2) P^{(0)}(q_1) P^{(0)}(|\mathbf{k}_1 - \mathbf{q}_1|) \\
&\qquad + \delta_D(\mathbf{k}_1 + \mathbf{k}_2) P^{(0)}(q_1) P^{(0)}(|\mathbf{k}_1 - \mathbf{q}_1|) \Big].
\end{aligned}
\tag{2.179}
$$

Now, we exploit the fact that $F_2(\mathbf{q}_1, \mathbf{k}_1 - \mathbf{q}_1) = F_2(\mathbf{q}_1 - \mathbf{k}_1, -\mathbf{q}_1)$, thus obtaining the final form for the second term:

$$
\langle \delta_2(\mathbf{k}_1)\delta_2(\mathbf{k}_2)\rangle = 2\delta_D(\mathbf{k}_1 + \mathbf{k}_2) \int d^3\mathbf{q} \Big[F_2(\mathbf{q}, \mathbf{k}_1 - \mathbf{q}) \Big]^2 P^{(0)}(q) P^{(0)}(|\mathbf{k}_1 - \mathbf{q}|). \tag{2.180}
$$

We move forward calculating the third term, which reads:

$$\begin{aligned}
\langle\delta_3(\mathbf{k}_1)\delta_1(\mathbf{k}_2)\rangle &= \langle\int d^3\mathbf{q}_1\int d^3\mathbf{q}_2\int d^3\mathbf{q}_3\delta_D(\mathbf{k}_1-\mathbf{q}_1-\mathbf{q}_2-\mathbf{q}_3)\\
&\qquad\times F_3(\mathbf{q}_1,\mathbf{q}_2,\mathbf{q}_3)\delta(\mathbf{q}_1)\delta(\mathbf{q}_2)\delta(\mathbf{q}_3)\delta(\mathbf{k}_2)\rangle\\
&= \int d^3\mathbf{q}_1\int d^3\mathbf{q}_2 F_3(\mathbf{q}_1,\mathbf{q}_2,\mathbf{k}_1-\mathbf{q}_1-\mathbf{q}_2)\\
&\qquad\times\langle\delta(\mathbf{q}_1)\delta(\mathbf{q}_2)\delta(\mathbf{k}_1-\mathbf{q}_1-\mathbf{q}_2)\delta(\mathbf{k}_2)\rangle\\
&= \int d^3\mathbf{q}_1\int d^3\mathbf{q}_2 F_3(\mathbf{q}_1,\mathbf{q}_2,\mathbf{k}_1-\mathbf{q}_1-\mathbf{q}_2)\\
&\quad\times\Big[\delta_D(\mathbf{q}_1+\mathbf{q}_2)P^{(0)}(q_1)\delta_D(\mathbf{k}_1+\mathbf{k}_2-\mathbf{q}_1-\mathbf{q}_2)P^{(0)}(|\mathbf{k}_1-\mathbf{q}_1-\mathbf{q}_2|)\\
&\qquad+\delta_D(\mathbf{k}_1-\mathbf{q}_2)P^{(0)}(q_1)\delta_D(\mathbf{k}_2+\mathbf{q}_2)P^{(0)}(k_2)\\
&\qquad+\delta_D(\mathbf{q}_1+\mathbf{k}_2)P^{(0)}(q_1)\delta_D(\mathbf{k}_1-\mathbf{q}_1)P^{(0)}(|\mathbf{k}_1-\mathbf{q}_1-\mathbf{q}_2|)\Big]\\
&= \delta_D(\mathbf{k}_1+\mathbf{k}_2)\int d^3\mathbf{q}_1 F_3(\mathbf{q}_1,-\mathbf{q}_1,\mathbf{k}_1)\Big[P^{(0)}(q_1)P^{(0)}(k_1)\\
&\qquad+P^{(0)}(q_1)P^{(0)}(k_2)+P^{(0)}(q_1)P^{(0)}(k_1)\Big].
\end{aligned}$$

The final form of the third term is then:

$$\langle\delta_3(\mathbf{k}_1)\delta_1(\mathbf{k}_2)\rangle = 3\delta_D(\mathbf{k}_1+\mathbf{k}_2)\int d^3\mathbf{q}F_3(\mathbf{q},-\mathbf{q},\mathbf{k}_1)P^{(0)}(q)P^{(0)}(k_1) \tag{2.181}$$

whereas the fourth term can be derived in the same way as the third one.
Thus, gathering all the four terms, we obtain the shape of the one-loop power spectrum:

$$\begin{aligned}
P_{1-loop}(k_1) = \delta_D(\mathbf{k}_1+\mathbf{k}_2)\Big[P^{(0)}(k_1)+2\int d^3\mathbf{q}\big[F_2(\mathbf{q},\mathbf{k}_1-\mathbf{q})\big]^2P^{(0)}(q)P^{(0)}(|\mathbf{k}_1-\mathbf{q}|)\\
+6\int d^3\mathbf{q}F_3(\mathbf{q},-\mathbf{q},\mathbf{k}_1)P^{(0)}(q)P^{(0)}(k_1)\Big].
\end{aligned} \tag{2.182}$$

where we have indicated $P_{1-loop}(k_1)\equiv\langle\tilde{\delta}(\mathbf{k}_1)\tilde{\delta}(\mathbf{k}_2)\rangle$.
In particular, we can write the power spectrum up to one-loop corrections as:

$$P_{1-loop}(k) = P^{(0)}(k)+P^{(1)}(k) \tag{2.183}$$

where the first order contributions can be written as

$$P^{(1)}(k) = P_{22}(k)+P_{13}(k), \tag{2.184}$$

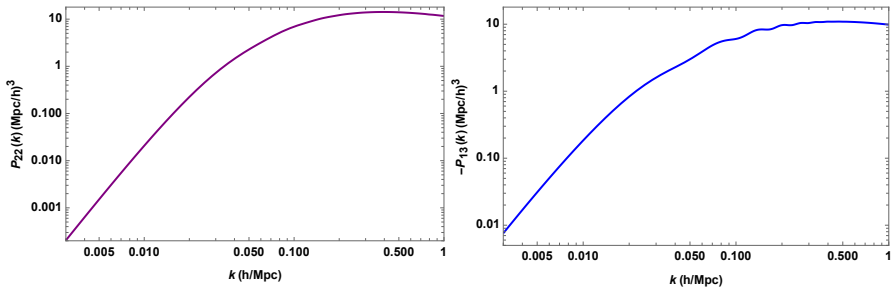

Figure 2.11: We have calculated explicitly from eq. (2.185) and eq. (2.186) $P_{22}(k)$ and $P_{13}(k)$, depicted in the left and right panel respectively. Note that we have plotted $-P_{13}(k)$. Both $P_{22}(k)$ and $P_{13}(k)$ assume small values at low k and they grow considerably going towards smaller scales.

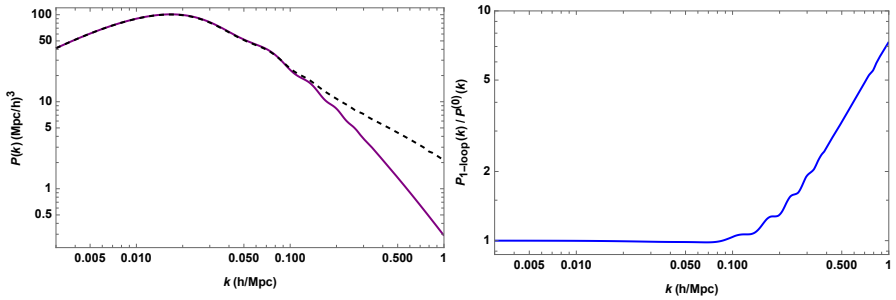

Figure 2.12: In the left panel is represented the linear power spectrum at $z = 0$, $P^{(0)}(k)$ (purple), and the power spectrum calculated up to one loop corrections, $P_{1-loop}(k)$ (dashed). In the right panel the ratio between $P_{1-loop}(k)$ and $P^{(0)}(k)$ is shown. We see that $k \sim 0.1$ represents the end of the validity of the linear regime.

so that

$$P_{22}(k) = 2 \int d^3\mathbf{q} \big[F_2(\mathbf{q}, \mathbf{k}-\mathbf{q})\big]^2 P^{(0)}(q) P^{(0)}(|\mathbf{k}-\mathbf{q}|), \tag{2.185}$$

$$P_{13}(k) = 6 \int d^3\mathbf{q} F_3(\mathbf{q}, -\mathbf{q}, \mathbf{k}) P^{(0)}(q) P^{(0)}(k), \tag{2.186}$$

which are depicted in Fig. 2.11. We see that the one loop corrections to the integral grow considerably with incresing wavenumber. However, the $P_{22}(k)$ is positive, whereas $P_{13}(k)$ is negative. In this way the two corrections almost equal each other, leading to an overall small correction.
In addition, we show in Fig. 2.12 the one-loop power spectrum P_{1-loop} compared to the linear matter power spectrum at $z = 0$, i.e. $P^{(0)}(k)$. Also, we show the ratio between P_{1-loop} and $P^{(0)}(k)$.
It is clear, looking at Fig. 2.12, that starting from $k \sim 0.1$ h/Mpc the corrections to the linear power spectrum are not small anymore and, in particular, $P^{(0)}(k)$ undertimates the power spectrum calculated with the perturbative corrections up to one-loop. This means that, starting indeed around $k \sim 0.1$ h/Mpc the linear regime is not valid anymore.

Chapter 3

Statistical Approach to Cosmology

In this chapter we shall go through some statistical concepts and review some useful tools which are widely employed in cosmology.
One question should arise: why do we need a statistical approach when, not only we are dealing with data analysis, but on general ground we are studying cosmology and its fundamental observables?
As we know, the present explanation of the large-scale structure of the universe is that the distribution of matter on cosmological scales we see today comes from the growth of primordial, small, seed fluctuations on an homogeneous universe amplified by gravitational instability [35]. The fact is, tests of cosmological theories, which actually help in characterizing these primordial seeds, are not deterministic, but *statistical*, for the following reasons. First, we do not have direct observational access to primordial fluctuations. This means that we do not have definite initial conditions. Second, the time scale for cosmological evolution is so much greater with respect to the time scale over which we can make observations, that it is absolutely impossible to follow the evolution of single systems. Thus, if we are willing to test the evolution of structures, we must do it statistically. Our present universe is therefore modeled as a stochastic realization of a statistical ensemble of different possibilities. The aim, therefore is to predict statistical realizations, which actually depend on the statistical characteristics of the primordial perturbations that led to the present-day large-scale structure configuration.

3.1 Parameter Estimation

Following [49] we will start reviewing some topics that are very common in cosmological data analysis. Most data analysis problems are, in some sense, called "inverse problems". We have a set of data $\mathbf{x}$ and we wish to interpret the data in some way. One typical example could be: *are large-scale structure observations consistent with the hypothesis that the universe is spatially flat?*
When dealing with cosmology, we collect some data and wish to interpret them in terms of a model, i.e. a theoretical framework which we assume to be true. The model will usually have some parameters $\boldsymbol{\theta}$ in it, which we want to determine: this is called

the parameter estimation process. Therefore, the main goal is to provide estimates of the parameters, and their errors, or preferably the whole probability distribution of $\boldsymbol{\theta}$, given the data $\mathbf{x}$, which is called *posterior probability* distribution. Basically, it is the probability that the parameters take certain values after doing the experiment, and we can indicate it in the following way:

$$p(\boldsymbol{\theta}|\mathbf{x}). \tag{3.1}$$

From $p(\boldsymbol{\theta}|\mathbf{x})$ one can calculate the expectation values of the parameters and their errors.

3.1.1 Forward Modeling

Often, instead of the posterior probability, it may be easier to calculate rather the opposite, namely

$$p(\mathbf{x}|\boldsymbol{\theta}) \tag{3.2}$$

referred to as *forward modeling* i.e., knowing the parameters beforehand, we can compute the expected distribution of the data. Examples of forward modeling distributions include the common ones, such as Binomial, Poisson, Gaussian and so on.
We can consider, as a concrete example, a model in which we have a Gaussian with mean μ and variance σ^2. The model has two parameters $\boldsymbol{\theta} = (\mu, \sigma)$, and, given the parameters, the probability of a single variable x reads

$$p(\mathbf{x}|\boldsymbol{\theta}) = \frac{1}{\sqrt{2\pi}\sigma} e^{-\frac{(x-\mu)^2}{2\sigma^2}}. \tag{3.3}$$

The interesting thing is that we can relate eq. (3.3) to the posterior probability $p(\boldsymbol{\theta}|\mathbf{x})$ thanks to the Bayes theorem, which states:

$$p(\boldsymbol{\theta}|\mathbf{x}) = \frac{p(\mathbf{x}|\boldsymbol{\theta})p(\boldsymbol{\theta})}{p(\mathbf{x})} \tag{3.4}$$

where we can call $p(\mathbf{x}|\boldsymbol{\theta})$ *Likelihood* and we indicate it with $L(\mathbf{x}, \boldsymbol{\theta})$. Moreover, $p(\boldsymbol{\theta})$ is called *prior*, and expresses our knowledge of the parameters before doing the experiment, which may come from previous experiments, or from a given theory. Finally, $p(\mathbf{x})$ is called *evidence*, which is defined is in the following way:

$$p(\mathbf{x}) = \int d\boldsymbol{\theta} p(\mathbf{x}|\boldsymbol{\theta})p(\boldsymbol{\theta}). \tag{3.5}$$

Let us note that, in the absence of any data, it is common to adopt the principle of indifference and assume a *flat prior*, i.e. all values of the parameters are equally likely, thus taking $p(\boldsymbol{\theta}) = const$. Hence, for flat priors, we have simply

$$p(\boldsymbol{\theta}|\mathbf{x}) \propto L(\mathbf{x}; \boldsymbol{\theta}) \tag{3.6}$$

3.1.2 Errors

Now, let us assume we have a posterior probability distribution $p(\boldsymbol{\theta}|\mathbf{x})$. One common estimator of the parameters, which we indicate with the hat symbol, is the mean:

$$\hat{\boldsymbol{\theta}} = \int d\boldsymbol{\theta} p(\boldsymbol{\theta}|\mathbf{x})\boldsymbol{\theta}. \tag{3.7}$$

We define an estimator *unbiased* if its expectation value coincides with the true value of the parameter, $\boldsymbol{\theta}_0$:

$$\langle\hat{\boldsymbol{\theta}}\rangle = \boldsymbol{\theta}_0. \tag{3.8}$$

Now, for simplicity, we assume that the probability distribution is single-peaked. Moreover, we assume a flat prior, so that the posterior probability is proportional to the likelihood. We can therefore study the behavior of $L(\mathbf{x};\boldsymbol{\theta})$ close to the peak, performing a Taylor expansion of the logarithm of the likelihood function:

$$\log L(\mathbf{x};\boldsymbol{\theta}) = \log L(\mathbf{x};\boldsymbol{\theta}_0) + \frac{1}{2}(\boldsymbol{\theta}_\alpha - \boldsymbol{\theta}_{0\alpha})\frac{\partial^2 \log L}{\partial\boldsymbol{\theta}_\alpha \partial\boldsymbol{\theta}_\beta}(\boldsymbol{\theta}_\beta - \boldsymbol{\theta}_{0\beta}) + \cdots \tag{3.9}$$

which implies that, locally, $L(\mathbf{x};\boldsymbol{\theta})$ is a multivariate Gaussian in the parameter space:

$$L(\mathbf{x};\boldsymbol{\theta}) = L(\mathbf{x};\boldsymbol{\theta}_0)e^{-\frac{1}{2}(\boldsymbol{\theta}_\alpha - \boldsymbol{\theta}_{0\alpha})H_{\alpha\beta}(\boldsymbol{\theta}_\beta - \boldsymbol{\theta}_{0\beta})}, \tag{3.10}$$

where we have used

$$H_{\alpha\beta} = -\frac{\partial^2 \log L}{\partial\boldsymbol{\theta}_\alpha \partial\boldsymbol{\theta}_\beta} \tag{3.11}$$

which is called Hessian matrix. The Hessian indicates whether the estimates of θ_α and θ_β are correlated or not. In fact, if $H_{\alpha\beta}$ is not diagonal, it means that the estimates are correlated. Let us note that, even if the quantities are uncorrelated, their estimates could have a similar effect on the data; in this case the estimates would be actually correlated, therefore leading to a non-diagonal Hessian.

3.2 Fisher Matrix Approach

Now we will deal with an important issue in cosmology, that is: how well can we measure model parameters from a given data set, without simulating the data set? In other words: are we able to make a forecast, given a data set, of some specific parameters? The accuracy, i.e. the error bar, with which cosmological parameters can be measured from a given data set is conveniently computed with the Fisher information matrix formalism [50].
Therefore, proceeding as we have done in Sec. 3.1, we can think of the data as an N-dimensional vector $\mathbf{x}$; the components (x_i) could be, for example, the fluctuations in the galaxy density with respect to the mean, in N disjoint bins that cover the three

dimensional survey volume; $\mathbf{x}$ is considered as a random variable whose probability distribution $L(\mathbf{x}, \boldsymbol{\theta})$ (the likelihood) depends on a vector of cosmological parameters $\boldsymbol{\theta}$. These parameters $\boldsymbol{\theta}$ are exactly what we want to estimate. In order to do so, we need the explicit expression of the Fisher matrix, which is defined as the expectation value of the Hessian (eq. (3.11)) and reads:

$$\mathbf{F}_{ij} \equiv -\left\langle \frac{\partial^2 \log L}{\partial\theta_i \partial\theta_j} \right\rangle . \tag{3.12}$$

3.2.1 The Cramer-Rao Inequality

What is extremely useful in this approach, is that the inverse of the Fisher matrix, $\mathbf{F}^{-1}$, can be thought as the best covariance matrix for the measurements errors on the parameters, namely:

$$\Delta\theta_i \Delta\theta_j \geq (\mathbf{F}^{-1})_{ij}. \tag{3.13}$$

It follows that, if all the parameters are estimated from the data, as well as the parameter we are interested in, we have:

$$\Delta\theta_i \geq (\mathbf{F}^{-1})_{ii}^{1/2} \tag{3.14}$$

whereas if all other parameters are fixed we simply obtain

$$\Delta\theta_i \geq \frac{1}{\sqrt{F_{ii}}}. \tag{3.15}$$

Equation (3.15) takes the name of Cramer-Rao inequality and we can derive it following [51].
Since $L(\mathbf{x}, \theta)$ is the joint frequency function of the observations, it holds that

$$\int dx_1 \cdots \int dx_n L(x_1, \ldots, x_n, \theta) = 1. \tag{3.16}$$

Now we suppose that the first two derivatives of L w.r.t. θ exist for all θ. If we differentiate both sides of eq. (3.16) w.r.t. θ we obtain:

$$\int dx_1 \cdots \int dx_n \frac{\partial L}{\partial\theta} = 0, \tag{3.17}$$

where we have simply written L for the sake of notation. We may rewrite the last equation as:

$$\langle \frac{\partial \log L}{\partial\theta} \rangle = \int dx_1 \cdots \int dx_n \left(\frac{1}{L} \frac{\partial L}{\partial\theta} \right) L = 0. \tag{3.18}$$

If we differentiate eq. (3.18) we obtain:

$$\int dx_1 \cdots \int dx_n \left[\left(\frac{1}{L} \frac{\partial L}{\partial \theta} \right) \frac{\partial L}{\partial \theta} + L \frac{\partial}{\partial \theta} \left(\frac{1}{L} \frac{\partial L}{\partial \theta} \right) \right] = 0, \tag{3.19}$$

which becomes

$$\int dx_1 \cdots \int dx_n \left[\left(\frac{1}{L} \frac{\partial L}{\partial \theta} \right)^2 + \frac{\partial^2 \log L}{\partial \theta^2} \right] = 0, \tag{3.20}$$

or

$$\langle \big(\frac{\partial \log L}{\partial \theta} \big)^2 \rangle = - \langle \frac{\partial^2 \log L}{\partial \theta^2} \rangle. \tag{3.21}$$

Now let us consider an estimator t of some function of θ, say $\tau(\theta)$ in complete generality. The estimator is unbiased if $\langle t \rangle = \tau(\theta)$. Now, if we suppose that t is unbiassed, we have:

$$\langle t \rangle = \int dx_1 \cdots \int dx_n t L = \tau(\theta). \tag{3.22}$$

We differentiate eq. (3.22), obtaining:

$$\int dx_1 \cdots \int dx_n t \frac{\partial \log L}{\partial \theta} L = \tau'(\theta), \tag{3.23}$$

which we may rewrite, using eq. (3.18), as

$$\tau'(\theta) = \int dx_1 \cdots \int dx_n \left[t - \tau(\theta) \right] \frac{\partial \log L}{\partial \theta} L. \tag{3.24}$$

Now, by the Cauchy-Schwarz inequality, we have from eq. (3.24)

$$\left[\tau'(\theta) \right]^2 \leq \int dx_1 \cdots \int dx_n \left[t - \tau(\theta) \right]^2 L \cdot \int dx_1 \cdots \int dx_n \left(\frac{\partial \log L}{\partial \theta} \right)^2 L, \tag{3.25}$$

which, on rearrangement, becomes

$$\left(\Delta \theta \right)^2 = \langle \left[t - \tau(\theta) \right]^2 \rangle \geq \frac{\left(\tau'(\theta) \right)^2}{\langle \big(\frac{\partial \log L}{\partial \theta} \big)^2 \rangle}, \tag{3.26}$$

and, using eq. (3.21), the last equation may be rewritten

$$\left(\Delta \theta \right)^2 \geq \frac{\left(\tau'(\theta) \right)^2}{- \langle \frac{\partial^2 \log L}{\partial \theta^2} \rangle}. \tag{3.27}$$

Now, in the case where t is estimating θ itself, we have that $\tau'(\theta) = 1$; therefore we come to:

$$(\Delta\theta)^2 \geq \frac{1}{-\langle \frac{\partial^2 \log L}{\partial \theta^2} \rangle}, \tag{3.28}$$

which is, using the definition of the Fisher matrix:

$$(\Delta\theta)^2 \geq \frac{1}{F_{\theta\theta}}, \tag{3.29}$$

i.e., the Cramer-Rao inequality. Note that, in the case of just a single parameter, the Fisher matrix has rank 1.

3.2.2 Gaussian Likelihood

Now we can assume the probability distribution L to be a Gaussian with mean $\boldsymbol{\mu} \equiv \langle \mathbf{x} \rangle$ and covariance matrix $\mathbf{C} \equiv \langle \mathbf{x}\mathbf{x}^t \rangle - \boldsymbol{\mu}\boldsymbol{\mu}^t$, thus we can write:

$$-2\log L = \log \det \mathbf{C} + (\mathbf{x} - \boldsymbol{\mu})\mathbf{C}^{-1}(\mathbf{x} - \boldsymbol{\mu})^t \tag{3.30}$$

where we have dropped the coefficients in front of the distribution function. If we now define $\mathbf{D} \equiv (\mathbf{x} - \boldsymbol{\mu})(\mathbf{x} - \boldsymbol{\mu})^t$ and consider that $\log(\det \mathbf{C}) = \mathrm{tr}(\log \mathbf{C})$, we can write eq. (3.30) as follows:

$$-2\log L = \mathrm{tr}\left[\log \mathbf{C} + \mathbf{C}^{-1}\mathbf{D}\right]. \tag{3.31}$$

Indicating $\mathbf{C}_{,i} \equiv \frac{\partial}{\partial \theta_i}\mathbf{C}$, it holds that $\mathbf{C}^{-1}{}_{,i} = -\mathbf{C}^{-1}\mathbf{C}_{,i}\,\mathbf{C}^{-1}$ and $(\log \mathbf{C})_{,i} = \mathbf{C}^{-1}\mathbf{C}_{,i}$. Therefore we can write eq. (3.31) in the following fashion:

$$-(2\log L)_{,i} = \mathrm{tr}\left[\mathbf{C}^{-1}\mathbf{C}_{,i} - \mathbf{C}^{-1}\mathbf{C}_{,i}\,\mathbf{C}^{-1}\mathbf{D} + \mathbf{C}^{-1}\mathbf{D}_{,i}\right], \tag{3.32}$$

thus

$$\begin{aligned} -(2\log L)_{,ij} = \mathrm{tr}\Big[& -\mathbf{C}^{-1}\mathbf{C}_{,i}\,\mathbf{C}^{-1}\mathbf{C}_{,j} + \mathbf{C}^{-1}\mathbf{C}_{,ij} + \mathbf{C}^{-1}\mathbf{C}_{,i}\,\mathbf{C}^{-1}\mathbf{C}_{,j}\,\mathbf{C}^{-1}\mathbf{D} \\ & - \mathbf{C}^{-1}\mathbf{C}_{,ij}\,\mathbf{C}^{-1}\mathbf{D} + \mathbf{C}^{-q}\mathbf{C}_{,j}\,\mathbf{C}^{-1}\mathbf{C}_{,i}\,\mathbf{C}^{-1}\mathbf{D} - \mathbf{C}^{-1}\mathbf{C}_{,j}\,\mathbf{C}^{-1}\mathbf{D}_{,i} \\ & - \mathbf{C}^{-1}\mathbf{C}_{,i}\,\mathbf{C}^{-1}\mathbf{D}_{,j} + \mathbf{C}^{-1}\mathbf{D}_{,i}\Big] \\ = \mathrm{tr}\Big[& \mathbf{C}^{-1}\mathbf{C}_{,ij} + \mathbf{C}^{-1}\mathbf{C}_{,j}\,\mathbf{C}^{-1}\mathbf{C}_{,i}\,\mathbf{C}^{-1}\mathbf{D} - \mathbf{C}^{-1}\mathbf{C}_{,i}\,\mathbf{C}^{-1}\mathbf{D}_{j} \\ & + \mathbf{C}^{-1}\mathbf{C}_{,j}\,\mathbf{C}^{-1}\mathbf{D}_{,i} - \mathbf{C}^{-1}\mathbf{C}_{,ij}\,\mathbf{C}^{-1}\mathbf{D} + \mathbf{C}^{-1}\mathbf{D}_{,ij}\Big]. \end{aligned} \tag{3.33}$$

Then, since we have that $\langle \mathbf{x} \rangle = \boldsymbol{\mu}$ and $\langle \mathbf{x}\mathbf{x}^t \rangle = \mathbf{C} + \boldsymbol{\mu}\boldsymbol{\mu}^t$, we obtain:

$$\begin{cases} \langle \mathbf{D} \rangle & = \mathbf{C}, \\ \langle \mathbf{D}_{,i} \rangle & = 0, \\ \langle \mathbf{D}_{,ij} \rangle & = \boldsymbol{\mu}_{,i}\,\boldsymbol{\mu}^{t}_{,j} + \boldsymbol{\mu}_{,j}\,\boldsymbol{\mu}^{t}_{,i} \end{cases} \tag{3.34}$$

Therefore, inserting this into eq. (3.33), and using the trace property $\mathrm{tr}[\mathbf{AB}] = \mathrm{tr}[\mathbf{BA}]$ we obtain:

$$-(2\log L)_{,ij} = \mathrm{tr}\big[\mathbf{C}^{-1}\mathbf{C}_{,i}\,\mathbf{C}^{-1}\mathbf{C}_{,j} + \mathbf{C}^{-1}(\boldsymbol{\mu}_{,i}\,\boldsymbol{\mu}_{,j}^{t} + \boldsymbol{\mu}_{,j}\,\boldsymbol{\mu}_{,i}^{t})\big], \tag{3.35}$$

and, taking into account the definition of the Fisher matrix, eq.(3.12), we can write:

$$\mathbf{F}_{ij} = \frac{1}{2}\mathrm{tr}\left[\mathbf{C}^{-1}\frac{\partial \mathbf{C}}{\partial \theta_i}\mathbf{C}^{-1}\frac{\partial \mathbf{C}}{\partial \theta_j}\right] + \mathrm{tr}\left[\mathbf{C}^{-1}\frac{\partial \boldsymbol{\mu}}{\partial \theta_i}\frac{\partial \boldsymbol{\mu}}{\partial \theta_j}^{t}\right]. \tag{3.36}$$

We have thus found an explicit form for the Fisher matrix when the probability distribution is a Gaussian. It is an interesting result because, as we have said before, if we know how $\boldsymbol{\mu}$ and $\mathbf{C}$ depends on the parameters we can calculate the Fisher matrix before doing the experiment so that we can have an estimate of the expected error on a given parameter.

Now, still following [50], we will derive a simple approximation for $\mathbf{F}$ which helps in an intuitive understanding of numerical results and shows the different contributions for each scale k. If we do not take into account non-linear clustering and redshift-space distortions all the cosmological information is carried by the galaxy power spectrum. If the volume of the survey we are considering is much larger than the scale of any feature in the power spectrum, it has been shown that all the cosmological information in the variable $\mathbf{x}$ is recovered when $P(k)$ is estimated with the FKP method [52, 53]. In particular we can think of x_n as the average power measured with the FKP method in a thin shell of radius k_n in Fourier space. Therefore, we can write the FKP results as:

$$\begin{aligned} \boldsymbol{\mu} &\approx P(k_n) \\ \mathbf{C}_{mn} &\approx 2\frac{P(k_n)P(k_n)}{V_n V_{eff}(k_n)}\delta_{mn} \end{aligned} \tag{3.37}$$

where

$$V_n \equiv \frac{4\pi}{(2\pi)^3}k_n^2 dk_n \tag{3.38}$$

$$V_{eff}(k) \equiv \int \left[\frac{\bar{n}(\mathbf{r})P(k)}{1+\bar{n}(\mathbf{r})P(k)}\right] d^3r. \tag{3.39}$$

We indicate with $\bar{n}(\mathbf{r})$ the selection function of the survey, that is the a priori expectation value for the number density of the galaxies; V_{eff} can therefore be interpreted as the effective volume used for measuring the power at wave number k. If we choose the shells thick enough, so that they contain a lot of uncorrelated modes, $V_n V_{eff}(k_n) \gg 1$, the central limit theorem states that $\mathbf{x}$ can be well approximated by a Gaussian.

Also, in this limit, we can neglect the first term in eq. (3.36) [50] and, using eq. (3.37) we have:

$$\mathbf{F}_{ij} \approx \frac{1}{4\pi^2} \sum_n \frac{\partial P(k_n)}{\partial \theta_i} \frac{\partial P(k_m)}{\partial \theta_j} \frac{V_{eff}(k_n) k_n^2 dk_n}{P(k_n)^2}. \tag{3.40}$$

Let us define

$$\omega(k) = \frac{V_{eff}}{\lambda^3} \tag{3.41}$$

where $\lambda = 2\pi/k$ is the wavelength. Hence we come to:

$$\mathbf{F}_{ij} = 2\pi \sum_n \frac{\partial P(k_n)}{\partial \theta_i} \frac{\partial P(k_m)}{\partial \theta_j} \frac{\omega(k)}{P(k_n)^2} \frac{dk_n}{k_n} \tag{3.42}$$

and, finally replacing the sum with an integral, we arrive to:

$$\mathbf{F}_{ij} \approx 2\pi \int_{k_{min}}^{k_{max}} \frac{\partial \log P(k)}{\partial \theta_i} \frac{\partial \log P(k)}{\partial \theta_j} \omega(k) d\log k. \tag{3.43}$$

Eq. (3.43) could be useful because it divides the effects of cosmology, which enter through the derivatives of the power spectrum, from those of the survey-specific details, which are considered via the weight function $\omega(k)$. Let us note, however, that eq. (3.43) is a rather crude approximation, since it ignores edge effects, redshift space distortions and, most importantly, non-linear clustering.

Chapter 4

Large Scale Structure Consistency Relations

4.1 Consistency Relations

In this chapter we want to derive and to study more in detail the large-scale structure consistency relations (CR). As stated in [11], the consistency relations, which come from the equivalence principle, are exact equalities among correlation functions of different order and hold for primordial perturbations generated by single-field models of inflation.
For the derivation of the consistency relations we will mainly follow [11]. We start with isolating the effects on the bispectrum of nearly uniform and time-dependent displacements fields:

$$\mathbf{x} + \mathbf{d}_\alpha(\mathbf{x}) \tag{4.1}$$

and, recalling eq. (2.169), the bispectrum is defined as

$$B_{\alpha\beta\gamma}(q, k_+, k_-) \equiv \langle \delta_\alpha(\mathbf{q})\delta_\beta(-\mathbf{k}_+)\delta_\gamma(\mathbf{k}_-)\rangle' \tag{4.2}$$

where the prime indicates that the expectation value has to be divided by the Dirac delta $\delta_D(\mathbf{q} - \mathbf{k} - \mathbf{q}/2 + \mathbf{k} - \mathbf{q}/2) = \delta_D(0)$. The subscripts α, β, γ indicate the different tracers we can use to measure the density contrast, such as baryons, dark matter, galaxies and so on.
It is helpful to shift back to the initial positions, defining new density fields,

$$\delta_\alpha(\mathbf{x}) \equiv \tilde{\delta}_\alpha(\mathbf{x} - \mathbf{d}_\alpha(\mathbf{x})) \simeq \tilde{\delta}_\alpha(\mathbf{x}) - \mathbf{d}_\alpha(\mathbf{x}) \cdot \nabla\tilde{\delta}_\alpha(\mathbf{x}). \tag{4.3}$$

We now take the Fourier transform of this last equation (note that we indicate with the same symbol fields in real and Fourier space):

$$\delta_\alpha(\mathbf{p}) \simeq \tilde{\delta}_\alpha(\mathbf{p}) - \mathcal{F}\big\{ - \mathbf{d}_\alpha(\mathbf{x}) \cdot \nabla\tilde{\delta}_\alpha(\mathbf{x})\big\}(\mathbf{p}). \tag{4.4}$$

The second term then becomes:

$$
\begin{aligned}
&= \int \frac{d^3\mathbf{x}}{(2\pi)^3} e^{-i\mathbf{p}\cdot\mathbf{x}} (-\mathbf{d}_\alpha(\mathbf{x}) \cdot \nabla \tilde{\delta}_\alpha(\mathbf{x})) \\
&= \int \frac{d^3\mathbf{x}}{(2\pi)^3} e^{-i\mathbf{p}\cdot\mathbf{x}} \left[- \int d^3\mathbf{q}' e^{i\mathbf{q}'\cdot\mathbf{x}} \mathbf{d}_\alpha(\mathbf{q}') \cdot \nabla \int d^3\mathbf{q}'' e^{i\mathbf{q}''\cdot\mathbf{x}} \tilde{\delta}_\alpha(\mathbf{q}'') \right] \\
&= - \int \frac{d^3\mathbf{x}}{(2\pi)^3} e^{-i\mathbf{p}\cdot\mathbf{x}} \int d^3\mathbf{q}' e^{i\mathbf{q}'\cdot\mathbf{x}} \mathbf{d}_\alpha(\mathbf{q}') \cdot \int d^3\mathbf{q}'' (i\mathbf{q}'') e^{i\mathbf{q}''\cdot\mathbf{x}} \tilde{\delta}_\alpha(\mathbf{q}'') \\
&= -i \int\int\int \frac{d^3\mathbf{x}}{(2\pi)^3} d^3\mathbf{q}' d^3\mathbf{q}'' e^{-i\mathbf{x}\cdot(\mathbf{p}-\mathbf{q}'-\mathbf{q}'')} (\mathbf{q}'' \cdot \mathbf{d}_\alpha(\mathbf{q}')) \tilde{\delta}_\alpha(\mathbf{q}'') \\
&= -i \int\int d^3\mathbf{q}' d^3\mathbf{q}'' \delta_D(\mathbf{p}-\mathbf{q}'-\mathbf{q}'') (\mathbf{q}'' \cdot \mathbf{d}_\alpha(\mathbf{q}')) \tilde{\delta}_\alpha(\mathbf{q}''),
\end{aligned}
$$

thus obtaining

$$
\delta_\alpha(\mathbf{p}) \simeq \tilde{\delta}_\alpha(\mathbf{p}) - i \int d^3\mathbf{q}' (\mathbf{p}-\mathbf{q}') \cdot \mathbf{d}_\alpha(\mathbf{q}') \tilde{\delta}_\alpha(\mathbf{p}-\mathbf{q}'). \tag{4.5}
$$

We proceed by inserting this into eq. (4.2) and obtain:

$$
\begin{aligned}
B_{\alpha\beta\gamma}(q, k_+, k_-) = &\langle \tilde{\delta}_\alpha(\mathbf{q}) \tilde{\delta}_\beta(-\mathbf{k}_+) \tilde{\delta}_\gamma(\mathbf{k}_-) \rangle' \\
&- i \int d^3\mathbf{q}' (\mathbf{k}_- - \mathbf{q}') \big\langle \tilde{\delta}_\alpha(\mathbf{q}) \tilde{\delta}_\beta(-\mathbf{k}_+) \mathbf{d}_\gamma(\mathbf{q}') \tilde{\delta}_\gamma(\mathbf{k}_- - \mathbf{q}') \big\rangle' \\
&- i \int d^3\mathbf{q}' (-\mathbf{k}_+ - \mathbf{q}') \big\langle \tilde{\delta}_\alpha(\mathbf{q}) \mathbf{d}_\beta(\mathbf{q}') \tilde{\delta}_\beta(-\mathbf{k}_+ - \mathbf{q}') \tilde{\delta}_\gamma(\mathbf{k}_-) \big\rangle' \\
&- i \int d^3\mathbf{q}' (\mathbf{q} - \mathbf{q}') \big\langle \mathbf{d}_\alpha(\mathbf{q}') \tilde{\delta}_\alpha(\mathbf{q} - \mathbf{q}') \tilde{\delta}_\beta(-\mathbf{k}_+) \tilde{\delta}_\gamma(\mathbf{k}_-) \big\rangle' \\
&+ \cdots
\end{aligned} \tag{4.6}
$$

Since we are in the $q \ll k$ limit, we assume that $\mathbf{d}_\alpha(\mathbf{q})$ correlates only with $\tilde{\delta}_\alpha(\mathbf{q})$, therefore we can write:

$$
\begin{aligned}
\big\langle \tilde{\delta}_\alpha(\mathbf{q}) \mathbf{d}_\beta(\mathbf{q}') \tilde{\delta}_\beta(-\mathbf{k}_+ - \mathbf{q}') \tilde{\delta}_\gamma(\mathbf{k}_-) \big\rangle' &\simeq \big\langle \tilde{\delta}_\alpha(\mathbf{q}) \mathbf{d}_\beta(\mathbf{q}') \big\rangle \big\langle \tilde{\delta}_\beta(-\mathbf{k}_+ - \mathbf{q}') \tilde{\delta}_\gamma(\mathbf{k}_-) \big\rangle' \\
&= \delta_D(\mathbf{q} + \mathbf{q}') \big\langle \tilde{\delta}_\alpha(\mathbf{q}) \mathbf{d}_\beta(-\mathbf{q}) \big\rangle' \big\langle \tilde{\delta}_\beta(-\mathbf{k}_-) \tilde{\delta}_\gamma(\mathbf{k}_-) \big\rangle'
\end{aligned} \tag{4.7}
$$

Thus, the Bispectrum takes the form:

$$
\begin{aligned}
\lim_{q/k \to 0} B_{\alpha\beta\gamma}(q, k_+, k_-) = &\langle \tilde{\delta}_\alpha(\mathbf{q}) \tilde{\delta}_\beta(-\mathbf{k}_+) \tilde{\delta}_\gamma(\mathbf{k}_-) \rangle' \\
&i\mathbf{k} \cdot \Big[\big\langle \tilde{\delta}_\alpha(\mathbf{q}) \mathbf{d}_\beta(-\mathbf{q}) \big\rangle' P_{\beta\gamma}(k_-) - \big\langle \tilde{\delta}_\alpha(\mathbf{q}) \mathbf{d}_\gamma(-\mathbf{q}) \big\rangle' P_{\beta\gamma}(k_+) \Big] \\
&+ \cdots
\end{aligned} \tag{4.8}
$$

where we have used the definition of the power spectrum. Now we take a closer look to $\mathbf{d}_\alpha(\mathbf{q})$. Actually, since the Equivalence Principle and the adiabatic initial conditions ensure that, at large scales, all species fall with the same acceleration under the effect of the potential generated by the total matter field, so that $\mathbf{d}_{\alpha,\beta,\gamma}(\mathbf{q}) \to \mathbf{d}_m(\mathbf{q})$, we will consider a common displacement, $\mathbf{d}_m(\mathbf{q})$.
By definition, suppressing the m subscript, we have:

$$\mathbf{d}(\mathbf{q},\tau) = \int^{\tau} d\tau' \mathbf{v}(q,\tau'), \tag{4.9}$$

then:

$$d\tau' = \frac{d\tau}{d\log D} d\log D = \frac{1}{\mathcal{H}f} d\log D = \frac{1}{\mathcal{H}f} d\eta, \tag{4.10}$$

where we have used $f = \frac{d\log D}{d\log a}$. Therefore:

$$\mathbf{d}(\mathbf{q},\tau) = \int^{\eta} d\eta' \frac{\mathbf{v}(q,\eta')}{\mathcal{H}f}. \tag{4.11}$$

We assume to be in linear theory, so that we have $\frac{\mathbf{v}(q,\eta')}{\mathcal{H}f} \sim e^{\eta} = D$. Hence:

$$\int_{\eta_i}^{\eta_f} d\eta' \frac{\mathbf{v}(\mathbf{q},\eta')}{\mathcal{H}f}\Big|_{\eta_f} e^{(\eta'-\eta_f)} = \frac{\mathbf{v}(\mathbf{q},\eta)}{\mathcal{H}f}\Big|_{\eta_f} e^{(\eta-\eta_f)}\Big|_{\eta_i}^{\eta f} \underset{\eta_f\to\infty}{=} \frac{\mathbf{v}(\mathbf{q},\eta)}{\mathcal{H}f}. \tag{4.12}$$

We then take the continuity equation in the linear regime, which reads:

$$\frac{\partial\delta(\mathbf{x},\tau)}{\partial\tau} + \nabla\cdot\mathbf{v}(\mathbf{x},\tau) = 0 \tag{4.13}$$

and, substituting $\frac{\mathrm{d}}{\mathrm{d}\tau} = \mathcal{H}f\frac{\mathrm{d}}{\mathrm{d}\log D}$ we arrive to:

$$\delta'(\mathbf{x},\eta) + \frac{\nabla'\cdot\mathbf{v}(\mathbf{x},\eta)}{\mathcal{H}f} = 0 \tag{4.14}$$

where $' \equiv \frac{\mathrm{d}}{\mathrm{d}\log D}$. Since $\delta \sim D = e^{\eta}$ we have that $\delta'(\mathbf{x},\eta) = \delta(\mathbf{x},\eta)$, thus obaining:

$$\delta(\mathbf{x},\eta) + \frac{\nabla'\cdot\mathbf{v}(\mathbf{x},\eta)}{\mathcal{H}f} = 0. \tag{4.15}$$

If we now Fourier transform eq. (4.15) we arrive to:

$$\frac{\mathbf{v}(\mathbf{q},\eta)}{\mathcal{H}f} = i\frac{\mathbf{q}}{q^2}\delta(\mathbf{q},\eta) \tag{4.16}$$

which leads to

$$\mathbf{d}_m(\mathbf{q}) = i\frac{\mathbf{q}}{q^2}\delta_m(\mathbf{q}). \tag{4.17}$$

Finally, using eq. (4.8), neglecting its first term and using eq. (4.17), we obtain the large-scale structure consistency relations:

$$\begin{aligned}\lim_{q/k\to 0}\frac{B_{\alpha\beta\gamma}(q,k_+,k_-)}{P_{\alpha\alpha}(q)P_{\beta\gamma}(k)} &= \frac{\mu}{b_\alpha(q)}\frac{k}{q}\frac{(P_{\beta\gamma}(k_-)-P_{\beta\gamma}(k_+))}{P_{\beta\gamma}(k)}+O\left(\left(\frac{q}{k}\right)^0\right)\\ &= -\frac{\mu^2}{b_\alpha(q)}\frac{\mathrm{d}\log P_{\beta\gamma}(k)}{\mathrm{d}\log k}+O\left(\left(\frac{q}{k}\right)^0\right),\end{aligned} \tag{4.18}$$

where $\mu\equiv(\mathbf{q}\cdot\mathbf{k})/(qk)$. We have also defined the bias parameter as a physical quantity in the following manner:

$$b_\alpha(q)\equiv\lim_{q\to 0}\frac{P_{\alpha\alpha}(q)}{P_{\alpha m}(q)}. \tag{4.19}$$

We note that the equal-time Consistency Relations (eq. (4.18)) contain no $1/q$ pole. As a first check, we can compute the matter bispectrum in the squeezed limit at the lowest order in standard perturbation theory. In fact we have:

$$\begin{aligned}B(\mathbf{q},\mathbf{k}-\mathbf{q}/2,-\mathbf{k}-\mathbf{q}/2) &= 2F_2(\mathbf{q},\mathbf{k}-\mathbf{q}/2)P_m^{(0)}(q)P_m^{(0)}(|\mathbf{k}-\mathbf{q}/2|)\\ &+2F_2(\mathbf{q},-\mathbf{k}-\mathbf{q}/2)P_m^{(0)}(q)P_m^{(0)}(|-\mathbf{k}-\mathbf{q}/2|)\\ &+2F_2(\mathbf{k}-\mathbf{q}/2,-\mathbf{k}-\mathbf{q}/2)P_m^{(0)}(|\mathbf{k}-\mathbf{q}/2|)P_m^{(0)}(|-\mathbf{k}-\mathbf{q}/2|)\end{aligned} \tag{4.20}$$

where we have denoted with $P_m^{(0)}$ the linear matter power spectrum. Around $q/k\ll 1$ we can write:

$$|\mathbf{k}-\mathbf{q}/2|=k\sqrt{1-\mu\frac{q}{k}+\frac{1}{4}\left(\frac{q}{k}\right)^2}\simeq k-\frac{1}{2}\mu q \tag{4.21}$$

so that we can expand the power spectrum as

$$P_m^{(0)}(|\mathbf{k}-\mathbf{q}/2|)\simeq P_m^{(0)}(k)-\frac{1}{2}q\mu\frac{\mathrm{d}P_m^{(0)}(k)}{\mathrm{d}k}. \tag{4.22}$$

The next step is to expand the three terms on the r.h.s. of eq. (4.20) around $q/k\to 0$. The first term is:

$$=2\left[\frac{1}{2}\mu\frac{k}{q}+\left(\frac{13}{28}+\frac{2}{7}\mu^2+O\left(\frac{q}{k}\right)\right)\right]P_m^{(0)}(q)\left(P_m^{(0)}(k)-\frac{1}{2}q\mu\frac{\mathrm{d}P_m^{(0)}(k)}{\mathrm{d}k}\right) \tag{4.23}$$

whereas the second term is:

$$=2\left[-\frac{1}{2}\mu\frac{k}{q}+\left(\frac{13}{28}+\frac{2}{7}\mu^2+O\left(\frac{q}{k}\right)\right)\right]P_m^{(0)}(q)\left(P_m^{(0)}(k)+\frac{1}{2}q\mu\frac{\mathrm{d}P_m^{(0)}(k)}{\mathrm{d}k}\right) \tag{4.24}$$

and the third is:

$$= O\left(\frac{q}{k}\right). \tag{4.25}$$

Putting all the pieces together we arrive to:

$$\lim_{q/k\to 0} \frac{B^{SPT}_{mmm}(q,k_+,k_-)}{P^{(0)}_m(q)P^{(0)}_m(k)} = -\mu^2 \frac{\mathrm{d}\log P^{(0)}_m(k)}{\mathrm{d}\log k} + \frac{13+8\mu^2}{7} + O\left(\frac{q}{k}\right) \tag{4.26}$$

The first term on the r.h.s. of this equation can be isolated from the rest because of its dependence on the scale. In order to see this effect we can do as follows.
We know, from Sec. 2.2, that, around some specific values of k, the power spectrum displays some oscillating features that we can, at first approximation, identify with the baryon acoustic oscillations. Thus, we can write the power spectrum as an oscillating part (wiggle) plus a smooth part (no-wiggle):

$$P^{(0)}_m(k) = P^{w}_m(k) + P^{nw}_m(k). \tag{4.27}$$

We can explicit the last expression in the following way:

$$P^{(0)}_m(k) = P^{nw}_m(k)\left(1 + A_{bao}(k)\sin(kr_s)\right) \tag{4.28}$$

r_s standing for comoving sound horizon and A_{bao} is the amplitude of the BAO oscillations.
Thus, performing the derivative of the power spectrum that appears in the consistency relations we have:

$$\begin{aligned}
\frac{\mathrm{d}\log P^{(0)}_m(k)}{\mathrm{d}\log k} &= \frac{\mathrm{d}\log\left[P^{nw}_m(k) + P^{nw}_m(k)A_{bao}(k)\sin(kr_s)\right]}{\mathrm{d}\log k} \\
&= \frac{k}{P^{(0)}_m(k)}\frac{\mathrm{d}P^{nw}_m(k)}{\mathrm{d}k} + \frac{k}{P^{(0)}_m(k)}\left[\frac{\mathrm{d}P^{nw}_m(k)}{\mathrm{d}k}A_{bao}(k)\sin(kr_s)\right] \\
&+ kr_sA_{bao}(k)\Bigg[\frac{1}{1+A_{bao}(k)\sin(kr_s)}\cos(kr_s) \\
&+ \frac{1}{r_s}\frac{1}{1+A_{bao}(k)\sin(kr_s)}\frac{1}{A_{bao}(k)}\frac{\mathrm{d}A_{bao}(k)}{\mathrm{d}k}\sin(kr_s)\Bigg] \\
&= \frac{\mathrm{d}\log P^{nw}_m(k)}{\mathrm{d}\log k} + \frac{kr_sA_{bao}(k)}{1+A_{bao}(k)\sin(kr_s)}\left[\cos(kr_s) + \alpha(k)\sin(kr_s)\right]
\end{aligned} \tag{4.29}$$

where we have defined

$$\alpha(k) \equiv \frac{1}{kr_s}\frac{\mathrm{d}\log A_{bao}(k)}{\mathrm{d}\log k}. \tag{4.30}$$

We see that the bispectrum in the squeezed limit contains an oscillating component whose amplitude is enhanced by $kr_s \sim 2\pi k/(0.05\mathrm{hMpc}^{-1})$ and it also has a smooth

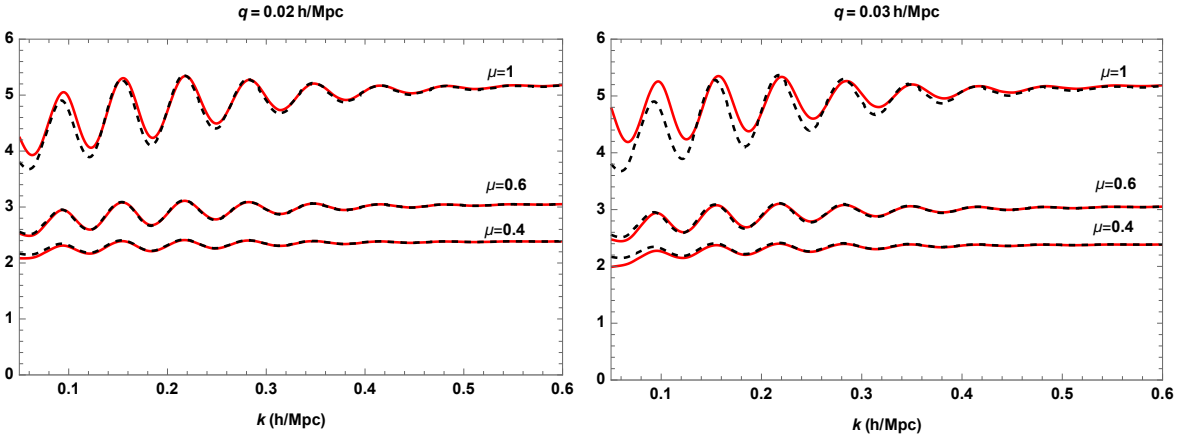

Figure 4.1: Comparison between the l.h.s. and the r.h.s. of eq. (4.26). The red solid line is the tree-level bispectrum (divided by $P_m^{(0)}(q)$ and $P_m^{(0)}(k)$), whereas the black dashed line is the r.h.s. of the equation. Note that the plot is made choosing $q = 0.02$ h/Mpc for the left panel and $q = 0.03$ h/Mpc for the right one. In addition, three different values of μ were chosen.

component given by the first term on the r.h.s of the last line of eq. (4.29).
In Fig. 4.1 we show the result of eq. (4.26), comparing the l.h.s and the r.h.s. of the equation, for $q = 0.02$ h/Mpc, $q = 0.03$ h/Mpc and for three different values of μ. We see, as we expect, that the consistency relations hold if the squeezed limit is true, i.e. as long as k is big enough. Also, if we choose a greater value for q, we clearly see less correspondence between the two sides of the consistency relations, especially for higher values of μ. We also note that, as we will see in the last chapter of this work, the amplitude of the oscillations of the two sides of the consistency relations are deeply related by the CR.

4.2 Damping of Baryon Acoustic Oscillations

A key advantage of the BAO as a cosmological probe is that nonlinearities such as those induced from nonlinear gravitational clustering induce predictable shifts in the oscillation scale and hence can be modelled both analytically and through numerical simulations [24]. There are, however, two important effects we want to investigate more in detail.
The first effect caused by nonlinearity is the shift in the peak of the correlation function due to mode-mode coupling [54]. This happens basically for two reasons. First, if the smooth part of the correlation function changes along with time, the acoustic peak will shift as well [24]. Secondly, let us go back at the model in which we considered the expanding wave from the initial point-like overdensity. When we are writing the two point correlation function we are asking ourselves: what is the probability of finding a galaxy at a given distance, assuming that there is a galaxy at the origin. But, taking into account the nonlinear evolution of the density shell, we would expect it to undergo some collapse during the expansion of the universe, due to its own self-gravity and due to the gravity provided by the galaxy at the center. This all lead to a shrinking of the radius of the shell hence shifting the peak of the two point correlation function.
The second effect caused by nonlinearity is the smoothing and broadening of the peak. Still qualitatively we can think of this effect as follows. Let us imagine that a galaxy forms on the BAP shell. Since we are considering nonlinearities, this galaxy will interact with all other over and under-densities, therefore generating a net force which may pull the galaxy outwards or inwards [24]. Since the correlation function is computed by averaging over all available galaxies, the average effect is to broaden and to smooth the BAP. These two effects are shown in Fig. (4.2).
In the fourier space, this broadening of the BAP can be translated into a damping of the oscillations in the power spectrum on small scales. We can understand this process analytically as follows. Let us think to the correlation function $\xi(r)$ as a shifted Gaussian:

$$\xi(r) = e^{-\frac{(r-r_\star)^2}{2\sigma^2}}. \tag{4.31}$$

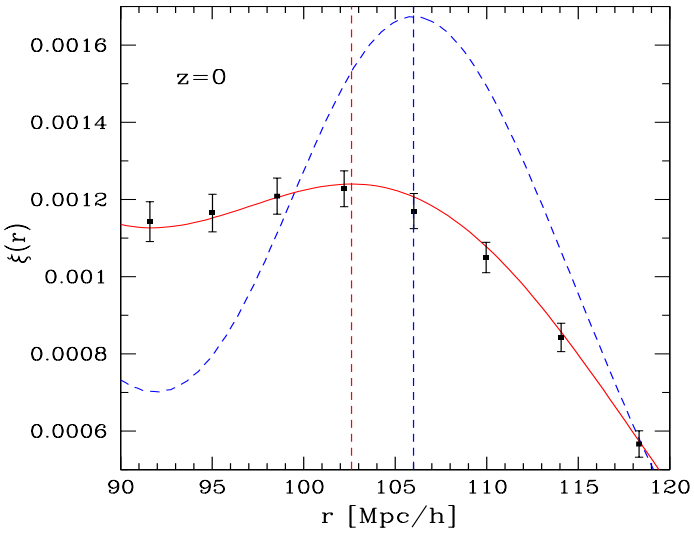

Figure 4.2: Movement of the Baryon Acoustic Peak at z=0. The linear peak (dashed line) is both broadened and shifted towards smaller scales. The solid line shows the prediction for the shift from renormalised perturbation theory (RPT) [55]. The vertical lines denote the corresponding maxima of the linear and nonlinear correlation functions. Figure taken from [56].

Therefore, using eq. (2.29) we have:

$$\begin{aligned} P(k) &= \int_{-\infty}^{\infty} e^{-\frac{(r-r_\star)^2}{2\sigma^2}} e^{-ikr} dr \\ &= \sqrt{\frac{\pi}{2}} e^{-ikr_\star} e^{-k^2\sigma^2}. \end{aligned} \tag{4.32}$$

In Fig. (4.3) is illustrated this model. We see that, as the Gaussian broadens, the oscillations in the power spectrum are washed out, making their detection harder.

We now want to investigate more quantitatively the behavior of BAO oscillations and understand more deeply the reason why they are damped. We can see this starting from the evolution equation of the power spectrum. We will follow [57] for this derivation.

Neglecting vorticity, the first two moments of the coarse-grained Vlasov equation give the continuity and Euler equations, which can be rewritten in a compact form in Fourier space as follows:

$$\begin{aligned} \left(\delta_{ab}\partial_\eta + \Omega_{ab}\right)\varphi_b(\mathbf{k},\eta) = \int \frac{d^3\mathbf{q}_1}{(2\pi)^3} \int \frac{d^3\mathbf{q}_2}{(2\pi)^3} (2\pi)^3 \delta_D(\mathbf{k}-\mathbf{q}_1-\mathbf{q}_2) \times \\ \left[e^\eta \gamma_{abc}(\mathbf{q}_1,\mathbf{q}_2)\varphi_b(\mathbf{q}_1,\eta)\varphi_c(\mathbf{q}_2,\eta) - h_a(\mathbf{k},\eta)\right] \end{aligned} \tag{4.33}$$

where:

$$\varphi_1(\mathbf{k},\eta) \equiv e^{-\eta}\tilde{\delta}(\mathbf{k},\eta) \qquad \varphi_2(\mathbf{k},\eta) \equiv e^{-\eta}\frac{-\tilde{\theta}(\mathbf{k},\eta)}{\mathcal{H}f}. \tag{4.34}$$

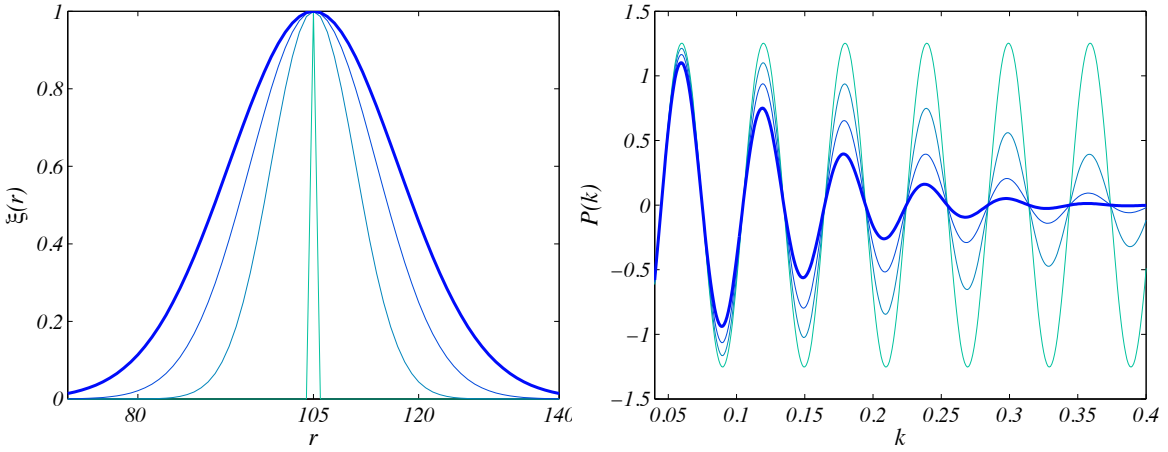

Figure 4.3: Smoothing out the baryon acoustic signal in the Fourier pair $\xi(r)$, $P(k)$. Increasing the width of the correlation function peak corresponds to the damping of the acoustic oscillations in the power spectrum. Figure taken from [24].

We have used $\eta = \log D(\tau)$ and the linear growth function $f(\eta) \equiv \frac{1}{\mathcal{H}}\frac{\mathrm{d}\eta}{\mathrm{d}\tau}$. The left hand side of of eq. (4.33) is the linearized part of the equation for the two dynamical modes, and in particular the matrix $\mathbf{\Omega}$ reads:

$$\mathbf{\Omega} = \begin{pmatrix} 1 & -1 \\ -\frac{3}{2}\frac{\Omega_m}{f^2} & \frac{3}{2}\frac{\Omega_m}{f^2} \end{pmatrix}. \tag{4.35}$$

Moreover, on the r.h.s, the first term on the square brackets encodes the mode-coupling between the fields. In particular the only non vanishing components of the vertex functions are:

$$\gamma_{121}(\mathbf{p},\mathbf{q}) = \frac{(\mathbf{p}+\mathbf{q})\cdot\mathbf{p}}{2p^2} \qquad \gamma_{112}(\mathbf{q},\mathbf{p}) = \gamma_{121}(\mathbf{p},\mathbf{q}) \qquad \gamma_{222} = \frac{(\mathbf{p}+\mathbf{q})^2\mathbf{p}\cdot\mathbf{q}}{2p^2q^2}. \tag{4.36}$$

It is useful to recast the mode-coupling term in this manner:

$$\begin{aligned} e^{\eta}\gamma_{abc}(\mathbf{q}_1,\mathbf{q}_2)\varphi_b(\mathbf{q}_1,\eta)\varphi_c(\mathbf{q}_2,\eta) =& e^{\eta}\delta_{a2}\tilde{\gamma}(\mathbf{q}_1,\mathbf{q}_2)\varphi_2(\mathbf{q}_1,\eta)\varphi_2(\mathbf{q}_2,\eta) + \\ & - ik^j\frac{\tilde{v}^j(\mathbf{q}_1)}{\mathcal{H}f}\varphi_a(\mathbf{q}_2,\eta) \end{aligned} \tag{4.37}$$

with

$$\tilde{\gamma}(\mathbf{q}_1,\mathbf{q}_2) = \frac{(\mathbf{q}_1\cdot\mathbf{q}_2)^2}{q_1^2q_2^2} - 1. \tag{4.38}$$

When $q_1 \ll k \simeq q_2$ the second term on the r.h.s. of eq. (4.37) discriminates the leading contributions to the mode-coupling induced by long velocity modes.

In particular, expressing the velocity through eq. (2.118), the second term gives

$$e^{\eta}\frac{\mathbf{k}\cdot\mathbf{q}_1}{q_1^2}\varphi_2(\mathbf{q}_1,\eta)\varphi_a(\mathbf{q}_2,\eta). \tag{4.39}$$

which is an IR divergent term. In addition, let us note that the vertex function, eq. (4.38), is never divergent; in fact it can be written as $\cos^2\theta_{12}-1$, where θ_{12} is the angle between $\mathbf{q}_1$ and $\mathbf{q}_2$, and also it vanishes for $\mathbf{k}=\mathbf{q}_1+\mathbf{q}_2\to 0$. Therefore, the only IR divergent term we need to account for is that of eq. (4.39).
We will now discuss the effects of the resummation at all orders. First of all we apply the equation of motion, eq. (4.33), to the correlator $\langle\varphi_a(\mathbf{k},\eta)\varphi_b(-\mathbf{k},\eta)\rangle'$ in order to attain the evolution equation for the power spectrum. As we have done before, the prime indicates that we have divided bu the overall momentum delta function. We get:

$$\underbrace{\langle\varphi_a(\mathbf{k},\eta)\left(\delta_{db}\partial_\eta+\Omega_{db}\right)\varphi_b(-\mathbf{k},\eta)\rangle'}_{\mathbf{A}}+\underbrace{\langle\left(\delta_{ac}\partial_\eta+\Omega_{ac}\right)\varphi_a(\mathbf{k},\eta)\varphi_b(-\mathbf{k},\eta)\rangle'}_{\mathbf{B}}, \tag{4.40}$$

we have:

$$\begin{aligned}\mathbf{A}&=\langle\varphi_a(\mathbf{k})\int\frac{d^3\mathbf{q}_1}{(2\pi)^3}\int\frac{d^3\mathbf{q}_2}{(2\pi)^3}(2\pi)^3\delta_D(-\mathbf{k}-\mathbf{q}_1-\mathbf{q}_2)\times\\&\qquad e^{\eta}\gamma_{dbc}(\mathbf{q}_1,\mathbf{q}_2)\varphi_b(\mathbf{q}_1)\varphi_c(\mathbf{q}_2)\rangle'\\&=\langle\varphi_a(\mathbf{k})\int\frac{d^3\mathbf{q}_1}{(2\pi)^3}\int\frac{d^3\mathbf{q}_2}{(2\pi)^3}(2\pi)^3\delta_D(-\mathbf{k}-\mathbf{q}_1-\mathbf{q}_2)\times\\&\qquad\left[e^{\eta}\delta_{d2}\tilde{\gamma}(\mathbf{q}_1,\mathbf{q}_2)\varphi_2(\mathbf{q}_1)\varphi_2(\mathbf{q}_2)+ik^j\frac{\tilde{v}^j}{\mathcal{H}f}\varphi_d(\mathbf{q}_2)\right]\rangle'.\end{aligned} \tag{4.41}$$

Thus, taking care only of the second term in square brackets:

$$\begin{aligned}\mathbf{A}&=\langle\varphi_a(\mathbf{k})\int\frac{d^3\mathbf{q}_1}{(2\pi)^3}\int\frac{d^3\mathbf{q}_2}{(2\pi)^3}(2\pi)^3\delta_D(-\mathbf{k}-\mathbf{q}_1-\mathbf{q}_2)\times\\&\qquad e^{\eta}\left(-\frac{\mathbf{k}\cdot\mathbf{q}_1}{q_1^2}\varphi_2(\mathbf{q}_1)\varphi_d(\mathbf{q}_2)\right)\rangle'\\&=\langle\varphi_a(\mathbf{k})\int\frac{d^3\mathbf{q}_1}{(2\pi)^3}\int\frac{d^3\mathbf{q}_2}{(2\pi)^3}(2\pi)^3\delta_D(-\mathbf{k}+\mathbf{q}_1-\mathbf{q}_2)\times\\&\qquad e^{\eta}\left(\frac{\mathbf{k}\cdot\mathbf{q}_1}{q_1^2}\varphi_2(-\mathbf{q}_1)\varphi_d(\mathbf{q}_2)\right)\rangle'\\&=e^{\eta}\int\frac{d^3\mathbf{q}_1}{(2\pi)^3}\frac{\mathbf{k}\cdot\mathbf{q}_1}{q_1^2}\langle\varphi_a(\mathbf{k})\varphi_2(-\mathbf{q}_1)\varphi_d(-\mathbf{k}+\mathbf{q}_1)\rangle'.\end{aligned} \tag{4.42}$$

Then, similarly, for the other term we have:

$$\begin{aligned}\mathbf{B} &= e^{\eta}\langle\int\frac{d^3\mathbf{q}_1}{(2\pi)^3}\int\frac{d^3\mathbf{q}_2}{(2\pi)^3}(2\pi)^3\delta_D(\mathbf{k}-\mathbf{q}_1-\mathbf{q}_2)\frac{\mathbf{k}\cdot\mathbf{q}_1}{q_1^2}\varphi_2(\mathbf{q}_1)\varphi_c(\mathbf{q}_2)\varphi_b(-\mathbf{k})\rangle' \\ &= e^{\eta}\langle\int\frac{d^3\mathbf{q}_1}{(2\pi)^3}(2\pi)^3\frac{\mathbf{k}\cdot\mathbf{q}_1}{q_1^2}\varphi_2(\mathbf{q}_1)\varphi_c(\mathbf{k}-\mathbf{q}_1)\varphi_b(-\mathbf{k})\rangle' \\ &= e^{\eta}\int\frac{d^3\mathbf{q}_1}{(2\pi)^3}\frac{\mathbf{k}\cdot\mathbf{q}_1}{q_1^2}\langle\varphi_2(\mathbf{q}_1)\varphi_c(\mathbf{k}-\mathbf{q}_1)\varphi_b(-\mathbf{k})\rangle'.\end{aligned} \tag{4.43}$$

So, in the evolution equation for the power spectrum, the last term of eq. (4.37) gives:

$$e^{\eta}\int\frac{d^3\mathbf{q}}{(2\pi)^3}\frac{\mathbf{k}\cdot\mathbf{q}}{q^2}\left[\langle\varphi_2(\mathbf{q})\varphi_a(\mathbf{k}-\mathbf{q})\varphi_b(-\mathbf{k})\rangle' + \langle\varphi_a(\mathbf{k})\varphi_b(-\mathbf{k}+\mathbf{q})\varphi_2(-\mathbf{q})\rangle'\right]. \tag{4.44}$$

The already derived consistency relations, eq. (4.18), can be written now as follows:

$$\langle\varphi_2(\mathbf{q})\varphi_a(\mathbf{k}-\mathbf{q})\varphi_b(-\mathbf{k})\rangle' \simeq -e^{\eta}\frac{\mathbf{k}\cdot\mathbf{q}}{q^2}P^{(0)}(q)\left(P_{ab}(k)-P_{ab}(|\mathbf{k}-\mathbf{q}|)\right)+O\left(\left(\frac{q}{k}\right)^0\right) \tag{4.45}$$

for $q \ll k$. Inserting eq. (4.45) into eq. (4.44) we arrive to:

$$\begin{aligned}&-2e^{2\eta}\int\frac{d^3\mathbf{q}}{(2\pi)^3}\left(\frac{\mathbf{k}\cdot\mathbf{q}}{q^2}\right)^2P^{(0)}(q)\left(P_{ab}(k)-P_{ab}(|\mathbf{k}-\mathbf{q}|)\right) \\ &\simeq -2e^{2\eta}\frac{k^2}{(2\pi)^2}\int dqP^{(0)}(q)\int_{-1}^{1}dxx^2\left(P_{ab}(k)-P_{ab}(k-qx)\right). \\ &= -2e^{2\eta}\frac{k^2}{(2\pi)^2}\int dqP^{(0)}(q)\bar{P}^1_{ab}(k,q)F^1(qr_s)\end{aligned} \tag{4.46}$$

In the last passage we have defined:

$$\bar{P}^n_{ab}(k,q)\equiv\frac{\int_{-1}^{1}dxx^{2n}\left(1-\frac{P_{ab}(k-qx)}{P_{ab}(k)}\right)}{F^n(qr_s)}P_{ab}(k), \tag{4.47}$$

with:

$$F^n(qr_s)\equiv\int_{-1}^{1}dxx^{2n}(1-\cos(qr_sx)) \tag{4.48}$$

so that $F^1(qr_s) = 2(1 - j_0(qr_s) + 2j_2(qr_s))/3$, where $j_n(x)$ are the spherical Bessel functions.[1]

As we have done in Sec. 4.1 we can write the power spectrum in the following way:

[1]Please note that $j_0(x) = \frac{\sin x}{x}$ and $j_2(x) = -\frac{\sin x}{x} - 3\frac{\cos x}{x^2} + 3\frac{\sin x}{x^3}$.

$$P_{ab}(k) = P^{nw}_{ab}(k)\,(1 + A_{bao}(k)\sin(kr_s)) \equiv P^{nw}_{ab}(k) + P^{w}_{ab}(k) \tag{4.49}$$

where $A_{bao}(k)$, as before, is the smooth modulating function which damps the oscillations. If we insert eq. (4.49) into eq. (4.47) we obtain:

$$\bar{P}^{n}_{ab}(k,q) = P^{w}_{ab}(k) + O\left(P^{nw\,\prime\prime}_{ab}(k)/r_s^2\right). \tag{4.50}$$

Hence, eq. (4.46) becomes:

$$-2e^{2\eta}k^2\epsilon^2(r_s)P^{w}_{ab}(k) + O\left(P^{nw\,\prime\prime}_{ab}\right) \tag{4.51}$$

using

$$\epsilon^2(r_s) \equiv \frac{1}{6\pi^2}\int dq P^{(0)}(q)(1 - j_0(qr_s) + 2j_2(qr_s)). \tag{4.52}$$

Now we follow the approach of [58], in which the class of loop diagrams that are most IR-enhanced are first identified and then resummed into the nonperturbative effect, that is the exponential BAO damping. Their L-loop diagram reads:

$$P^{w}_{L-\mathrm{loop,LO}}(k) = \frac{1}{L!}\prod_{i=1}^{L}\left[\frac{1}{2}\int^{\Lambda} d^3q_i P^{nw}(q_i)\mathcal{D}_{\mathbf{q}_i}\mathcal{D}_{-\mathbf{q}_i}\right]P^{w}(k), \tag{4.53}$$

where 'LO' stands for leading-order IR-enhanced loops; moreover we have defined

$$\mathcal{D}_{\mathbf{q}_i}P^{w}(k) = \frac{\mathbf{q}_i\cdot\mathbf{k}}{q_i^2}\left(P^{w}\left(|\mathbf{k}+\mathbf{q}|\right) - P^{w}(k)\right) = \frac{\mathbf{q}_i\cdot\mathbf{k}}{q_i^2}\left(e^{\mathbf{q}_i\cdot\nabla_{\mathbf{k}'}} - 1\right)P^{w}(k')\Big|_{k'=k}. \tag{4.54}$$

In order to calculate the wiggle power spectrum at L^{th} order we can exploit eq. (4.51), that is (setting $\eta = 0$ and suppressing the ab subscript):

$$P^{w}_{1-\mathrm{loop}}(k) = -k^2\epsilon^2 P^{w}(k). \tag{4.55}$$

In fact, we see that, at first order, eq. (4.53) must coincide to eq. (4.55). Therefore, it is straightforward to see that, for the L^{th} order we simply have:

$$P^{w}_{L-\mathrm{loop,LO}}(k) = \frac{(-k^2\epsilon^2)^L}{L!}P^{w}(k). \tag{4.56}$$

Finally, resumming all these terms at all orders we obtain the exponential damping above mentioned:

$$P^{w}_{\mathrm{IR,LO}}(k) = \sum_{L=0}^{\infty}P^{w}_{L-\mathrm{loop,LO}}(k) = e^{-k^2\epsilon^2}P^{w}(k). \tag{4.57}$$

Therefore, referring to eq. (4.49) we can write the power spectrum as:

$$P(k) = P^{nw}(k) + e^{-k^2\epsilon^2}P^{w}(k). \tag{4.58}$$

Chapter 5

Forecast of Cosmological Parameters

5.1 Bias Parameter Forecast

In this section we will perform a forecast on the bias parameter derived in the previous chapter. We will achieve this goal using the Fisher matrix formalism.
To this aim, we will start from the consistency relations we derived in the last chapter, which we report here:

$$\lim_{q/k\to 0} \frac{B_{\alpha\beta\gamma}(q,k_+,k_-)}{P_{\alpha\alpha}(q)P_{\beta\gamma}(k)} = -\frac{\mu^2}{b_\alpha(q)}\frac{\mathrm{d}\log P_{\beta\gamma}(k)}{\mathrm{d}\log k} + O\left(\left(\frac{q}{k}\right)^0\right). \tag{5.1}$$

Let us recall that we have defined the bias parameter as the ratio between the power spectrum of a specific tracer (galaxies, CMB photons, dark matter and so on) and the cross correlator between dark matter and the given tracer, i.e.

$$b_\alpha(q) = \lim_{q\to 0}\frac{P_{\alpha\alpha}(q)}{P_{\alpha m}(q)}. \tag{5.2}$$

Therefore, for dark matter ($\alpha = m$) we have that $b_m(q) = 1$.
In the last chapter we checked eq. (5.1) in perturbation theory computing also the leading smooth term, namely

$$\lim_{q/k\to 0} \frac{B^{SPT}_{mmm}(q,k_+,k_-)}{P^0_m(q)P^0_m(k)} = -\mu^2\frac{\mathrm{d}\log P^0_m(k)}{\mathrm{d}\log k} + \frac{13+8\mu^2}{7} + O\left(\frac{q}{k}\right) \tag{5.3}$$

which, at first order, is exactly scale independent.
We will base our forecast of the error on the bias parameter on the Fisher matrix approach, introduced in Sec. 3.2. In particular, from eq. (3.15) we can have an estimate of the best error we get on the bias parameter, given the dark matter bispectrum and power spectrum. As we have already pointed out, in order to evaluate the error on the bias, in this approach we do not need to simulate any set of data. All we need is the probability distribution of the data given the parameters of the theory we assume to be true.

Hence, we start writing the Likelihood associated to our calculation, which reads

$$L \propto \exp\left[-\frac{1}{2}\sum_i \left(\frac{\frac{B(q,|\mathbf{k}_i+\mathbf{q}/2|,|\mathbf{k}_i-\mathbf{q}/2|)}{P(k_i)P(q)} + \frac{1}{b_m(q)}\mu^2\frac{\mathrm{d}\log P(k_i)}{\mathrm{d}\log k_i} - f(k_i,q,\mu)}{\sigma_i}\right)^2\right] \tag{5.4}$$

that is, a Gaussian distribution obtained using the consistency relations. Note that we have added $f(k_i, q, \mu)$, which is simply a polynomial fit of the difference of the two sides of the CR having set $b_m(q) = 1$. Thus, $f(k_i, q, \mu)$ is a smooth function and subtracting it in eq. (5.4) actually allows us to compare only the oscillatory parts of the two sides of the consistency relations.
Note that the sum in eq. (5.4) is made over the i-th k-bin. As we shall see more in details, since we are comparing the oscillatory parts of the two side of the consistency relations, the k-range we will take into account will be the range in which the power spectrum shows oscillating features. Lastly, the error σ_i associated to our distribution is the error we anticipate from the future measurements of the bispectrum and the power spectrum. We will give more details on this in what follows.
We will assume that the only parameter of the theory is b_m. This means that the Fisher matrix has rank equal to 1. Moreover, the Fisher matrix is obtained recalling that

$$F_{bb} = -\left\langle \frac{\partial^2 \log L}{\partial b_m^2} \right\rangle \tag{5.5}$$

evaluated in $b_m = 1$ and, using eq. (3.15), the best error we can obtain on b_m is simply

$$\sigma_b = \frac{1}{\sqrt{F_{bb}}}. \tag{5.6}$$

The power spectrum we will use for our calculations is the linear matter power spectrum obtained using CAMB [59].
The next step, in order to perform the calculation of eq. (5.5), is to understand what should we put as σ_i, i.e. what is the error associated to our probability distribution. As we have said before, the numerator of eq. (5.4) is made up of three terms; we can actually consider only the first two terms, which are respectively the l.h.s and minus the r.h.s of eq. (5.1). Therefore, assuming that the two are uncorrelated, we have:

$$\sigma_i = \sqrt{(\sigma^2_{LHS})_i + (\sigma^2_{RHS})_i} \tag{5.7}$$

where LHS and RHS indicate the left and the right hand sides of the consistency relations. We therefore need to understand how to compute these errors for given survey specifications. We will follow [60].

5.1.1 Power Spectrum and Bispectrum Error

An estimator for the power spectrum may be written as

$$P_{obs}(k) = \frac{1}{N_k}\sum_{i=1}^{N_k}|\delta(\mathbf{k}_i)|^2\Big|_{|\mathbf{k}_i-k|\leq\Delta k} \tag{5.8}$$

where Δk is the bin width, which is greater or equal than k_f, the fundamental wavenumber of the survey, given by

$$k_f = \frac{2\pi}{V^{1/3}} \tag{5.9}$$

where V is the survey volume. Moreover, N_k is the number of independent k-modes available per bin. This estimator is unbiased, namely

$$\langle P_{obs}(k)\rangle = \frac{1}{N_k}\sum_{i=1}^{N_k}\langle|\delta(\mathbf{k}_i)|^2\rangle\Big|_{|\mathbf{k}_i-k|\leq\ k_f} = \langle|\delta(k)|^2\rangle = P(k). \tag{5.10}$$

The variance of this estimator is given by

$$\langle\left(\frac{P_{obs}(k)-P(k)}{P(k)}\right)^2\rangle = 1-2\frac{\langle P_{obs}\rangle}{P(k)}+\frac{1}{N_k^2P(k)^2}\sum_{i=1}^{N_k}\sum_{j=1}^{N_k}\langle\delta^\star(\mathbf{k}_i)\delta(\mathbf{k}_i)\delta^\star(\mathbf{k}_j)\delta(\mathbf{k}_j)\rangle. \tag{5.11}$$

We use Wick theorem and evaluate the summation neglecting the connected contribution to the four point function:

$$\begin{aligned}\sum_{i=1}^{N_k}\sum_{j=1}^{N_k}\langle\delta^\star(\mathbf{k}_i)\delta(\mathbf{k}_i)\delta^\star(\mathbf{k}_j)\delta(\mathbf{k}_j)\rangle &= \sum_{i=1}^{N_k}\sum_{j=1}^{N_k}\Big[\langle\delta^\star(\mathbf{k}_i)\delta(\mathbf{k}_i)\rangle\langle\delta^\star(\mathbf{k}_j)\delta(\mathbf{k}_j)\rangle \\ &+ \langle\delta^\star(\mathbf{k}_i)\delta(\mathbf{k}_j)\rangle\langle\delta^\star(\mathbf{k}_j)\delta(\mathbf{k}_i)\rangle \\ &+ \langle\delta^\star(\mathbf{k}_i)\delta^\star(\mathbf{k}_j)\rangle\langle\delta(\mathbf{k}_i)\delta(\mathbf{k}_j)\rangle\Big] \\ &= N_k^2P(k)^2+2N_kP(k)^2,\end{aligned} \tag{5.12}$$

where the first contribution comes from the first line and the second one from the last two lines. Thus, the variance is:

$$\langle(P_{obs}(k)-P(k))^2\rangle = 2\frac{P(k)^2}{N_k} \tag{5.13}$$

therefore leading to the standard deviation

$$\sigma_{P(k)} = \sqrt{\frac{2}{N_k}}P(k). \tag{5.14}$$

We need now to calculate N_k, which reads:

$$N_k = \frac{4\pi k^2 \Delta k}{k_f^3} = 4\pi \left(\frac{k}{k_f}\right)^2 \frac{\Delta k}{k_f} \tag{5.15}$$

which, expressing k_f through eq. (5.9), leads to the following form for the error on the power spectrum:

$$\sigma_{P(k)} = 2\pi \frac{P(k)}{k\sqrt{V\Delta k}}. \tag{5.16}$$

Instead, for the bispectrum, we have that an estimator is given by [61]:

$$B_{obs}(k_1, k_2, k_3) = \frac{k_f^3}{V_B} \int_{k_1} d^3\mathbf{q}_1 \int_{k_2} d^3\mathbf{q}_2 \int_{k_3} d^3\mathbf{q}_3 \delta_D(\mathbf{q}_{123}) \delta(\mathbf{q}_1)\delta(\mathbf{q}_2)\delta(\mathbf{q}_3) \tag{5.17}$$

where the integration is over the bin defined by $q_i \in (k_i - \Delta k/2, k_i + \Delta k/2)$ and

$$V_B \equiv \int_{k_1} d^3\mathbf{q}_1 \int_{k_2} d^3\mathbf{q}_2 \int_{k_3} d^3\mathbf{q}_3 \delta_D(\mathbf{q}_{123}) \simeq 8\pi^2 k_1 k_2 k_3 \Delta k^3. \tag{5.18}$$

Let us now derive the variance associated to this estimator:

$$\Delta B^2 = \langle B_{obs}(k_1, k_2, k_3)^2 \rangle - \langle B(k_1, k_2, k_3) \rangle^2. \tag{5.19}$$

The first term is:

$$\begin{aligned} \langle B_{obs}(k_1, k_2, k_3)^2 \rangle = & \frac{k_f^3}{V_B^2} \int_{k_1} d^3\mathbf{q}_1 \int_{k_2} d^3\mathbf{q}_2 \int_{k_3} d^3\mathbf{q}_3 \int_{k_1} d^3\mathbf{p}_1 \int_{k_2} d^3\mathbf{p}_2 \int_{k_3} d^3\mathbf{p}_3 \times \\ & \delta_D(\mathbf{q}_{123}) \delta_D(\mathbf{p}_{123}) \langle \delta(\mathbf{q}_1)\delta(\mathbf{q}_2)\delta(\mathbf{q}_3)\delta(\mathbf{p}_1)\delta(\mathbf{p}_2)\delta(\mathbf{p}_3) \rangle. \end{aligned} \tag{5.20}$$

The expectation value of the 6 delta's is equal to:

$$\begin{aligned} = & s_{123} \langle \delta(\mathbf{q}_1)\delta(\mathbf{p}_1) \rangle \langle \delta(\mathbf{q}_2)\delta(\mathbf{p}_2) \rangle \langle \delta(\mathbf{q}_3)\delta(\mathbf{p}_3) \rangle + \langle \delta(\mathbf{q}_1)\delta(\mathbf{q}_2)\delta(\mathbf{q}_3) \rangle \langle \delta(\mathbf{p}_1)\delta(\mathbf{p}_2)\delta(\mathbf{p}_3) \rangle \\ & + O\left(P(q_1)T(q_1, q_2, p_1, p_2)\right) + O\left(H(q_1, q_2, q_3, p_1, p_2, p_3)\right) \end{aligned} \tag{5.21}$$

where $s_{123} = 6, 2, 1$ for equilateral, isosceles, and general triangles, respectively. Moreover, T denotes the trispectrum and H the hexaspectrum, and we can neglect them. The last term of the first line in eq. (5.21) cancels out with the second term of eq. (5.19), so that we have:

$$\begin{aligned} \Delta B^2 \simeq & s_{123} \frac{k_f^3}{V_B^2} \int_{k_1} d^3\mathbf{q}_1 \cdots \int_{k_3} d^3\mathbf{p}_3 \delta_D(\mathbf{q}_{123}) \delta_D(\mathbf{p}_{123}) \times \\ & \delta_D(\mathbf{q}_1 + \mathbf{p}_1) \delta_D(\mathbf{q}_2 + \mathbf{p}_2) \delta_D(\mathbf{q}_3 + \mathbf{p}_3) P(q_1) P(q_2) P(q_3) \end{aligned} \tag{5.22}$$

leading to:

$$\Delta B^2 \simeq s_{123}\frac{k_f^3}{V_B^2}\int_{k_1} d^3\mathbf{q}_1 \int_{k_1} d^2\mathbf{q}_2 \int_{k_3} d^3\mathbf{q}_3 \left[\delta_D(\mathbf{q}_{123})\right]^2 P(q_1)P(q_2)P(q_3). \tag{5.23}$$

Since we can write that

$$\frac{1}{V_B}\int_{k_1} d^3\mathbf{q}_1 \int_{k_1} d^2\mathbf{q}_2 \int_{k_3} d^3\mathbf{q}_3 \left[\delta_D(\mathbf{q}_{123})\right]^2 P(q_1)P(q_2)P(q_3) \simeq \frac{P(q_1)P(q_2)P(q_3)}{k_f^3} \tag{5.24}$$

we can finally write the variance as

$$\Delta B^2 \simeq k_f^3 \frac{s_{123}}{V_B} P(k_1)P(k_2)P(k_3). \tag{5.25}$$

We can recast eq. (5.25) and write the error on the bispectrum in the following way:

$$\sigma_{B(k_1,k_2,k_3)} \simeq \sqrt{\frac{\pi s_{123}}{V k_1 k_2 k_3 \Delta k^3}} \left[P(k_1)P(k_2)P(k_3)\right]^{1/2}. \tag{5.26}$$

Recalling that, given a function of n-independent variables $f(x_1, \ldots, x_n)$, it holds that

$$\sigma_f = \left(\sum_{i=1}^{n}\left(\frac{\partial f}{\partial x_i}\sigma_{x_i}\right)^2\right)^{1/2} \tag{5.27}$$

we are interested in the derivation of σ_{RHS}, the error of the r.h.s. of the consistency relations. Looking at eq. (4.18), we may rewrite the r.h.s. of the CR as

$$\mu\frac{k}{q}\frac{(P_m(k_-) - P_m(k_+))}{P_m(k)} \tag{5.28}$$

where we have set $b_m(q) = 1$. Then, assuming no error on k, q and μ, we have that

$$\sigma\left(\frac{(P_m(k_-) - P_m(k_+))}{P_m(k)}\right)^2 = \frac{\sigma\left(P(k_-) - P(k_+)\right)^2}{P(k)^2} + \frac{\left(P(k_-) - P(k_+)\right)^2}{P(k)^4}\sigma^2_{P(k)} \tag{5.29}$$

leading to

$$\sigma_{RHS} = \mu\frac{k}{q}\sqrt{\frac{\sigma^2_{P(k_-)} + \sigma^2_{P(k_+)}}{P(k)^2} + \frac{\left(P(k_-) - P(k_+)\right)^2}{P(k)^4}\sigma^2_{P(k)}} \tag{5.30}$$

which, in the squeezed limit, gives

$$\sigma_{RHS} = \sqrt{2}\mu\frac{k}{q}\frac{\sigma_{P(k)}}{P(k)}. \tag{5.31}$$

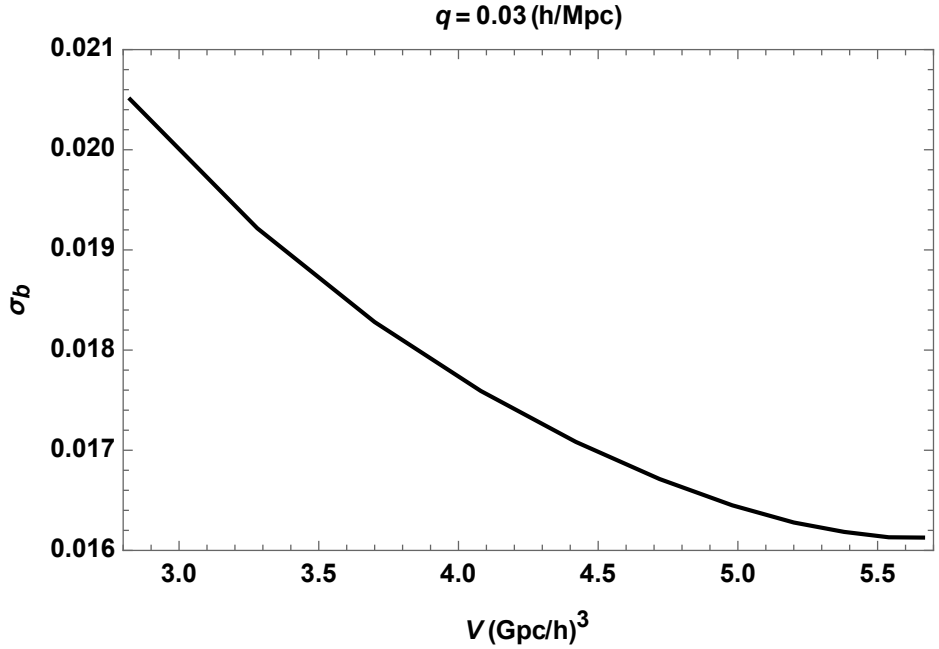

Figure 5.1: The error on the bias parameter defined in eq. (5.6). Since the value of the bias, in this case, is exactly 1, the error shown coincides with the relative error. For this plot we have chosen $b_m = 1, s_{123} = 2, \mu = 1$, $q = 0.03$ h/Mpc and $\Delta k = 0.016$ h/Mpc.

Similarly, we derive the standard deviation for the l.h.s. of the consistency relations. We obtain:

$$\sigma_{LHS} = \sqrt{\frac{\sigma^2_{B(q,k_+,k_-)}}{\left(P(k)P(q)\right)^2} + \frac{B(q,k_+,k_-)^2}{\left(P(k)P(q)\right)^4}\left(P(q)^2\sigma^2_{P(k)} + P(k)^2\sigma^2_{P(q)}\right)} \tag{5.32}$$

We have thus found the two contribution to the standard deviation in eq. (5.4), that we will add in quadrature according to eq. (5.7).

5.1.2 Error on the Bias Parameter

Now we have all the ingredients to proceed in the calculation of σ_b. Let us note that, from eqs. (5.4, 5.5, 5.16, 5.26, 5.31, 5.32) we have that the Fisher matrix is $\mathbf{F}_{bb} = \mathbf{F}_{bb}(k, q, \mu, s_{123}, V)$ with $\mu = \frac{\mathbf{k}\cdot\mathbf{q}}{kq}$, s_{123} is a geometrical factor and V is the survey volume. However, as already mentioned, we are doing this calculation at fixed q, μ, s_{123} and V and we are summing over the k-bins. The Fisher matrix therefore has only one parameter (b_m) and it is actually a matrix of rank 1, i.e. a number.

The first result obtained is the error on the bias parameter as a function of the survey volume. The computation was done using 25 linearly-spaced bins, from $k_{min} = 0.05$ h/Mpc up to $k_{max} = 0.45$ h/Mpc, using therefore a bin width of $\Delta k = 0.016$ h/Mpc. The result is shown in Fig. 5.1. We find, for $\mu = 1$, $\sigma_b \simeq 0.0161 - 0.0205$. We

have obtained what we have expected, namely we find lower values of the bias error as we increase the survey volume.
We also show, in Fig. 5.2 the value of the bias error as a function of k_{max}. For the computation we have used linearly-spaced bins from $k_{min} = 0.05$ h/Mpc up to different k_{max}. What is left unchanged, for any given k_{max} is the width of the bin, which was fixed at $\Delta k = 0.016$ h/Mpc. Note that, as we expect, if we go towards greater k_{max}, the error on the bias becomes smaller. This trend, however, seems to be more important at low k_{max} whereas, around $k_{max} \sim 0.35$ h/Mpc this effect starts to be less visible: this is because the oscillations amplitude of the power spectrum, around that value, becomes very small, see Fig. 5.6. Furthermore, still looking at Fig. 5.2, we note that, as the value of q increases, we get a better (smaller) error. This surely happens because if the value of q is bigger, the phase space volume is greater, and we have more triangles which we can make statistic with, therefore we expect this behavior. However, as we have said in Sec. 4.1 and in Fig. 4.1, since we have derived the consistency relations in the squeezed limit we expect them to be less reliable as q increases. But, how much exactly? What we can do, simply, is to calculate the reduced chi-squared of our probability distribution function, namely the numerator of the exponentiated part of eq. (5.4). In this way we can have a statistical description of how accurately the oscillating part of the l.h.s. resembles the r.h.s. one. In Fig. 5.3 we show the result for three different values of q. In particular we have obtained that for $q = 0.01$ (h/Mpc) $\chi^2_\nu = 0.002$ and $b_m = 1.002$, for $q = 0.02$ (h/Mpc) $\chi^2_\nu = 0.11$ and $b_m = 1.008$ and for $q = 0.03$ (h/Mpc) $\chi^2_\nu = 0.97$ and $b_m = 1.02$. We thus have that, indeed, as q increases, the CR are less precise; however, for example, still for $q = 0.03$ (h/Mpc) we obtain a value of χ^2_ν which is still satisfactory.
Now, since the galaxy clustering statistic is affected by shot noise, from now on we will take into account this effect. To this aim, we can rewrite the power spectrum as:

$$P(k)_{shot} = P(k) + n_g^{-1} \tag{5.33}$$

where n_g is the galaxy number density, with values of n_g taken from [62]. We repeat the same calculations of Fig. 5.2, but taking into account this correction. The result is showed in Fig. 5.4. We see that the results are very similar to the previous one; moreover we see, as expected, the values of σ_b are a little bit higher and tend to saturate, as k_{max} increases, a little bit before with respect to 5.2. As a result, the effect of shot noise is to roughly double the error at the plateau, for any of the considered q values.

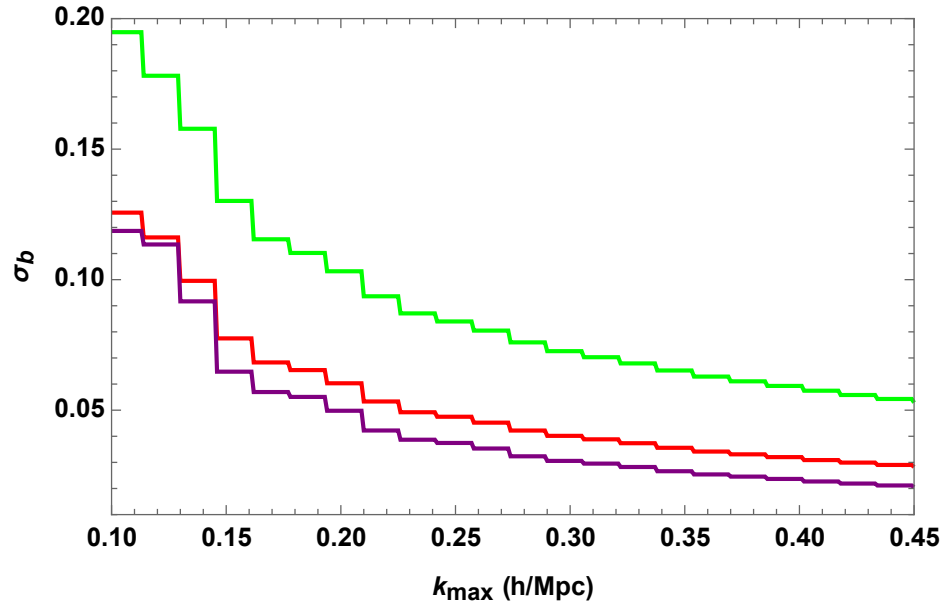

Figure 5.2: We show the value of the bias estimated error σ_b calculated at different k_{max} and at different q: $q = 0.01$ h/Mpc (green), $q = 0.02$ h/Mpc (red) and $q = 0.03$ h/Mpc (purple). The behaviour is what we were expecting: the more k_{max} reduces, the worse becomes the error on the bias. In this calculation we have set $b_m = 1, \mu = 1$ and $V = 2.82$ h^{-3}Gpc^3.

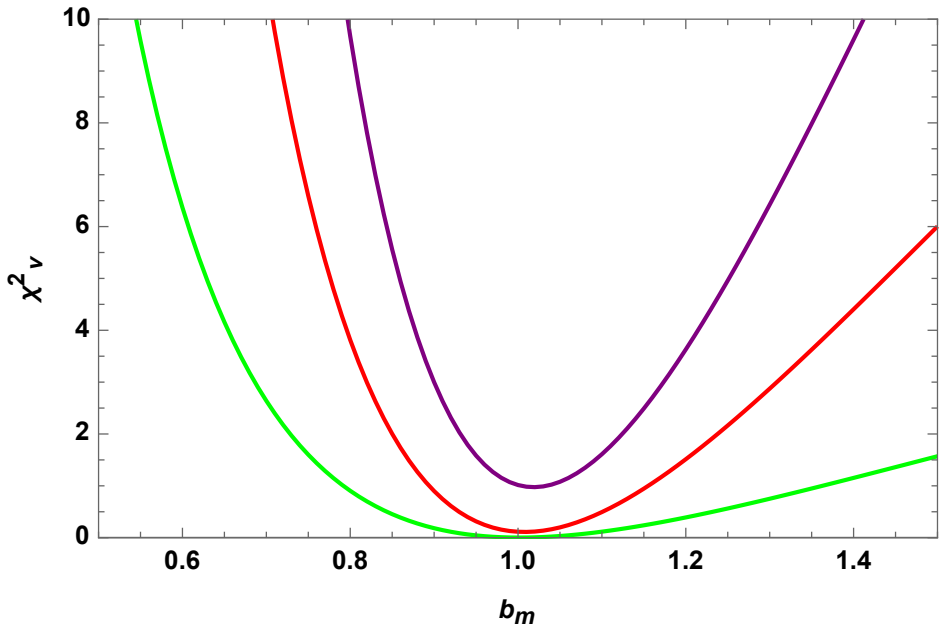

Figure 5.3: We show the χ^2_ν distribution for three different values of q: $q = 0.01$ h/Mpc (green), $q = 0.02$ h/Mpc (red) and $q = 0.03$ h/Mpc (purple). We see that, as q increases, the value of the minimum gets bigger and also the minimum point tends to be less precise (with respect to the fiducial value $b_m = 1$).

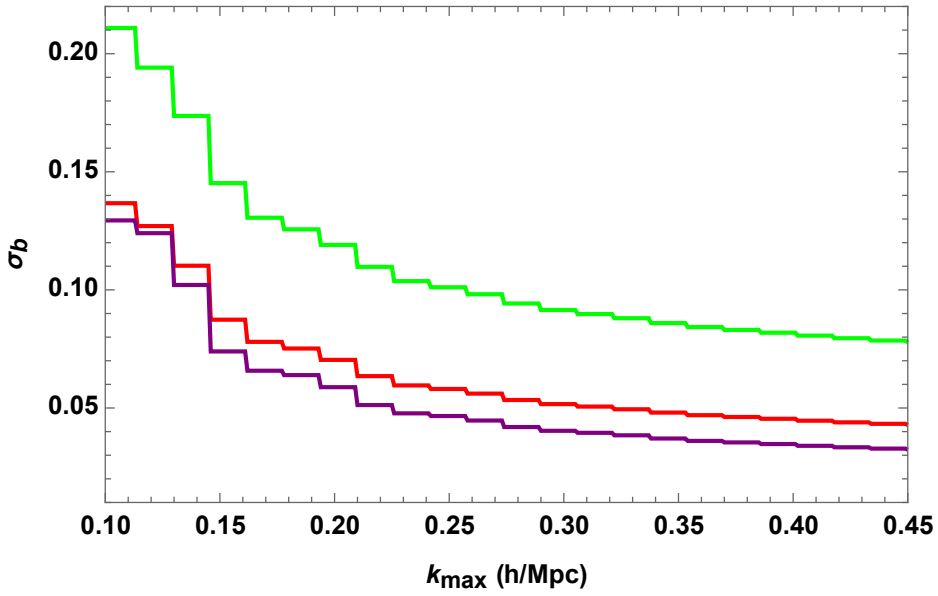

Figure 5.4: We show the value of the bias estimated error σ_b calculated at different k_{max} and at different q: $q = 0.01$ h/Mpc (green), $q = 0.02$ h/Mpc (red) and $q = 0.03$ h/Mpc (purple) including shot noise corrections. We note that, with respect to Fig. 5.2, σ_b is greater and that its values tends to saturate earlier. In this calculation we have set $b_m = 1, \mu = 1$ and $V = 2.82$ h^{-3}Gpc^3.

5.1.3 Bias Parameter Error with Damped Oscillations

As we have said, in our calculations we have used the linear matter power spectrum obtained with CAMB. However, we have seen in Sec. 4.2 that the BAO oscillations are actually suppressed. In this section we want to consider this effect which we have neglected so far.

As we have already derived, we can write the matter power spectrum in the following way:

$$P(k) = P^{nw}(k) + e^{-k^2\epsilon^2} P^{w}(k) \tag{5.34}$$

where we can, at least for now, think to the wiggle part as the oscillating features caused by the BAO's phenomenon. Note that, integrating eq. (4.52) we obtain the following values of ϵ^2: $\epsilon^2 = 35$ at $z = 0$, $\epsilon^2 = 12$ at $z = 1$ and $\epsilon^2 = 6$ at $z = 2$. Therefore, what we want to do, is to perform the same calculations we did in the last section, but taking a power spectrum which shows an exponentially suppressed wiggle term.

In order to do so, we perform a polynomial fit of the power spectrum with the following function:

$$p(k, V) = \sum_{i=-3}^{i=3} a_i(V) k^i \tag{5.35}$$

where we have decided to go from k^{-3} to k^3 because it was the best trade off option

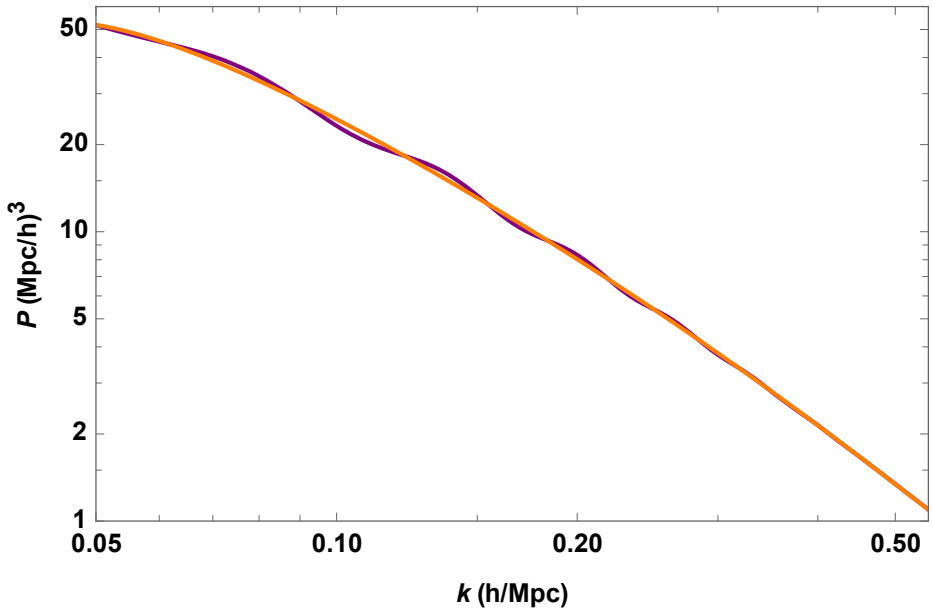

Figure 5.5: We show, between $k \sim 0.05$ and $k \sim 0.5$ the linear power spectrum $P(k)$ at zero redshift (purple), which exhibits the characteristic oscillatory features. We also display the polynomial fit $p(k, V)$ (orange) which represents the smooth part of the power spectrum.

between fitting only the smooth part of $P(k)$ and still obtaining a good χ^2 of the fitting distribution, see Fig. 5.5.
Afterward, subtracting from the power spectrum the fitting polynomial $p(k, V)$ we have obtained the wiggle part, i.e.

$$P^w(k) = P(k) - p(k, V), \tag{5.36}$$

which is shown in Fig. 5.6.

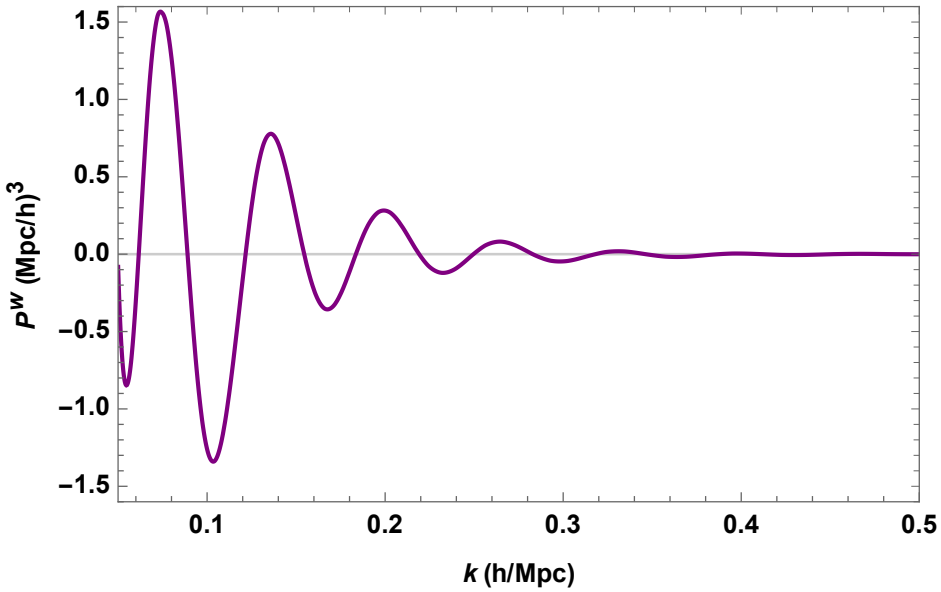

Figure 5.6: In this plot the wiggle part of the linear power spectrum $P^w(k)$ is shown. We can see that, even if they become really small in amplitude, the oscillations continue up to $k \sim 0.45$ h/Mpc.. This means that, referring to Fig. (5.2), in the calculation of the bias error we can extend the computation up to $k_{max} \sim 0.45$ h/Mpc.

The wiggle part was then multiplied by the exponential factor $e^{-k^2\epsilon^2}$, thus obtaining an explicit function that represents the wiggle suppressed part we were searching for, which we show in Fig. (5.7). Finally, summing the wiggle suppressed part to the smooth part allowed us to obtain the same exact power spectrum we started from, but with suppressed oscillating features, i.e.

$$P_{damped}(k, \epsilon, V) = p(k, V) + e^{-k^2\epsilon^2} \left[P(k) - p(k, V)\right]. \tag{5.37}$$

Let us note that the damped power spectrum depends on ϵ, therefore we expect σ_b to assume different values for each ϵ we choose. The process that allows us to obtain σ_b is the same we have done in the previous section and we show, in Fig. 5.8 the results of our calculations. Again, we have used linearly-spaced k-bins, keeping fixed $\Delta k = 0.016$ h/Mpc. We see what we have just said, namely that for any given value of ϵ the error on the bias assumes different values. In particular, as ϵ increases, the error gets worse. This is due to the fact that, if the oscillations are more suppressed, we have less information we can gain from the power spectrum, i.e. k_{max} will be smaller.

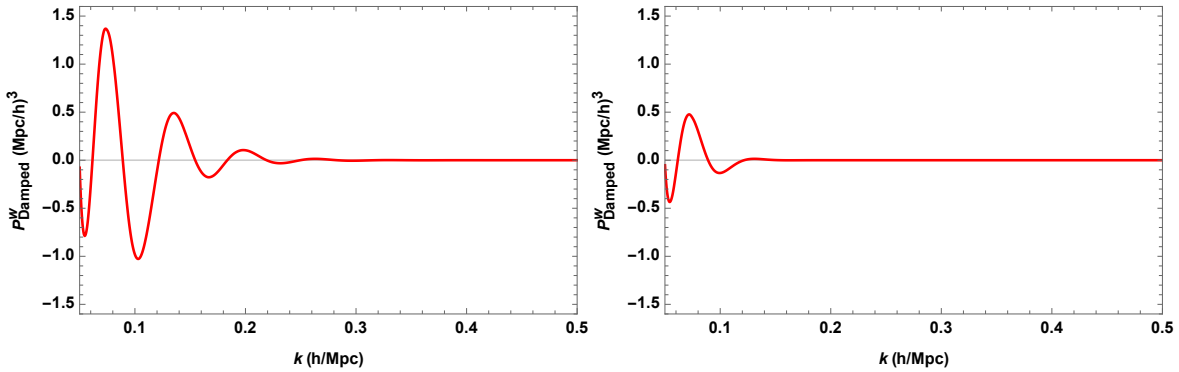

Figure 5.7: We show the damped wiggle part of the power spectrum, i.e. $e^{-k^2\epsilon^2}P^w(k)$. In the left panel we have chosen $\epsilon^2 = 5$ (Mpc/h)^2, whereas in right panel $\epsilon^2 = 15$ (Mpc/h)^2. We see that, obviously, the oscillations are suppressed both in amplitude and in extension: in fact, we note that the oscillations stop at $k \sim 0.3$ h/Mpc in the left panel and at $k \sim 0.14$ h/Mpc in the right one. Thus, when calculating σ_b, we have to take into account at what k_{max} the oscillations extend to.

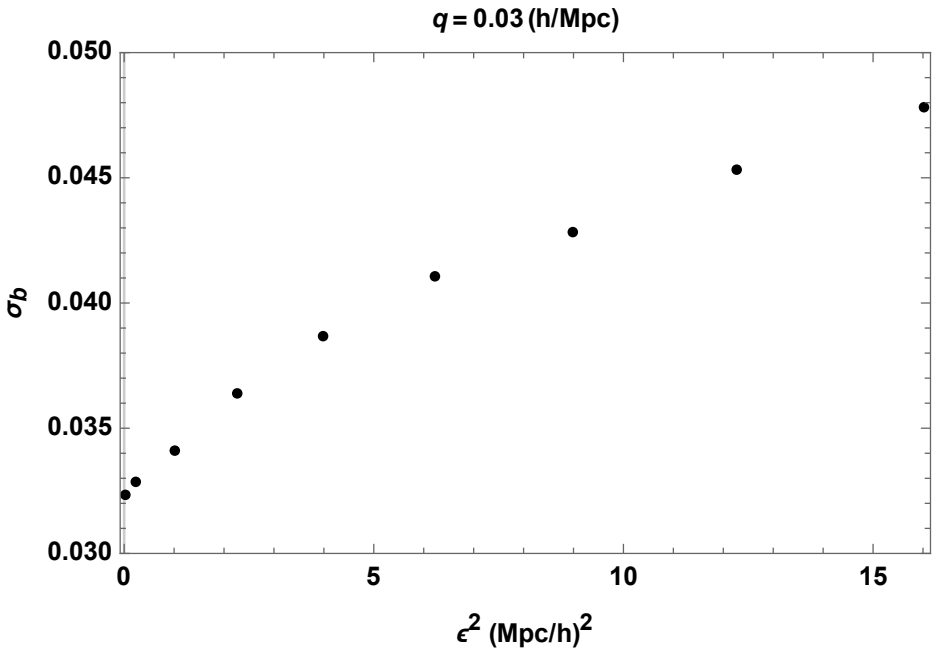

Figure 5.8: In this plot we show the estimated value of the bias error against the damping constant ϵ^2, see eq. (5.34). We see that, as we expect, the more the oscillations of the linear power spectrum are suppressed, the more the bias error increases. For this calculation we have chosen $b_m = 1, \mu = 1, s_{123} = 2$, $V = 2.82$ h^{-3}Gpc^3 and $q = 0.03$ h/Mpc.

5.2 Primordial Oscillations

Standard slow-roll inflation predicts a primordial power spectrum of curvature perturbations which goes as a power law as we have seen in Sec. 2.1.2. However, the study of departures from a simple power-law in the primordial power spectrum (PPS) has been studied extensively, since a lot of inflationary models consider these type of solutions [63].
From the theoretical point of view, departures from a simple power-law PPS could be a signature of the failure of any of the assumptions of the standard single field slow-roll inflation with Bunch-Davies initial conditions for quantum fluctuations, which we have introduced in Chapter 1 and 2. The detection of these features could be extremely useful in differentiating between inflation and alternative scenarios, or could provide hints for inflaton dynamics beyond slow-roll, and new heavy particles [63].
The upcoming cosmological observations, such as the large-scale structure surveys, will help in describing if the hints for departures from a power-law power spectrum have a physical origin or are simply some statistical fluctuation.
The type of inflationary oscillatory features on the primordial power spectrum we will deal with are predicted in various theoretical frameworks. For example, these features are present in the context of axion inflation [64], or could be created by a periodic signal present in the inflationary field potential [65]. They are also present in axion monodromy inflation [66] or in small-field models such as brane inflation [67] or also in models which display oscillations of massive fields [68].
As from [69] or also [70] we will study models in which these primordial oscillations appear as superimposed oscillations in the primordial power spectrum. In particular we can write:

$$P_\zeta(k) = P_{\zeta,0}(k)\,(1 + A_{lin}\sin(kr_{lin} + \phi)) \tag{5.38}$$

where $P_{\zeta,0}(k) = A_s(k/k_0)^{n_s-1}$ is the already introduced standard power-law primordial power spectrum.
However, in this work we are more in interested in the linear matter power spectrum. From [71] we know that the matter overdensity in Fourier space $\delta(\mathbf{k})$ is related to the curvature perturbations $\Phi(\mathbf{k})$ by Poisson equation as

$$\delta(\mathbf{k}, z) = M(k, z)\Phi(\mathbf{k}) \tag{5.39}$$

where

$$M(k, z) = \frac{2}{3}\frac{k^2 T(k) D(z)}{\Omega_m H_0^2} \tag{5.40}$$

and where $T(k)$ is the matter transfer function and $D(z)$ the growth factor. Hence we can write:

$$\langle\delta(\mathbf{k}_1)\delta(\mathbf{k}_2)\rangle = M(k_1, z)M(k_2, z)\langle\Phi(\mathbf{k}_1)\Phi(\mathbf{k}_2)\rangle \tag{5.41}$$

namely:

$$P_m^{(0)}(k) = M^2(k,z)P_\zeta(k). \tag{5.42}$$

5.2.1 Superimposed Linear Oscillations and Consistency Relations

We have seen in eq. (4.28) that, at first approximation, we can write the linear matter power spectrum as a smooth part plus an oscillating part which comes from the BAO's phenomenon. Now we want to consider a scenario in which the PS has further oscillatory feature, besides BAO's, of inflationary origin.
In this context, we assume a PS of the form

$$P_m^{(0)}(k) = P_m^{nw}\left[1 + A_{bao}(k)\sin(kr_s) + A_{lin}(k)\sin(kr_{lin}+\phi)\right] \tag{5.43}$$

where $A_{lin}(k)$ and r_{lin} are the amplitude and the scale-length of the new oscillations we want to investigate. We also included a phase ϕ, with respect to BAO oscillations. Using this power spectrum we can see what is the new form of the logarithmic derivative in the CR, i.e. eq. (4.26); we will suppress, for the sake of notation, the m subscript.

$$\begin{aligned}\frac{\mathrm{d}\log P^{(0)}(k)}{\mathrm{d}\log k} = &\frac{k}{P^{(0)}(k)}\frac{\mathrm{d}}{\mathrm{d}k}\left[P^{nw}(k) + P^{nw}(k)A_{bao}(k)\sin(kr_s)\right] \\ &+ \frac{k}{P^{(0)}(k)}\frac{\mathrm{d}}{\mathrm{d}k}\left[P^{nw}(k)A_{lin}(k)\sin(kr_{lin}+\phi)\right].\end{aligned} \tag{5.44}$$

Thus, for the first term of eq. (5.44), we have:

$$\begin{aligned}&= \frac{k}{P^{(0)}(k)}\Big[\frac{\mathrm{d}P^{nw}(k)}{\mathrm{d}k} + \frac{\mathrm{d}P^{nw}(k)}{\mathrm{d}k}A_{bao}(k)\sin(kr_s) + P^{nw}(k)\frac{\mathrm{d}A_{bao}(k)}{\mathrm{d}k}\sin(kr_s) + \\ &\quad + r_s P^{nw}(k)A_{bao}(k)\cos(kr_s)\Big] \\ &= \frac{1}{1 + A_{bao}(k)\sin(kr_s) + A_{lin}(k)\sin(kr_{lin}+\phi)}\frac{\mathrm{d}\log P^{nw}(k)}{\mathrm{d}\log k} + \frac{\mathrm{d}\log P^{nw}(k)}{\mathrm{d}\log k}\times \\ &\quad \times\left[\frac{A_{bao}(k)\sin(kr_s)}{1 + A_{bao}(k)\sin(kr_s) + A_{lin}(k)\sin(kr_{lin}+\phi)}\right] + kr_s A_{bao}(k)\Big[\frac{P^{nw}(k)\cos(kr_s)}{P^{(0)}(k)} + \\ &\quad + \frac{1}{r_s}\frac{P^{nw}(k)}{P^{(0)}(k)}\frac{1}{A_{bao}(k)}\frac{\mathrm{d}A_{bao}(k)}{\mathrm{d}k}\sin(kr_s)\Big].\end{aligned}$$

Therefore, the first term of eq. (5.44) reads:

$$\begin{aligned}&= \frac{\mathrm{d}\log P^{nw}(k)}{\mathrm{d}\log k}\left[\frac{1 + A_{bao}(k)\sin(kr_s)}{1 + A_{bao}(k)\sin(kr_s) + A_{lin}(k)\sin(kr_{lin}+\phi)}\right] \\ &\quad + \frac{kr_s A_{bao}(k)}{1 + A_{bao}(k)\sin(kr_s) + A_{lin}(k)\sin(kr_{lin}+\phi)}\Big[\cos(kr_s) + \alpha(k)\sin(kr_s)\Big]\end{aligned} \tag{5.45}$$

where we have already defined $\alpha(k)$ in eq. (4.30). Similarly, for the second term of eq. (5.44) we obtain:

$$= \frac{\mathrm{d}\log P^{nw}(k)}{\mathrm{d}\log k}\left[\frac{A_{lin}(k)\sin(kr_{lin}+\phi)}{1+A_{bao}(k)\sin(kr_s)+A_{lin}(k)\sin(kr_{lin}+\phi)}\right] + \frac{kr_{lin}A_{lin}(k)}{1+A_{bao}(k)\sin(kr_s)+A_{lin}(k)\sin(kr_{lin}+\phi)}\left[\cos(kr_{lin}+\phi)+\alpha'(k)\sin(kr_{lin}+\phi)\right] \tag{5.46}$$

where

$$\alpha'(k) \equiv \frac{1}{kr_{lin}}\frac{\mathrm{d}\log A_{lin}(k)}{\mathrm{d}\log k}. \tag{5.47}$$

Thus, taking into account two different oscillations, eq. (4.29) changes into:

$$\frac{\mathrm{d}\log P_m^{(0)}(k)}{\mathrm{d}\log k} = \frac{\mathrm{d}\log P_m^{nw}(k)}{\mathrm{d}\log k} + \frac{kr_s A_{bao}(k)}{1+A_{bao}(k)\sin(kr_s)+A_{lin}(k)\sin(kr_{lin}+\phi)}\times \left[\cos(kr_s)+\alpha(k)\sin(kr_s)\right] + \frac{kr_{lin}A_{lin}(k)}{1+A_{bao}(k)\sin(kr_s)+A_{lin}(k)\sin(kr_{lin}+\phi)} \times \left[\cos(kr_{lin}+\phi)+\alpha(k)\sin(kr_{lin}+\phi)\right]. \tag{5.48}$$

In Fig. (5.9) we show the results of the calculation of eq. (5.3), taking into account the presence of two different oscillations. We clearly see that, if we let the parameters of the linear oscillations to change, both sides of the CR change very similarly. This happens because, obviously, both sides of the equation contain the power spectrum with the two superimposed oscillations. However, we stress the fact that, since both sides of the consistency relations change in a similar way, the CR are still valid. We note, though, that especially when r_{lin} is different from the BAO scale-length (r_s) the CR seem to be less accurate.

Finally, let us point out that the we have chosen $A_{lin}(k)$ to be exponentially suppressed in a way similar to $A_{bao}(k)$, that is:

$$A_{lin}(k) = A_{0,lin}e^{-k^2\epsilon^2}. \tag{5.49}$$

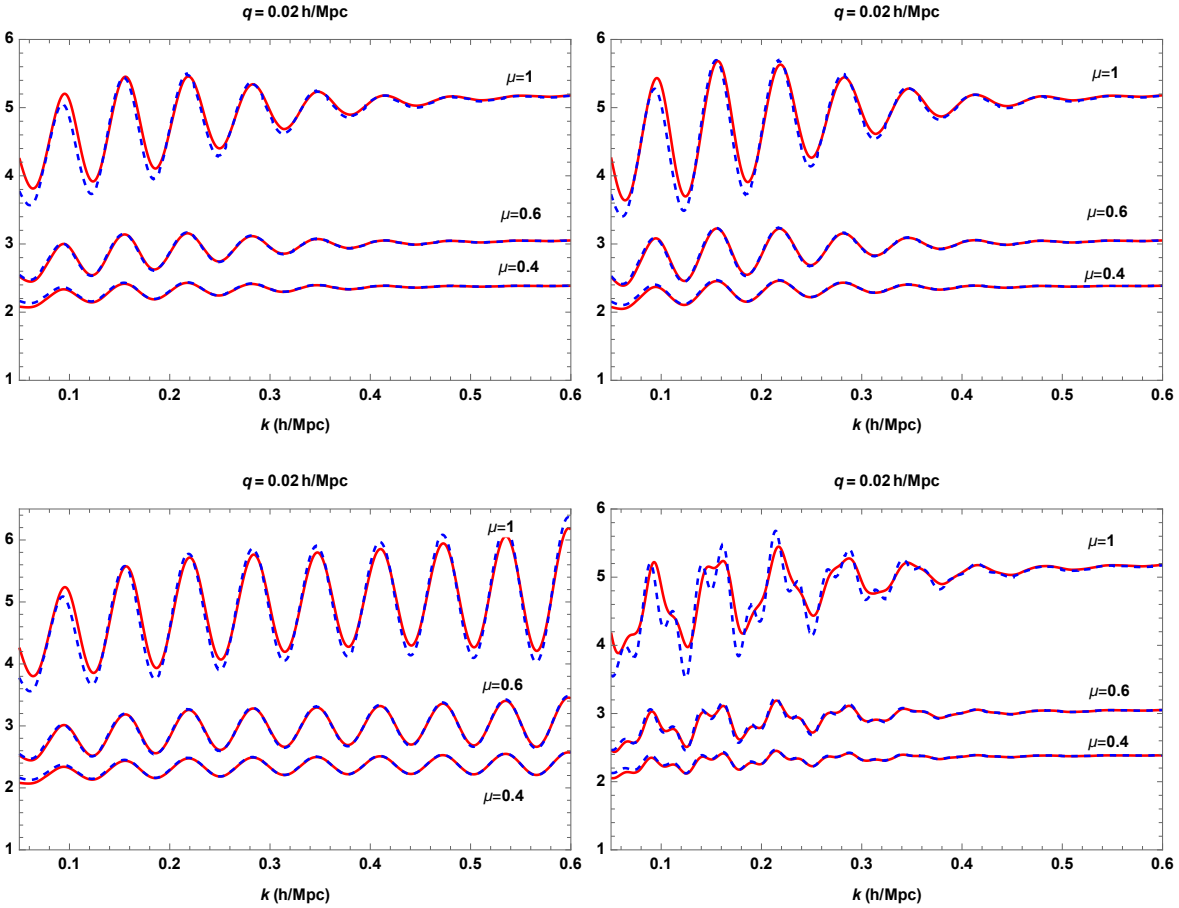

Figure 5.9: Comparison between the l.h.s. and r.h.s. of eq. (5.3), considering the power spectrum described by eq. (5.43). The red solid line is the l.h.s. whereas the blue dashed line is the r.h.s. of the equation. *Top left*: the plot was made choosing $q = 0.02$ h/Mpc, $A_{0,lin} = 0.02$, $r_{lin} = 100$ Mpc/h, $\phi = 0$ and $\epsilon = 5$. *Top right*: the plot was made choosing $q = 0.02$ h/Mpc, $A_{0,lin} = 0.05$, $r_{lin} = 100$ Mpc/h, $\phi = 0$ and $\epsilon = 5$. *Bottom left*: the plot was made choosing $q = 0.02$ h/Mpc, $A_{0,lin} = 0.02$, $r_{lin} = 100$ Mpc/h, $\phi = 0$ and $\epsilon = 0$. *Bottom right*: the plot was made choosing $q = 0.02$ h/Mpc, $A_{0,lin} = 0.02$, $r_{lin} = 250$ Mpc/h, $\phi = 0$ and $\epsilon = 5$. We clearly see that the oscillations of the two sides of the CR are deeply related. In the first three panels, since we have chosen $r_{lin} = 100$ Mpc/h, there is no much difference with respect to the case in which we have only BAO's, Fig. 4.1. However, when the linear oscillations scale-length happens to be different from the BAO's one, especially for high μ, the consistency relations seem to be less accurate.

5.3 2-D Fisher Matrix Forecast: Linear Oscillations

In this section, considering the power spectrum defined by eq. (5.43) and the consistency relations, we will perform a two-dimensional forecast still using the Fisher information matrix.
In order to do so, we assume the same probability distribution function defined by eq. (5.4) and the same definition of the Fisher matrix:

$$\mathbf{F}_{ij} = -\left\langle \frac{\partial^2 \log L}{\partial\theta_i \partial\theta_j} \right\rangle \tag{5.50}$$

and

$$\sigma_{\theta_i} \geq (\mathbf{F}^{-1})_{ii}^{1/2}. \tag{5.51}$$

Now we must be careful because the Fisher matrix is, in general, a matrix with rank different from one, since the vector of parameters we are considering is $\boldsymbol{\theta} = (b_m, A_{0,lin}, r_{lin}, \epsilon, \phi)$, where recall that ϵ is the damping constant of the linear oscillations. Thus, the Fisher matrix reads

$$\mathbf{F} = \mathbf{F}(b_m, A_{0,lin}, r_{lin}, \epsilon, \phi). \tag{5.52}$$

Now we take eq. (3.9), i.e.

$$\log L(\boldsymbol{\theta}) = \log L(\boldsymbol{\theta}_0) + \frac{1}{2}(\boldsymbol{\theta}_\alpha - \boldsymbol{\theta}_{0\alpha}) \frac{\partial^2 \log L}{\partial\boldsymbol{\theta}_\alpha \partial\boldsymbol{\theta}_\beta} (\boldsymbol{\theta}_\beta - \boldsymbol{\theta}_{0\beta}) + \cdots \tag{5.53}$$

and, since we have that

$$\log L(\boldsymbol{\theta}) = -\frac{1}{2}\chi^2(\boldsymbol{\theta}) \tag{5.54}$$

we can write

$$-\frac{1}{2}\chi^2(\boldsymbol{\theta}) = -\frac{1}{2}\chi^2(\boldsymbol{\theta}_0) - \frac{1}{2}\sum_{i,j}(\boldsymbol{\theta} - \boldsymbol{\theta}_0)_i \mathbf{F}_{ij} (\boldsymbol{\theta} - \boldsymbol{\theta}_0)_j + \cdots \tag{5.55}$$

which leads to

$$\Delta\chi^2 \simeq \sum_{i,j}(\boldsymbol{\theta} - \boldsymbol{\theta}_0)_i \mathbf{F}_{ij} (\boldsymbol{\theta} - \boldsymbol{\theta}_0)_j. \tag{5.56}$$

Eq. (5.56) defines an ellipsoid in the parameter space. In particular, we compute the elements of the Fisher matrix at a given fiducial parameter $\theta_{0,i}$ and then we keep fixed 3 out of 5 parameters at their fiducial value and let the remaining parameters pair to assume values around their fiducial value.

Therefore, if the indices i, j can assume only one value and $i \neq j$, we can expand eq. (5.56) as follows:

$$F_{\theta_i\theta_i}(\theta_i-\theta_{0,i})^2+F_{\theta_j\theta_j}(\theta_j-\theta_{0,j})^2+F_{\theta_i\theta_j}(\theta_i-\theta_{0,i})(\theta_j-\theta_{0,j})+F_{\theta_j\theta_i}(\theta_j-\theta_{0,j})(\theta_i-\theta_{0,i}) < \Delta\chi^2. \tag{5.57}$$

Note that eq. (5.57) has only four terms: this is, indeed, because we have evaluated eq. (5.56) at the fiducial value for three of the parameters we are considering. Moreover, we have used the symbol $<$ because we are interested to find those values of the parameters which give us a certain confidence level we are searching for. In particular, from [49], we know that the $\Delta\chi^2$ for joint parameter estimation for 2 parameters assumes the following values:

$$\begin{aligned} 1\sigma\ (68.3\,\%) &\implies \Delta\chi^2 = 2.30 \\ 2\sigma\ (95.4\,\%) &\implies \Delta\chi^2 = 6.17 \\ 3\sigma\ (99.7\,\%) &\implies \Delta\chi^2 = 11.8 \end{aligned} \tag{5.58}$$

We show, in Fig. 5.10, 5.11, 5.12 and 5.13 the 2 dimensional joint probability calculated, at 1 and 2 σ for the parameters $A_{0,lin}$ (which will be indicated simply with A_0), b_m and r_{lin}.
In particular, in Fig. 5.10 we show the confidence plot for the parameters A_0 and b_m, having chosen the fiducial value $b_m = 1$, $A_0 = 0.02$ and 4 different values of r_{lin}. Moreover, we have chosen $\epsilon = 0$, where recall that ϵ is the damping constant that suppresses both the BAO oscillations and the linear ones, see eq. (4.58) and eq. (5.49). Thus we are supposing in this case that the oscillations are not damped. We see that, while r_{lin} (the frequency) increases, we gain more information on the amplitude of the oscillations, as the error on A_0 becomes smaller. We also see, however, that A_0 and b_m are more correlated at higher value of the frequency.
In fig. 5.11, instead, we have chosen to damp both the two oscillations, having set $A_0 = 0.02$ and $r_{lin} = 100$ Mpc/h. We clearly see that, as the damping constant increases, the error on A_0 becomes bigger and A_0 becomes compatible with 0.
We see a similar behavior for r_{lin} in Fig. 5.12, where the error on r_{lin} becomes bigger as we increase the damping constant.
Finally, we have plotted in Fig. 5.13 the joint probability for A_0 and r_{lin}. Choosing $\epsilon^2 = 16$ $\mathrm{h}^{-2}\mathrm{Mpc}^2$ we do see that A_0 is compatible with 0. Moreover, we see that the two parameters A_0 and r_{lin} are strongly correlated.

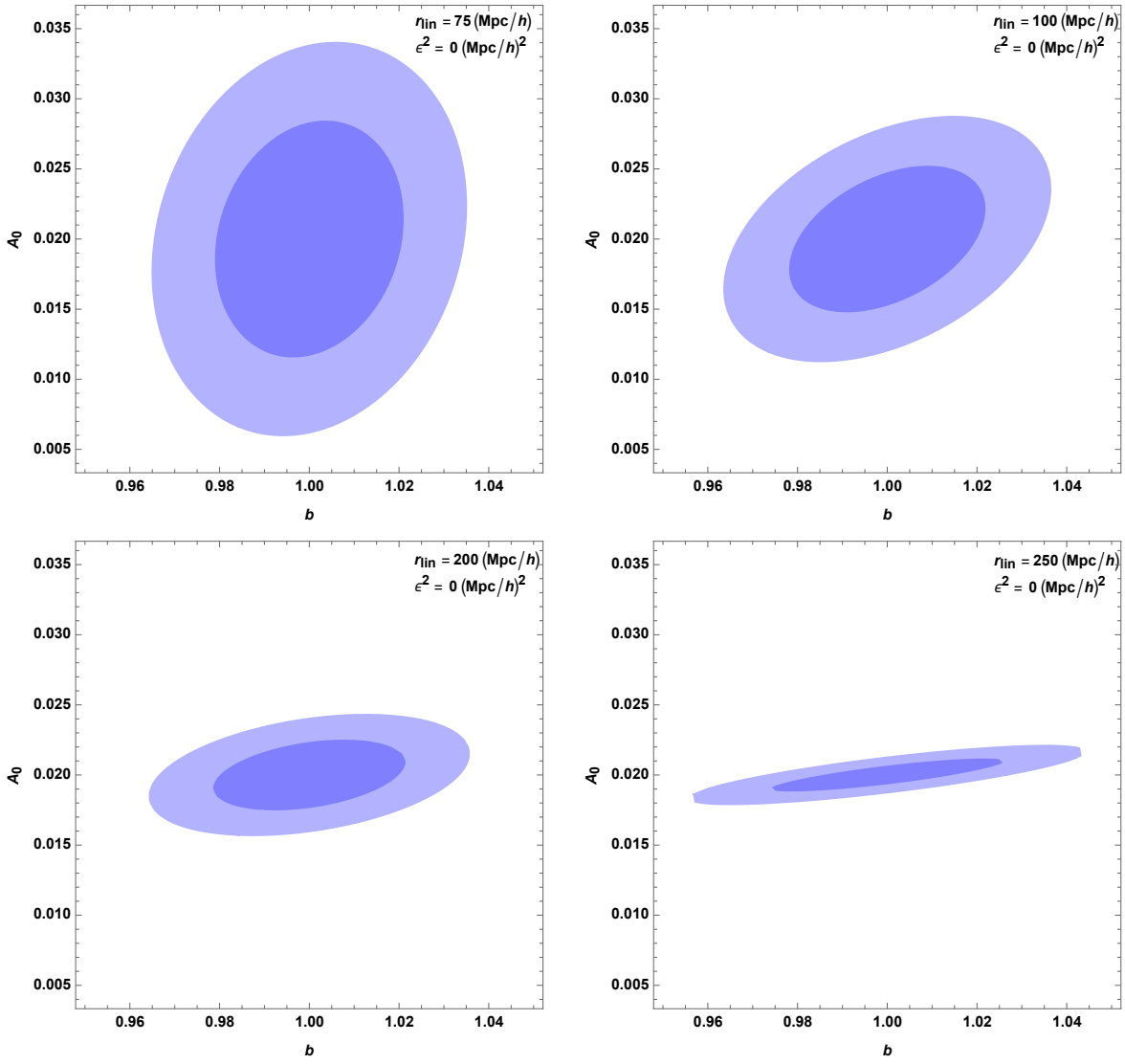

Figure 5.10: Two dimensional joint probability calculated at 1 σ (dark region) and 2 σ (light region) for $A_{0,lin}$, simply indicated with A_0, and b_m. All plots were computed having set $V = 2.82\ \mathrm{h}^{-3}\mathrm{Gpc}^3$ and $b_m = 1$. The damping constant of both the BAO oscillations and the linear oscillations, ϵ, was set equal to 0. We see that, as the value of r_{lin} increases (clockwise, from top-left), the error on A_0 gets smaller.

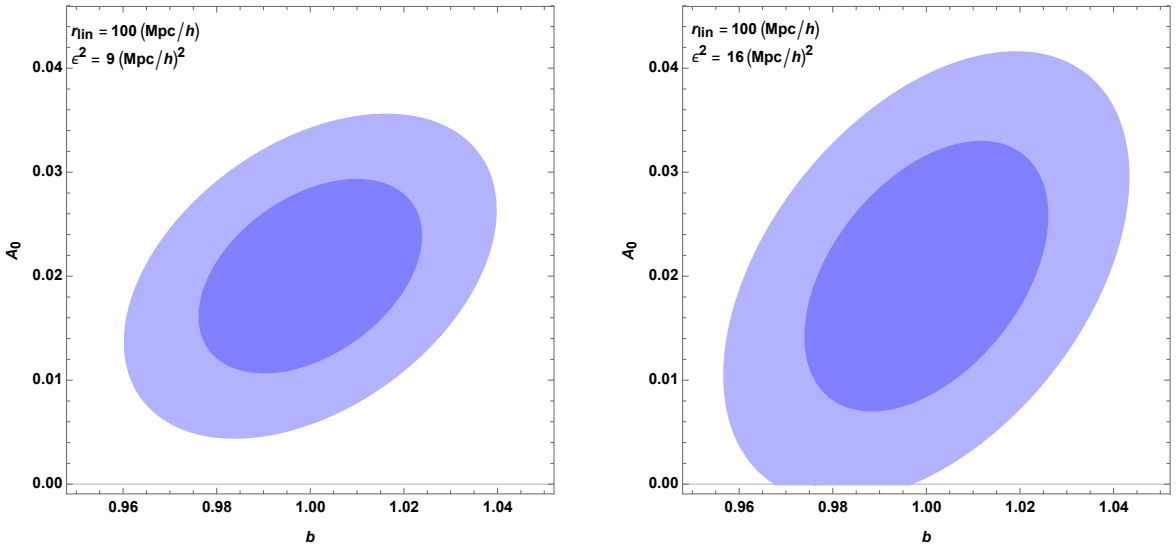

Figure 5.11: Two dimensional joint probability calculated at 1 σ (dark region) and 2 σ (light region) for A_0 and b_m. All plots were computed having set $V = 2.82$ h^{-3}Gpc^3, $b_m = 1$ and $r_{lin} = 100$ Mpc/h. We see that, as the damping constant ϵ increases the error on A_0 gets bigger and A_0 becomes compatible with 0.

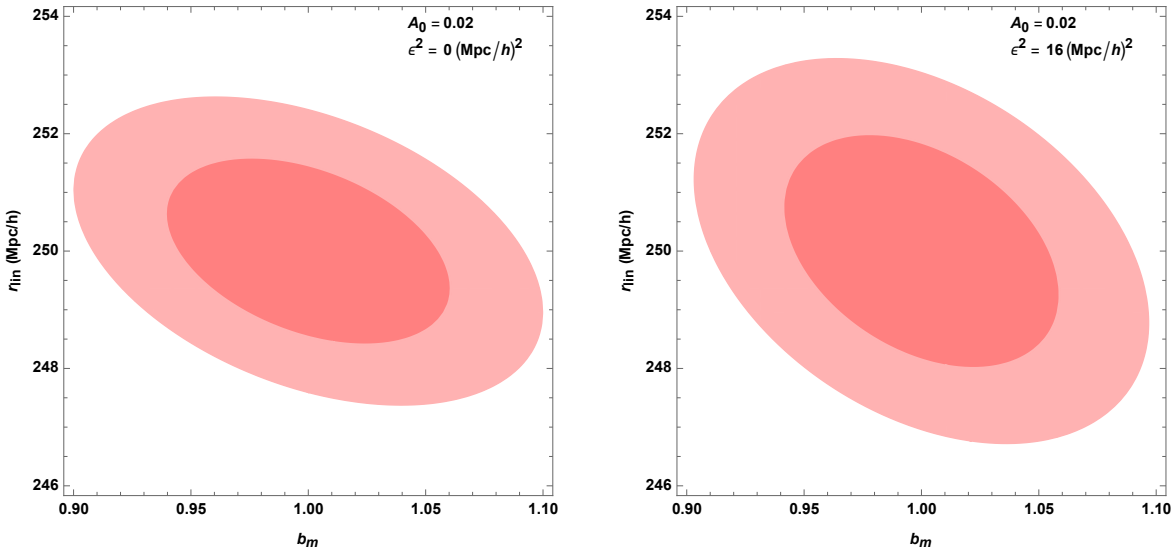

Figure 5.12: Two dimensional joint probability calculated at 1 σ (dark region) and 2 σ (light region) for r_{lin} and b_m. Again, we see that as ϵ increases, the error on r_{lin} becomes greater. These two plots were done choosing $V = 2.82$ h^{-3}Gpc^3 and $b_m = 1$.

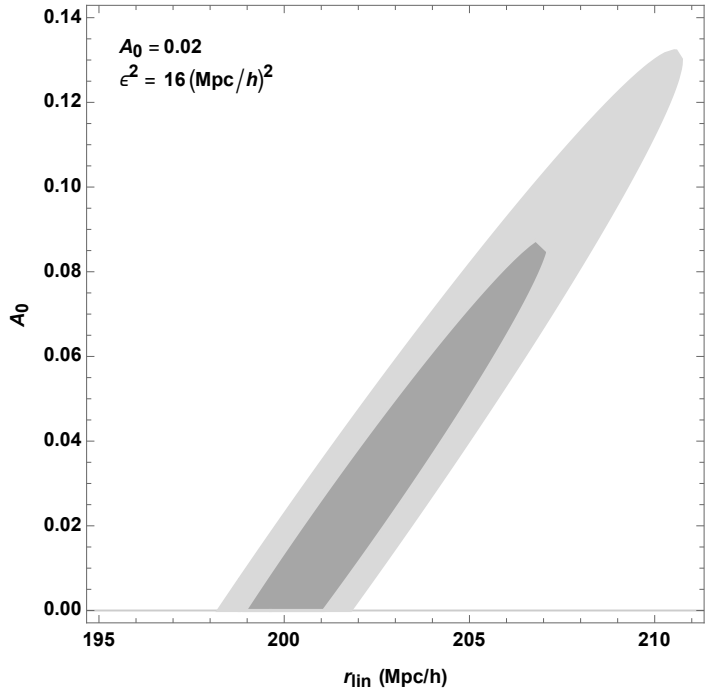

Figure 5.13: Two dimensional joint probability calculated at 1 σ (dark region) and 2 σ (light region) for A_0 and r_{lin}. We see that the two parameters are correlated and that A_0 is compatible with 0. For this plot we have set $V = 2.82\ \mathrm{h}^{-3}\mathrm{Gpc}^3$, $b_m = 1$ and $\epsilon^2 = 16\ \mathrm{h}^{-2}\mathrm{Mpc}^2$.

Chapter 6

Conclusions

We have started our work introducing standard cosmology and slow-roll inflation. Then we have studied cosmological perturbation theory (PT) in the Eulerian framework. In particular, we have derived the tree-level bispcetrum, eq. (2.175), and the power spectrum for the dark matter density field at first order in PT, eq. (2.185) and eq. (2.186).

Afterward, we have introduced the Fisher matrix formalism which was used in our forecasts. We have derived the Cramer-Rao inequality, eq. (3.14), which tells us the best error we can make on a given parameter of the theory, i.e.

$$\Delta\theta_i \geq (\mathbf{F}^{-1})_{ii}^{1/2}$$

where $\mathbf{F}_{ij}$ is the Fisher matrix.

In Chapter 4, then, we have derived the large-scale structure consistency relations (CR):

$$\lim_{q/k\to 0} \frac{B_{\alpha\beta\gamma}(q,k_+,k_-)}{P_{\alpha\alpha}(q)P_{\beta\gamma}(k)} = -\frac{\mu^2}{b_\alpha(q)}\frac{\mathrm{d}\log P_{\beta\gamma}(k)}{\mathrm{d}\log k} + O\left(\left(\frac{q}{k}\right)^0\right)$$

and defined the bias parameter as

$$b_\alpha(q) \equiv \lim_{q\to 0}\frac{P_{\alpha\alpha}(q)}{P_{\alpha m}(q)}.$$

Later, we have checked the CR computing the matter bispectrum at lowest order in perturbation theory, and we have obtained that

$$\lim_{q/k\to 0} \frac{B^{SPT}_{mmm}(q,k_+,k_-)}{P^0_m(q)P^0_m(k)} = -\mu^2\frac{\mathrm{d}\log P^0_m(k)}{\mathrm{d}\log k} + \frac{13+8\mu^2}{7} + O\left(\frac{q}{k}\right)$$

finding that we can write the r.h.s as a subdominant scale dependent term plus a smooth term which at first order is scale independent.

Next, in the last Chapter, the original work of this *Thesis* is presented. Using the Fisher matrix formalism we have performed different forecasts. We have assumed a Gaussian Likelihood obtained using the consistency relations, i.e. eq. (5.4). Then, as a first step we have derived the errors associated to the power spectrum and the bispectrum, obtaining:

$$\sigma_{P(k)} = 2\pi \frac{P(k)}{k\sqrt{V\Delta k}},$$

$$\sigma_{B(k_1,k_2,k_3)} = \sqrt{\frac{\pi s_{123}}{V k_1 k_2 k_3 \Delta k^3}} \left[P(k_1)P(k_2)P(k_3)\right]^{1/2}.$$

We have thus obtained Fig. (5.1), where we have computed the error of the bias as a function of the survey volume using 25 linearly-spaced bins, from $k_{min} = 0.05$ h/Mpc up to $k_{max} = 0.45$ h/Mpc, with a bin width of $\Delta k = 0.016$ h/Mpc. We note that, as the survey volume is increased, we get a lower value for the error. For $\mu = 1$, we find that $\sigma_b \simeq 0.0161 - 0.0205$. This is an interesting result, telling us that Euclid will potentially be able to measure the bias parameter up to 1-2 % of precision. Moreover, we know that in general the parameter f, which we have defined in eq. (2.110), is measured in the combination $f\sigma_8$. However, we can also write the coefficient of the r.h.s of the CR as a function of b_m and f [11]. Therefore, being able to measure precisely b_m would give a unique opportunity to break the degeneracy between f and σ_8.
Then we have computed the error on the bias using different k_{max}, i.e. Fig. 5.2. The more we lower k_{max}, using therefore a smaller range, the more the error on the bias gets worse. In addition we see that increasing k_{max} after $\sim 0.25 - 0.30$ h/Mpc, does not lower the error on the bias with the same trend we see for smaller values of k_{max}. This is because we calculated σ_b using the CR, which give information as long as there is a given scale which breaks the scale-invariance of the correlation function, such as the baryon acoustic oscillations [72]. Therefore, since BAO become really small around $k \sim 0.3$ h/Mpc, we do not gain much information thereafter.
Next, we have introduced shot noise corrections. In particular we have repeated the calculation of σ_b at varying k_{max}. The results, Fig. 5.4, show that the value of the error is slightly higher and that σ_b saturates earlier with increasing k_{max}.
In all previous results we have not considered the fact that the BAO are damped at late times. Therefore, we have used eq. (4.58), i.e.

$$P(k) = P^{nw}(k) + e^{-k^2\epsilon^2} P^{w}(k)$$

and implemented the same calculations using damped baryon acoustic oscillations. We presented the results in Fig. (5.8), where we performed the calculations using $\Delta k = 0.016$ Mph/h and $V = 2.82$ h^{-3}Gpc^3. We clearly see that, as the damping constant increases, the error on the bias gets bigger: this is indeed what we expect, as damping degrades the information content of the BAO's.

We have later introduced the following power spectrum:

$$P_m^{(0)}(k) = P_m^{nw}\left[1 + A_{bao}(k)\sin(kr_s) + A_{lin}(k)\sin(kr_{lin} + \phi)\right]$$

which displays further oscillations besides BAO's, of inflationary origin. First we checked the CR with this power spectrum and we found, in Fig. (5.9), that if r_{lin} is different from r_s the two oscillations interfere. Thus, measuring precisely the BAO could help in discriminating between the two oscillations and detect the inflationary features through the consistency relations.
Finally, in the last section, we performed a two-dimensional Fisher forecast on the parameters which are displayed in the above mentioned power spectrum. The results are reported in Figures 5.10-5.13. First, in Fig. 5.10, we have plotted the two dimensional joint probability for A_0 and b_m, having set $V = 2.82\ \mathrm{h}^{-3}\mathrm{Gpc}^3$. We note that, as we would expect, the more r_{lin} is different from r_s the more the error on A_0 gets smaller. At the same time, though, we see that A_0 and b_m becomes more correlated. In Fig. (5.11) instead, we have studied the behavior of A_0 and b_m for different values of ϵ^2. Again, as we expect, the more we suppress the oscillations the more the errors increase: in particular we see that A_0 becomes compatible with 0. In Fig. 5.12 we display the confidence plot of r_{lin} and b_m which exhibits the same features of the previous plots. Finally, Fig. 5.13 shows the confidence plot for A_0 and r_{lin}. The interesting result is that the two parameters are strongly correlated and, again, A_0 is compatible with 0.

The possible extensions of this work are numerous. First, redshift space distorsions can be taken into account, leading for example to modifications of the coefficient in front of the r.h.s of the CR, as we were discussing before. In addition, the same calculations can be made considering, besides dark matter, biased tracers. Finally, the results obtained in the two dimensional forecast could be used to constrain different inflationary parameters.

References

[1] Laura C Parker et al. "The masses and shapes of dark matter halos from galaxy-galaxy lensing in the CFHT legacy survey". In: *The Astrophysical Journal* 669.1 (2007), p. 21.

[2] Gary Hinshaw et al. "Nine-year Wilkinson Microwave Anisotropy Probe (WMAP) observations: cosmological parameter results". In: *The Astrophysical Journal Supplement Series* 208.2 (2013), p. 19.

[3] Planck Collaboration et al. "Planck 2013 results. XVI. Cosmological parameters". In: *Astron. Astrophys* 571 (2014), A16.

[4] Christopher P Ahn et al. "The tenth data release of the sloan digital sky survey: First spectroscopic data from the sdss-iii apache point observatory galactic evolution experiment". In: *The Astrophysical Journal Supplement Series* 211.2 (2014), p. 17.

[5] Alan H Guth. "Inflationary universe: A possible solution to the horizon and flatness problems". In: *Physical Review D* 23.2 (1981), p. 347.

[6] Chris A Blake et al. "Cosmology with the SKA". In: *New Astronomy Reviews* 48.11-12 (2004), pp. 1063–1077.

[7] Željko Ivezić et al. "LSST: from science drivers to reference design and anticipated data products". In: *The Astrophysical Journal* 873.2 (2019), p. 111.

[8] Rene Laureijs et al. "Euclid definition study report". In: *arXiv preprint arXiv:1110.3193* (2011).

[9] A Kehagias and A Riotto. "Symmetries and consistency relations in the large scale structure of the universe". In: *Nuclear Physics B* 873.3 (2013), pp. 514–529.

[10] Marco Peloso and Massimo Pietroni. "Galilean invariance and the consistency relation for the nonlinear squeezed bispectrum of large scale structure". In: *Journal of Cosmology and Astroparticle Physics* 2013.05 (2013), p. 031.

[11] Marco Marinucci, Takahiro Nishimichi, and Massimo Pietroni. "Measuring bias via the consistency relations of the large scale structure". In: *Physical Review D* 100.12 (2019), p. 123537.

[12] S Weinberg. *Gravitation and Cosmology*. Canada: John Wiley and Sons, 1972.

[13] S Dodelson. *Modern Cosmology*. Amsterdam: Academic Press, 2003.

[14] Edwin Hubble. "A relation between distance and radial velocity among extra-galactic nebulae". In: *Proceedings of the national academy of sciences* 15.3 (1929), pp. 168–173.

[15] Daniel Baumann. "TASI lectures on inflation". In: *arXiv preprint arXiv:0907.5424* (2009).

[16] Ralph A Alpher, Hans Bethe, and George Gamow. "The origin of chemical elements". In: *Physical Review* 73.7 (1948), p. 803.

[17] Arno A Penzias and Robert Woodrow Wilson. "A measurement of excess antenna temperature at 4080 Mc/s." In: *The Astrophysical Journal* 142 (1965), pp. 419–421.

[18] N Aghanim et al. "Planck 2018 results. VI. Cosmological parameters". In: *arXiv preprint arXiv:1807.06209* (2018).

[19] Joel R Primack. "The nature of dark matter". In: *arXiv preprint astro-ph/0112255* (2001).

[20] E Kolb and M Turner. *The Early Universe*. 1988.

[21] Maria Chiara Guzzetti et al. "Gravitational waves from inflation". In: *arXiv preprint arXiv:1605.01615* (2016).

[22] David H Lyth and Andrew R Liddle. *The primordial density perturbation: Cosmology, inflation and the origin of structure*. Cambridge University Press, 2009.

[23] Andrew R Liddle and David H Lyth. *Cosmological inflation and large-scale structure*. Cambridge University Press, 2000.

[24] Bruce Bassett and Renée Hlozek. "Baryon acoustic oscillations". In: *Dark energy: observational and theoretical approaches* (2010), p. 246.

[25] Daniel J Eisenstein, Hee-Jong Seo, and Martin White. "On the robustness of the acoustic scale in the low-redshift clustering of matter". In: *The Astrophysical Journal* 664.2 (2007), p. 660.

[26] Daniel Eisenstein and Martin White. "Theoretical uncertainty in baryon oscillations". In: *Physical Review D* 70.10 (2004), p. 103523.

[27] Eiichiro Komatsu et al. "Five-year wilkinson microwave anisotropy probe* observations: cosmological interpretation". In: *The Astrophysical Journal Supplement Series* 180.2 (2009), p. 330.

[28] Sergei Bashinsky and Edmund Bertschinger. "Dynamics of cosmological perturbations in position space". In: *Physical Review D* 65.12 (2002), p. 123008.

[29] Adam Hincks. *Baryon Acoustic Oscillations Tutorial*. `https://adh-sj.info/bao_cmb.php`. 2020.

[30] Hiroo Totsuji and T Kihara. "The correlation function for the distribution of galaxies". In: *Publications of the Astronomical Society of Japan* 21 (1969), p. 221.

[31] Daniel J Eisenstein et al. "Detection of the baryon acoustic peak in the large-scale correlation function of SDSS luminous red galaxies". In: *The Astrophysical Journal* 633.2 (2005), p. 560.

[32] David N Spergel et al. "Three-year Wilkinson Microwave Anisotropy Probe (WMAP) observations: implications for cosmology". In: *The Astrophysical Journal Supplement Series* 170.2 (2007), p. 377.

[33] Max Tegmark et al. "Cosmological constraints from the SDSS luminous red galaxies". In: *Physical Review D* 74.12 (2006), p. 123507.

[34] Idit Zehavi et al. "Galaxy clustering in the completed SDSS redshift survey: The dependence on color and luminosity". In: *The Astrophysical Journal* 736.1 (2011), p. 59.

[35] Francis Bernardeau et al. "Large-scale structure of the Universe and cosmological perturbation theory". In: *Physics reports* 367.1-3 (2002), pp. 1–248.

[36] PJE Peebles. "Large-scale background temperature and mass fluctuations due to scale-invariant primeval perturbations". In: (1982).

[37] EM Lifshitz and LD Landau. *Fluid Mechanics*. Pergamon Press, 1987.

[38] C Pichon and F Bernardeau. "Vorticity generation in large-scale structure caustics". In: *arXiv preprint astro-ph/9902142* (1999).

[39] Bhuvnesh Jain and Edmund Bertschinger. "Second order power spectrum and nonlinear evolution at high redshift". In: *arXiv preprint astro-ph/9311070* (1993).

[40] MH Goroff et al. "Coupling of modes of cosmological mass density fluctuations". In: *The Astrophysical Journal* 311 (1986), pp. 6–14.

[41] Francis Bernardeau. "The gravity-induced quasi-Gaussian correlation hierarchy". In: *The Astrophysical Journal* 392 (1992), pp. 1–14.

[42] FR Bouchet et al. "Weakly nonlinear gravitational instability for arbitrary Omega". In: *The Astrophysical Journal* 394 (1992), pp. L5–L8.

[43] Francis Bernardeau. "Skewness and kurtosis in large-scale cosmic fields". In: *arXiv preprint astro-ph/9312026* (1993).

[44] Roman Scoccimarro et al. "Nonlinear evolution of the bispectrum of cosmological perturbations". In: *The Astrophysical Journal* 496.2 (1998), p. 586.

[45] DJ Heath. "The growth of density perturbations in zero pressure Friedmann–Lemaitre universes". In: *Monthly Notices of the Royal Astronomical Society* 179.3 (1977), pp. 351–358.

[46] Ofer Lahav et al. "Dynamical effects of the cosmological constant". In: *Monthly Notices of the Royal Astronomical Society* 251.1 (1991), pp. 128–136.

[47] Stephen W Hawking. "The development of irregularities in a single bubble inflationary universe". In: *Physics Letters B* 115.4 (1982), pp. 295–297.

[48] James N Fry. "The Galaxy correlation hierarchy in perturbation theory". In: *The Astrophysical Journal* 279 (1984), pp. 499–510.

[49] Alan Heavens. "Statistical techniques in cosmology". In: *arXiv preprint arXiv:0906.0664* (2009).

[50] Max Tegmark. "Measuring cosmological parameters with galaxy surveys". In: *Physical Review Letters* 79.20 (1997), p. 3806.

[51] Maurice George Kendall and Alan Stuart. *The advanced theory of statistics: in 3 volumes*. C. Griffin, 1963.

[52] AJS Hamilton. "Towards optimal measurement of power spectra-I. Minimum variance pair weighting and the Fisher matrix". In: *Monthly Notices of the Royal Astronomical Society* 289.2 (1997), pp. 285–294.

[53] Hume A Feldman, Nick Kaiser, and John A Peacock. "Power spectrum analysis of three-dimensional redshift surveys". In: *arXiv preprint astro-ph/9304022* (1993).

[54] Robert E Smith, Román Scoccimarro, and Ravi K Sheth. "Scale dependence of halo and galaxy bias: Effects in real space". In: *Physical Review D* 75.6 (2007), p. 063512.

[55] Martin Crocce and Roman Scoccimarro. "Renormalized cosmological perturbation theory". In: *Physical Review D* 73.6 (2006), p. 063519.

[56] Martin Crocce and Roman Scoccimarro. "Nonlinear evolution of baryon acoustic oscillations". In: *Physical Review D* 77.2 (2008), p. 023533.

[57] Eugenio Noda, Marco Peloso, and Massimo Pietroni. "A robust BAO extractor". In: *Journal of Cosmology and Astroparticle Physics* 2017.08 (2017), p. 007.

[58] Diego Blas et al. "Time-sliced perturbation theory II: baryon acoustic oscillations and infrared resummation". In: *Journal of Cosmology and Astroparticle Physics* 2016.07 (2016), p. 028.

[59] Antony Lewis, Anthony Challinor, and Anthony Lasenby. "Efficient computation of cosmic microwave background anisotropies in closed Friedmann-Robertson-Walker models". In: *The Astrophysical Journal* 538.2 (2000), p. 473.

[60] Donghui Jeong. "Cosmology with High (z>1) Redshift Galaxy Surveys". PhD thesis.

[61] Emiliano Sefusatti and Eiichiro Komatsu. "Bispectrum of galaxies from high-redshift galaxy surveys: Primordial non-Gaussianity and nonlinear galaxy bias". In: *Physical Review D* 76.8 (2007), p. 083004.

[62] Victoria Yankelevich and Cristiano Porciani. "Cosmological information in the redshift-space bispectrum". In: *Monthly Notices of the Royal Astronomical Society* 483.2 (2019), pp. 2078–2099.

[63] Mario Ballardini et al. "Non-linear damping of superimposed primordial oscillations on the matter power spectrum in galaxy surveys". In: *arXiv preprint arXiv:1912.12499* (2019).

[64] Xiulian Wang et al. "Natural inflation, Planck scale physics and oscillating primordial spectrum". In: *International Journal of Modern Physics D* 14.08 (2005), pp. 1347–1364.

[65] Xingang Chen, Richard Easther, and Eugene A Lim. "Generation and characterization of large non-Gaussianities in single field inflation". In: *Journal of Cosmology and Astroparticle Physics* 2008.04 (2008), p. 010.

[66] Raphael Flauger et al. "Oscillations in the CMB from axion monodromy inflation". In: *Journal of Cosmology and Astroparticle Physics* 2010.06 (2010), p. 009.

[67] Rachel Bean et al. "Duality cascade in brane inflation". In: *Journal of Cosmology and Astroparticle Physics* 2008.03 (2008), p. 026.

[68] Xingang Chen. "Primordial features as evidence for inflation". In: *Journal of Cosmology and Astroparticle Physics* 2012.01 (2012), p. 038.

[69] Anže Slosar et al. "Scratches from the past: Inflationary archaeology through features in the power spectrum of primordial fluctuations". In: *arXiv preprint arXiv:1903.09883* (2019).

[70] Florian Beutler et al. "Primordial Features from Linear to Nonlinear Scales". In: *arXiv preprint arXiv:1906.08758* (2019).

[71] Emiliano Sefusatti. "One-loop perturbative corrections to the matter and galaxy bispectrum with non-Gaussian initial conditions". In: *Physical Review D* 80.12 (2009), p. 123002.

[72] Tobias Baldauf et al. "Equivalence principle and the baryon acoustic peak". In: *Physical Review D* 92.4 (2015), p. 043514.

Ringraziamenti

Desidero ringraziare il professor Pietroni per avermi permesso di lavorare con lui in questi mesi. Il suo spiccato senso fisico e la sua intelligenza nella ricerca sono stati fonte d'ispirazione per me. Lo ringrazio anche per la sua disponibilità a rispondere alle mie numerose domande e dubbi, ho davvero apprezzato il tempo che mi ha dedicato. Inoltre vorrei ringraziare anche il professor Peloso per la sua disponibilità e gentilezza: i consigli che mi ha dato sono stati sempre molto utili.
Un grato pensiero anche a tutta la mia numerosa famiglia. Mio papà e mia mamma che, oltre ad aver finanziato tutti questi anni di studi, mi hanno sempre appoggiato e voluto bene, anche non capendo praticamente niente di quello che stavo studiando. A mio fratello e le mie sorelle, impegnati nel bellissimo compito di crescere dei bambini, non mi hanno mai fatto mancare il loro bene. Un pensiero anche per tutti i miei zii. Un ricordo speciale anche ai nonni Nicola e Adriano, alle nonne Rosa e Nice e allo zio Wilder.
Ringrazio tutti i miei amici di Milano. Ringrazio particolarmente Trimo per la sua amicizia, il lavoro di questa tesi è stato possibile anche grazie al confronto con lui. Ricordo anche Simo Molinelli: è sempre stato per me una fonte di ispirazione come fisico e come uomo. Ringrazio il Don Andrea per la sua paternità e per il bene che mi vuole: occuperà sempre un posto nel mio cuore. Ricordo Palche, Becca, Edi, Piter, Marta, Giulia P. e Giulia C., Bianca, Bona, Muso, Visco, Gino e Richi Panza: la lontananza da loro non è facile, ma li porto con me.
Ringrazio tutti i miei amici di Padova, dal primo all'ultimo. Ringrazio Jack, perchè la sua disponibilità verso gli altri e verso di me mi commuove ogni volta. Ringrazio Samuele, che mi insegna sempre un modo semplice e profondo di stare davanti alla vita. Lo ringrazio anche per questi giorni in quarantena, la sua compagnia per me è fondamentale. Ricordo anche tutti i miei compagni di appartamento: con loro quest'anno mi sono sentito davvero a casa. Ringrazio la Vale Zap: la sua compagnia e la sua guida sono sempre illuminanti per me. Ringrazio la Chiara Ruzza, che non si stanca mai di cercare il meglio dalla vita: è per me sempre fonte di grande incoraggiamento. Ringrazio anche la Cristiana, vedere come mi vuole bene e come vuole bene a Dan è bellissimo.
Ringrazio tutti i miei amici fisici, in particolar modo tutti quelli che mi hanno dato una mano a correggere la tesi: Camilla, Cate, Cops, Piga, Matte Guida, Matte Scialpi e Nicolas. Grazie a Cops, Piga e Cate: condividere con loro questi anni di magistrale è stato speciale e affascinante, spero che l'amicizia con loro possa durare a lungo.

Non posso non ricordare anche tutti i miei amici di Reggio: Lollo, Chicchi, Ele, Losi, Brock, Meri, Matte Platani e Gianlu, quando riesco a vederli è sempre molto bello. Un particolare pensiero a Sabba e Jack, perchè l'amicizia con loro ha fondamenta profonde e sono per me una solida roccia a cui appoggiarmi.
Un pensiero anche ai miei amici americani: Brian, Emmalisa, Susan, Reinhard, Erik e Olivia. C'è un oceano che ci divide, ma li porto sempre con me.
Ringrazio Padre Enzo: in questi ultimi anni è stato per me guida e padre. Lo ringrazio per la profonda compagnia che mi fa e per come mi indica, sempre molto liberamente, la strada da percorrere.
Un grazie smisurato a Marco. Non ho parole per descrivere la gratitudine nei suoi confronti. Primo perchè questa tesi non sarebbe stata assolutamente possibile senza il suo aiuto. Ma ancora di più per la sua profonda amicizia. Ogni volta confrontarmi con lui non solo mi insegna tanto ma, soprattutto, mi porta gioa e serenità. Sei un grande.
Inoltre desidero ringraziare l'Anna, che è per me al contempo rifugio e apertura alla vita. La ringrazio per la sua disarmante semplicità, ogni volta guardarla come sta davanti alle circostanze mi commuove e mi insegna tanto. La ringrazio per come si impegna nella vita perchè osservare la dedizione e la passione che mette nei suoi studi è splendido, sono sicuro che un giorno sarà una bravissima infermiera. La ringrazio anche per come mi vuole bene gratuitamente: sentirsi amati e accolti non è mai scontato, e posso dire di avere incontrato una persona con la quale mi sento libero fino in fondo.
Un pensiero speciale a Marco Gallo e Chiara Corbella Petrillo. Sono l'esempio che la morte non ha l'ultima parola sulla vita: la loro storia è fonte di speranza e mi ha profondamente segnato e cambiato, dall'alto mi guardano e spero di poterli incontrare un giorno. Ringrazio infine Dio, per avermi donato questi amici e questi anni di università: sono stati per me fondamentali nel formarmi come fisico e soprattutto come uomo.